siam

6th Annual Meeting of the Bulgarian Section of SIAM
December 21-22, 2011
Sofia

BGSIAM'11

PROCEEDINGS

HOSTED BY THE INSTITUTE OF MATHEMATICS AND INFORMATICS
BULGARIAN ACADEMY OF SCIENCES

6th Annual Meeting of the Bulgarian Section of SIAM
December 21-22, 2011, Sofia

BGSIAM'11 Proceedings

ISSN: 1313-3357

Printed in Sofia, Bulgaria
Cover design: Boris Staikov
Printing and binding: Demetra Ltd.

PREFACE

The 6th Annual Meeting of Bulgarian Section of SIAM (BGSIAM) took part on December 21 and 22, 2011 and was hosted by the Institute of Mathematics and Informatics, Bulgarian Academy of Sciences, Sofia. The conference support provided by SIAM, as the major international organization for Industrial and Applied Mathematics, is very highly appreciated.

The Bulgarian Section of SIAM was founded on January 18, 2007 and the accepted Rules of Procedure were officially approved by the SIAM Board of Trustees on July 15, 2007. The activities of BGSIAM follow the general objectives of SIAM, as established in its Certificate of Incorporation. The role of SIAM is very important for promotion of interdisciplinary collaboration between applied mathematics and science, engineering and technology in the Republic of Bulgaria.

During the 6th Annual Meeting of BGSIAM (BGSIAM'11) a wide range of problems concerning recent achievements in the field of industrial and applied mathematics were presented. Following the established tradition, the conference provided a forum for exchange of ideas between scientists, who develop and study mathematical methods and algorithms, and researchers, who apply them for solving real life problems.

More than 50 participants from eight universities, five institutes of the Bulgarian Academy of Sciences and also from outside the traditional academic departments took part in BGSIAM'11. They represent most of the strongest Bulgarian research groups in the field of industrial and applied mathematics. We are very glad to report that special session for young researchers and students with 6 talks and 8 participants was organized during BGSIAM'11. Organization of such sessions for young researchers is the main goal of BGSIAM in the future conferences.

LIST OF INVITED LECTURES:

- ROUMEN ANGELOV
  Department of Mathematics and Applied Mathematics, University of Pretoria, Pretoria, South Africa
  METHODS OF ANALYSIS OF DYNAMICAL MODELS IN BIOSCIENCE
- ROSSEN IVANOV
  School of Mathematical Sciences, Dublin City University, Dublin 9, Ireland
  SINGULAR SOLUTIONS OF CROSS-COUPLED EPDIFF EQUATIONS: WALTZING PEAKONS AND COMPACTONS PAIRS
- TSVIATKO RANGELOV
  Institute of Mathematics and Informatics, Bulgarian Academy of Sciences, Bulgaria
  TIME-HARMONIC FRACTURE BEHAVIOR OF PIEZOELECTRIC SOLIDS WITH DEFECT

- JULIAN REVALSKI
  Institute of Mathematics and Informatics, Bulgarian Academy of Sciences, Bulgaria and Universite des Antilles et de la Guyane, France
  APPLICATIONS OF TOPOLOGICAL GAMES IN OPTIMIZATION AND NONLINEAR ANALYSIS

The present volume contains extended abstracts of the conference talks (Part A) and list of participants (Part B).

Angela Slavova
Chair of BGSIAM Section

Geno Nikolov
Vice-Chair of BGSIAM Section

Krassimir Georgiev
Secretary of BGSIAM Section

Sofia, February 2012

Contents

Part A
Extended abstracts[1]

[1] Arranged alphabetically according to the family name of the first author.

High-Order Difference Schemes for Singular Problems 1 Weakly Degeneration

Ivanka Tr. Angelova and Lubin G. Vulkov

1 Introduction

The main object of this report is the following Sturm-Liouvile equation

$$Au \equiv A_0 u + q(x)u = f(x), \quad A_0 = -\varepsilon^2 \frac{d}{dx}\left(\varphi(x)\frac{du}{dx}\right), \; u(1) = 0, \tag{1}$$

where $\varphi \in [0,1] \cap C^1(0,1]$ and $q(x) \geq 0$ is a measurable, bounded function. Suppose that $\varphi(0) = 0, \; \varphi(x) > 0, \; x > 0$, so that the equation (1) is degenerate at the point $x = 0$. The main feature of the degeneration could be illustrated with the case $\varphi(x) = x^\alpha p(x), \; \alpha > 0, p \in C^k[0,1]$ k is an integer and $p(x) \geq p_0$. S. G. Mihlin [4](also see [5]) for $\varepsilon = 1$ pointed three important cases concerning the integrals $I_1 = \int_0^1 \frac{dx}{\varphi(x)}$ and $I_2 = \int_0^1 \frac{xdx}{\varphi(x)}$ **a)** I_1 is convergent **b)** I_1 is nonconvergent but I_2 is convergent **c)** I_2 is nonconvergent.
If the integral I_3 is convergent then the operator A_0 (respectively A) is positive definite; it is also positive definite in the case $\alpha = 2$. If I_2 is nonconvergent, the operator A_0 is only positive and in this case A is positive definite, if $q(x) \geq q_0 = const.0$. As it is well known, if the operator A is positive definite, the equation $Au = f$ has one weak solution from the energy space H_A: this solution is also from $L_2(0,1)$. The scalar product $[\cdot,\cdot]_A$ and corresponding *energetic norm* $\|\cdot\|_A$ are as follows

$$[u,v]_A = \int_0^1 (\varphi u'v' + quv)dx, \quad \|u\|_A^2 = \int_0^1 (\varphi u'^2 + qu^2)dx.$$

The behavior of (1) for $p(x) = 1$ was recently analyzed in :H. Gastro & H. Wang, J. F. Anal (in press). It was shown that: *Suppose that* $0 \leq \alpha < 1$ and $\varepsilon = 1$. *Then there exists a function* $f \in C_0^\infty(0,1)$ *such that near the origin the solution can be expanded in the following way*

$$u(x) = a_1 x^{1-\alpha} + a_2 x^{3-2\alpha} + a_3 x^{5-3\alpha} + \cdots, \; a_1 \neq 0.$$

It follows from here that $u' \sim x^{-\alpha} \to \infty$ *near the origin and this is the main difficulty at the numerical solution of (1).*

2 Construction of Difference Schemes

We rewrite the problem (1) as follows:

$$-w' + q(x)u = f(x), \quad x \in (0,1),$$

where $w(x) = x^\alpha p(x) u'(x)$ is the flux and $0 \le \alpha < 1$ (weakly degeneration) $p(x), q(x) \in L_\infty(0,1),\ f(x) \in L_2(0,1),\ 0 < p_0 \le p(x) \le p_1;\ p_0, p_1$ are constants, $q(x) \ge 0$.
Let consider on $[0,1]$ arbitrary system of mesh points: $0 = x_0 < ... < x_i < ... < x_N = 1,\ h_i = x_i - x_{i-1},\ i = 1, \ldots, N-1$. Let

$$\xi_i^{(0)}(x) = \begin{cases} 1\,, x \in (x_{i-1}, x_{i+1}), \\ 0\,, x \notin (x_{i-1}, x_{i+1}),\ i = 1, \ldots\ N-1. \end{cases}$$

For $n = 0, 1, \ldots$ we introduce:

$$\xi_i^{(2n+1)}(x) = \begin{cases} \int\limits_{x_{i-1}}^{x} \frac{\xi_i^{(2n)}(t)}{x^\alpha p(t)} dt,\ x \in (x_{i-1}, x_i), \\ \int\limits_{x}^{x_{i+1}} \frac{\xi_i^{(2n)}(t)}{x^\alpha p(t)} dt,\ x \in (x_i, x_{i+1}), \\ 0 \quad ,\ x \notin (x_{i-1}, x_{i+1}),\ i = 1, \ldots\ N-1. \end{cases}$$

$$\xi_i^{(2n+2)}(x) = \begin{cases} \int\limits_{x_i - 1}^{x} q(t) \xi_i^{(2n+1)}(t) dt,\ x \in (x_{i-1}, x_i), \\ \int\limits_{x}^{x_{i+1}} q(t) \xi_i^{(2n+1)}(t) dt,\ x \in (x_i, x_{i+1}), \\ 0 \quad ,\ x \notin (x_{i-1}, x_{i+1}),\ i = 1, \ldots\ N-1. \end{cases}$$

Then, letting

$$\psi_i^{(n)}(x) = \sum_{k=1}^{n} \xi_i^{(2k-1)}(x);\ n = 1, 2, \ldots,$$

we derive on the base of Marchuk-type identities [1, 3], the schemes for $n = 1, 2, \ldots$:

$$-a_i^{(n)} U_{i-1} + c_i^{(n)} U_i - b_i^{(n)} U_{i+1} = f_i^{(n)}, U_0 = U_N = 0,\ \ i = 1, \ldots,\ N-1,$$

$$a_i^{(n)} = \frac{1}{\psi_i^{(n)}(x_i - 0)},\ b_i^{(n)} = \frac{1}{\psi_i^{(n)}(x_i + 0)},$$

$$c_i^{(n)} = a_i^{(n)} + b_i^{(n)} + \int\limits_{x_{i-1}}^{x_i} q(x) \frac{\psi_i^{(n)}(x)}{\psi_i^{(n)}(x_i - 0)} dx + \int\limits_{x_i}^{x_{i+1}} q(x) \frac{\psi_i^{(n)}(x)}{\psi_i^{(n)}(x_i + 0)} dx,$$

$$f_i^{(n)} = \int\limits_{x_{i-1}}^{x_i} f(x) \frac{\psi_i^{(n)}(x)}{\psi_i^{(n)}(x_i - 0)} dx + \int\limits_{x_i}^{x_{i+1}} f(x) \frac{\psi_i^{(n)}(x)}{\psi_i^{(n)}(x_i + 0)} dx.$$

Let us define for $0 \le a < b \le 1$

$$I^\alpha[g; a, b] = \int_a^b \frac{g(x)}{x^\alpha} dx,\ \xi = \xi(\alpha; a, b) = \frac{I^\alpha[x; a, b]}{I^\alpha[1; a, b]}.$$

For $\xi = \xi(\alpha; a, b)$ we get

$$I^\alpha[g; a, b] = g(\xi) I^\alpha[1; a, b] + \frac{1}{2} g''(\eta) \int_a^b \frac{x^2 - \xi^2}{x^\alpha} dx,\ \eta \in (a, b). \tag{2}$$

Note that for $\alpha = 0$, $\xi(0;a,b) = \frac{a+b}{2}$ and (2) reduces to the classical midpoint formula. Let us approximate $g(x)$ by the Lagrange polynomial.One can check that for $\xi = \xi(\alpha;a,b)$ we have:

$$I^{\alpha}[g;a,b] = \frac{g(a)(b-\xi)+g(b)(\xi-a)}{b-a} I^{\alpha}[1;a,b] + \frac{g''(\eta)}{2}\int_a^b \frac{x^2+ab-(a+b)\xi}{x^{\alpha}}dx. \tag{3}$$

Note that for $\alpha = 0$ (3) reduces to the classical trapezoid formula.
For $n = 2$ we choose $\xi = \xi(\alpha;a,b)$ such that

$$\int_a^b \frac{(b-x)(\xi-x)(x-a)}{x^{\alpha}}dx = 0.$$

Then we obtain a "Simpson's" type formula

$$\begin{aligned} I^{\alpha}[g;a,b] &= \frac{g(a)I_a[a,b]}{(b-a)(\xi-a)} + \frac{g(\xi)I_k[a,b]}{(b-\xi)(\xi-a)} + \frac{g(b)I_b[a,b]}{(b-a)(b-\xi)} \\ &+ O((b-a)^4 I^{\alpha}[1;a,b]), \text{ where} \end{aligned} \tag{4}$$

$I_a[a,b] = \int_a^b \frac{(b-x)(\xi-x)}{x^{\alpha}}dx,\ I_k[a,b] = \int_a^b \frac{(b-x)(x-a)}{x^{\alpha}}dx,\ I_b[a,b] = \int_a^b \frac{(x-a)(x-\xi)}{x^{\alpha}}dx.$

Note that for $\alpha = 0$ with $\xi(0;a,b) = \frac{a+b}{2}$ (4) reduces to the Simpson's formula.
The computational finite difference scheme for $n = 1$ as follows is:

$$p(\xi_{i-1/2})\frac{U_i - U_{i-1}}{\hbar_i I^{\alpha}[1;x_{i-1},x_i]} + p(\xi_{i+1/2})\frac{U_i - U_{i+1}}{\hbar_i I^{\alpha}[1;x_i,x_{i+1}]} + q_i U_i = f_i, \tag{5}$$

$\hbar_i = \xi_{i+1/2} - \xi_{i-1/2},\ \xi_{i-1/2} = \xi(\alpha;x_{i-1},x_i),\ \xi_{i+1/2} = \xi(\alpha;x_i,x_{i+1}),\ i = 1,\ldots,N-1.$

Let consider on $[0,1]$ system of mesh points: $0 = x_0 < \xi_{1/2} < x_1 < ... < \xi_{i-1/2} < x_i < \xi_{i+1/2} < ... < \xi_{N-1/2} < x_N = 1$ such that $x_i = (ih)^{\mu},\ i = 0,\ldots N,\ \mu \geq 1,\ hN = 1,$ see the concrete for $\alpha = 0.9,\ \mu = 2/(2-\alpha),\ N = 8.$

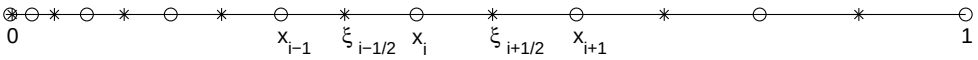

We introduce the functions:

$$Q_i^{(1)}(x) = \begin{cases} \xi_i^{(1)}(x)/\xi_i^{(1)}(x_i - 0) & , x \in (x_{i-1}, x_i), \\ \xi_i^{(1)}(x)/\xi_i^{(1)}(x_i + 0) & , x \in (x_i, x_{i+1}), \\ 0 & , x \notin (x_{i-1}, x_{i+1}),\ i = 1,\ldots\ N-1. \end{cases}$$

$$u_h(x) = \sum_{i=1}^{N-1} U_i Q_i^{(1)}(x),\ u_I(x) = \sum_{i=1}^{N-1} u(x_i) Q_i^{(1)}(x).$$

Then, for $\varepsilon = 1$, we prove second order convergence in the *energetic norm* on the graded mesh $\{x_i\}$ for $\mu = 2/(2-\alpha)$ of the Galerkin solution $u_h(x)$.

3 Numerical Experiments

In this section are presented samples of numerical experiments illustrating the accuracy of schemes derived in Section 2. The reported experiments were performed on the model problem (1).

Example 1. We take $\varepsilon = 1,\ p(x) = e^x,\ q(x) = 1 + x^2,\ u(0) = u(1) = 0$ in (1) with exact solution $u(x) = x^{1-\alpha}(1 - \sin \pi x/2)$ - the typical singular behavior at zero. Numerical results are presented in Tables 1, 2.

Table 1: $Example1 : \alpha = 0.9;\ 0.999,\ n = 1.$

α	0.9				0.999			
μ	1		$2/(2-\alpha)$		1		$2/(2-\alpha)$	
N	$\|z_h\|$	p	$\|z_h\|$	p	$\|z_h\|$	p	$\|z_h\|$	p
2^3	1,601E-2	1,4392	1,182E-2	1,9956	2,146E-2	1,3047	1,418E-2	1,9832
2^4	5,904E-3	1,6049	2,963E-3	1,9950	8,767E-3	1,4746	3,585E-3	1,9972
2^5	1,941E-3	1,7031	7,433E-4	1,9999	3,183E-3	1,5740	8,981E-4	1,9987
2^6	5,961E-4	1,7692	1,859E-4	2,0000	1,079E-3	1,6412	2,247E-4	1,9999
2^7	1,749E-4	1,8166	4,646E-5	2,0000	3,489E-4	1,6902	5,619E-5	2,0000
2^8	4,964E-5	1,8524	1,162E-5	2,0000	1,091E-4	1,7276	1,405E-5	2,0000
2^9	1,375E-5	1,8802	2,904E-6	2,0000	3,324E-5	1,7570	3,512E-6	2,0000
2^{10}	3,735E-6	1,9024	7,260E-7	2,0000	9,922E-6	1,7807	8,780E-7	2,0000
2^{11}	9,990E-7	1,9206	1,815E-7	2,0000	2,913E-6	1,8002	2,195E-7	1,9999
2^{12}	2,639E-7		4,537E-8		8,437E-7		5,488E-8	

$$\|z_h\| = \max_{0 \le i \le N} |U_i - u(x_i)|,\ p = \log_2 \|z_{2h}\|/\|z_h\|.$$

Table 2: $Example1. : \alpha = 0.5;\ 0.9;\ 0.999,\ n = 2.$

α	0.5		0.9		0.999	
μ	$4/(2-\alpha)$					
N	$\|z_h\|$	p	$\|z_h\|$	p	$\|z_h\|$	p
8	5,291E-6	3,9729	8,243E-5	3,9729	3,271E-4	3,5758
16	3,369E-7	3,9877	5,485E-6	3,9877	2,743E-5	3,6778
32	2,124E-8	3,9914	3,558E-7	3,9914	2,143E-6	3,7385
64	1,335E-9	3,9978	2,275E-8	3,9978	1,606E-7	3,7799
128	8,358E-11	4,0030	1,444E-9	4,0030	1,169E-8	3,8104
256	5,213E-12		9,126E-11	4,0458	8,333E-10	3,8184
512			5,526E-12		5,907E-11	

Example 2. We take $0 < \varepsilon < 1,\ p(x) = 1,\ q(x) = 1 + x^2,\ \alpha = 0.5,\ u(0) = u(1) = 0$ in (1).

Let consider on $[0,1]$ system of mesh points: $0 = y_0 < ... < y_i < ... < y_N = 1,\ i = 0, \dots N$. We get $\tau = \min\{1/2, 2\varepsilon \ln N\}$. Set $\tau = y_{N/2}$. We decompose $[0,\tau]$, $[\tau,1]$ in $N/2$ subintervals. $h = \frac{2\tau}{N}$ for $[0,\tau]$ and $H = \frac{2(1-\tau)}{N}$ for $[\tau,1]$. Then $x_i = y_i^{\mu},\ \mu \geq 1$ and the composite mesh [2, 6] for $\varepsilon = 0.05,\ \mu = 2/(2-\alpha),\ N = 8$ is shown below.

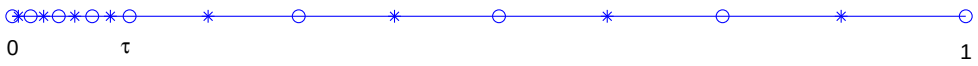

For this boundary value problem we do not know the exact solution. For exact solution we take the numerical one $\{U_i\}_0^N$ at $N = 2^{13}$. Numerical results are presented in Table 3 for scheme (5).

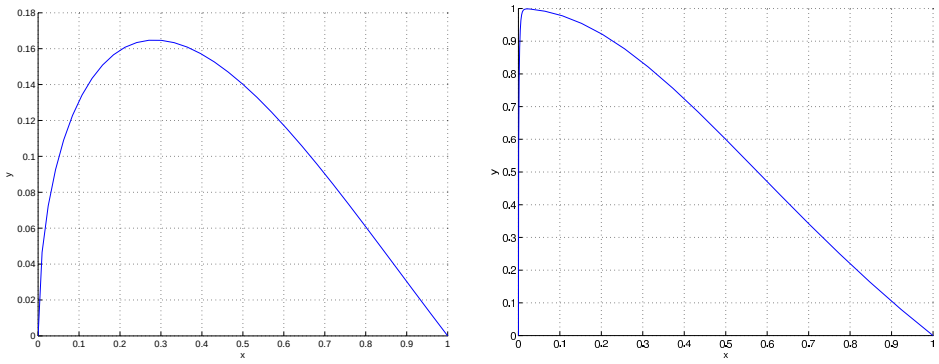

Figure 1: Numerical solution for $\varepsilon = 1$ (left) and $\varepsilon = 0.01$ (right).

Table 3: *Example* 2. $\alpha = 0.5,\ \mu = 4/3, \varepsilon = 10^{-1};\ 10^{-2};\ 10^{-6},\ n = 1$.

ε	10^{-1}		10^{-2}		10^{-6}	
N	$\|z_h\|$	p	$\|z_h\|$	p	$\|z_h\|$	p
2^3	2,147E-2	1,0342	2,169E-2	0,7914	2,168E-2	0,7907
2^4	1,048E-2	1,9646	1,253E-2	1,2280	1,253E-2	1,2280
2^5	2,686E-3	2,0613	5,350E-3	1,5290	5,350E-3	1,5290
2^6	6,435E-4	2,0812	1,854E-3	1,6143	1,854E-3	1,6143
2^7	1,521E-4	2,0591	6,055E-4	1,6866	6,055E-4	1,6866
2^8	3,649E-5	2,0432	1,881E-4	1,7307	1,881E-4	1,7307
2^9	8,854E-6	2,0422	5,668E-5	1,7820	5,668E-5	1,7820
2^{10}	2,150E-6	2,0860	1,648E-5	1,8085	1,648E-5	1,8085
2^{11}	5,063E-7		4,705E-6		4,705E-6	

Acknowledgments: This work is supported by the Bulgarian Fund for Science under the Project DID 02/37 form 2009.

References

[1] I. Angelova, L. Vulkov, High-order difference schemes based on new Marchuck integral identities for one-dimensional interface problems, *J. Numer. Math.*, Vol. 13, No. 1 (2005), 1-18

[2] C. Grosmann, L. Ludwig and H. Roos, Layer-adapted methods for a singularly perturved singular problem,*Comp. Methods in Appl. Math.*, Vol. 11, No. 2 (2011), 192-205

[3] G. Marchuk, V. Agoshkov, Introduction in projection-mesh methods. *Moscow, Nauka* (1981),(Russian).

[4] S. G. Mihlin, Varational-grid approximation of one-dimensional degenerate second-order differential equation, *Uestnik of LGU*, No.1(1973), 52-67

[5] T. Shaposhnikova, Grid point approximation of solutions of degenerate second-order ordinary differential equations, *Math. Notes*, Vol.24, No.1 (1978), 95-101

[6] J.J.H. Miller, E.O'Riordan and G.I. Shishkin, Fitted Numerical Methods for Singularly Perturbed Problems, *World-Scientific, Singapore*, (1996).

Computer-Aided Proof of Basin of Attraction of Asymptotically Stable Equilibria

Roumen Anguelov, Neli Dimitrova

1 Introduction

It is often the case in the modelling of biosystems, that the constructed mathematical model is a continuous dynamical system. The qualitative analysis of such systems regarding the long term behavior often deals only with local stability properties of the equilibria. One reason is that such properties are easy to establish by the nearly universal method of using the eigenvalues of the Jacobian of the right hand side. Except when the Jacobian has an eigenvalue with a zero real part (indicating possible bifurcation) these eigenvalues characterize completely the local stability properties of the equilibrium.
In a contradistinction, the only general purpose method for proving properties of global nature (global asymptotic stability or basin of attraction) is via a Lyapunov function [7]. Although there are many special types of systems for which Lyapunov functions are known, e.g. [2], there is no general method for constructing Lyapunov functions. Hence the difficulty in proving global properties particularly in high dimensional systems.
While the importance of the local stability properties is not in doubt, the fact that they characterize the behavior of the solutions only in a *sufficiently small* neighborhoods of the equilibria is an essential limitation in practical applications.
We propose a method of computer based proof of stability and basin of attraction of equilibria. It cannot be claimed that the method always gives result. However, in a typical situation it does. Moreover, if it does, this result constitutes a rigorous mathematical proof.

2 General Setting

Let $\Omega \subseteq \mathbb{R}^d$ and for every $p \in P \subset \mathbb{R}^m$ let $f(p,\cdot) : \Omega \to \mathbb{R}^d$. We assume that for every $p \in P$ the system of ODEs

$$\frac{dx}{dt} = f(p,x) \tag{1}$$

defines a (positive) dynamical system on $\Omega \subseteq \mathbb{R}^d$, that is, for every $x^0 \in \Omega$ it has a solution $x = x(p,x^0;t) \in \Omega$, $t \in [0,+\infty)$ such that $x(p,x^0;0) = x^0$.
Any equilibrium a satisfies the algebraic equation

$$f(p,a) = 0$$

We consider a typical situation when this equation has a solution $a(p)$ which is unique on some domain $D(p) = a(p) + M$, where M is compact and $0 \in M$, that is, $f(p,x) =$

0, $x \in D(p) \Rightarrow x = a(p)$. Equivalently, for every $p \in P$, function $f(p, \cdot)$ is invertible on $D(p)$.
Suppose that, motivated by empirical evidence, e.g. numerical simulations, intuition, insight into the physical process, etc, we make the following hypothesis:

Statement 1. *For every $p \in P$, (i) the set $D(p)$ is positively invariant and (ii) the equilibrium $a(p)$ is stable and attractive with basin of attraction containing $D(p)$.*

Statements of this sort are often formulated explicitly or implicitly implied in the literature. In most cases some numerical experiments provide support. We need to remark that in multidimensional problems, i.e. $x \in \mathbb{R}^{10}$ depending on a multidimensional parameter, e.g. $p \in P \subseteq \mathbb{R}^{10}$, numerical experiments can hardy be considered to generate a representative set of solutions. Naturally, this increases the value of statements that can be proved in a rigorous mathematical way.

3 Computer verification of basin of attraction

Let us make the substitution $x = a(p) + u$. Then the new variable satisfies the system

$$\frac{du}{dt} = f(p, a(p) + u) =: g(p, u) \tag{2}$$

It is easy to see that Statement 1 is equivalent to the following

Statement 2. *For every $p \in P$, (i) the set M is positively invariant for the system (2) and (ii) the origin is a stable and attractive equilibrium of (2) with basin of attraction containing M.*

We denote by $u(p, u^0; t)$ the solution of (2) for value of the parameters p which satisfies the initial condition $u(p, u^0; 0) = u^0$. Then we consider the multivalued function $u(P, M; \cdot) : [0, \infty) \to \mathcal{P}(\Omega)$ (the power set of Ω, i. e. the set of all subsets of Ω) given by

$$u(P, M; t) = \{u(p, u^0; t) : p \in P, u^0 \in M\}.$$

Function f is assumed continuous, thus, given that M and P are compact, the function $u(P, M; t)$ is compact-valued. Now Statement 2 is equivalently formulated as follows:

Statement 3. *For every $p \in P$, (i) there exists $\tau > 0$ such that $u(P, M; [0, \tau]) \subseteq M$ and (ii) $\lim_{t\to\infty} u(P, M; t) = 0$ in the topology of $\mathbb{R}^d$.*

Remark 4. *The equivalence of Statement 2 and Statement 3, especially of part (i), is not obvious and a proof is to be provided. In particular, part (i) in Statement 3 is equivalent to $u(P, M; t)$ being monotone decreasing in t with respect to inclusion.*

Under the additional assumption that M is an interval, Statement 3 assumes yet another equivalent formulation in terms of interval functions. Denote by $[u](P, M; t) = [u(P, M; t)]$ the interval hull of $u(P, M; t)$. At $t = 0$ we have $[u](P, M; 0)=u(P, M; 0)= M$, but in general we have the inclusion $u(P, M, t) \subseteq [u](P, M; t)$. Statement 3 is equivalent to

Statement 5. *(i) There exists $\tau > 0$ such that $[u(P, M; [0, \tau])] \subseteq M$ and (ii) $\lim_{t\to\infty}[u](P, M; t) = 0$ in the topology of $\mathbb{R}^d$.*

Using a numerical method for computing interval enclosure of the set of solutions of the system (2) point (i) in Statement 5 is computer verifiable. We can weaken a bit point (ii) to have also computer verifiable statement. We replace the statement that 0 is stable and attractive by the statement that for some $\varepsilon > 0$ the set $\mathcal{E} = [-\varepsilon, \varepsilon]^d$ contains an invariant set which is attractive and ε-stable. Let us recall that an equilibrium a is stable if for every $\gamma > 0$ there exists $\delta > 0$ such that any trajectory initiated in a δ-neighborhood of a remains within the γ-neighborhood of a for all times. We say that an equilibrium is **ε-stable** if this definition holds for $\gamma > \varepsilon$. We should remark that in practical applications the statement "the set $\mathcal{E} = [-\varepsilon, \varepsilon]^d$ contains an invariant set which is attractive and ε-stable" can be made to be virtually as strong as "0 is asymptotically stable" by taking ε sufficiently small.
In this way we obtain the following theorem.

Theorem 6. *If for some $\tau > 0$, $T > 0$, $\varepsilon > 0$ we have that (i) $[u(P, M; [0, \tau])] \subseteq M$ and (ii) $[u(P, M; T)] \subseteq \mathcal{E}$, then for every $p \in P$ the set $D(p)$ is positively invariant set of (1) and $a(p) + \mathcal{E}$ contains an attractive and ε-stable invariant set of (1) with basin of attraction containing $D(p)$.*

We can again remark that in practical applications the statement "$a(p) + \mathcal{E}$ contains an attractive and ε-stable invariant set" can be made to be virtually as strong as "$a(p)$ is asymptotically stable" by taking ε sufficiently small. This is true for example, if ε equals the width of the smallest computer interval containing $a(p)$. Using such small ε would be seldom necessary.
In some cases the inclusion (i) in Theorem 6 is difficult or impossible to obtain. This is due to the fact that M may not be an interval or instead of the interval hull, we have only some wider interval enclosure $\langle u\rangle(P, M, t)$ of $u(P, M, t)$. The inclusion (i) implies that M is an invariant set. But its actually more important function is to provide the monotonicity of $u(P, M, t)$ in t with respect to inclusion. Using this property we deduce from $u(P, M, T) \subseteq \mathcal{E}$ that $u(P, M, t) \subseteq \mathcal{E}$ for $t > T$. Furthermore, this monotonicity implies that the limit when $t \to \infty$ of $u(P, M; t)$ exists. This limit is the attractive invariant set. In the next theorem a slightly different condition leads to the same result.

Theorem 7. *If for some $\tau > 0$, $T > 0$, $\varepsilon > 0$ we have that (i) $\langle u\rangle(P, M; [\tau, 2\tau]) \subseteq M$ and (ii) $\langle u\rangle(P, M; [T, T + \tau])] \subseteq \mathcal{E}$, then for every $p \in P$ the set $u(p, D(p); [0, \tau])$ is positively invariant set of (1) and $a(p)+\mathcal{E}$ contains an attractive and ε-stable invariant set of (1) with basin of attraction containing $u(p, D(p); [0, \tau])$ (and also $D(p)$).*

Proof. Let $p \in P$ and let $\hat{M}(p) = u(p, M; [0, \tau])$. Then (i) implies that $u(p, \hat{M}(p); [0, \tau]) \subseteq \hat{M}(p)$. Therefore, $u(p, M; [t, t + \tau]) = u(p, \hat{M}(p); t)$ is monotone decreasing with respect to inclusion. Then so is $u(P, M; [t, t + \tau])$. The rest follows from Theorem 6 using $u(P, M; [t, t + \tau])$ instead of $u(P, M; t)$. □

4 A model example

We would like to test if the whole procedure is feasible on a simple example: the well-known "single substrate–single biomass" chemostat model with Monod specific growth rate function [1]

$$\frac{dx}{dt} = -\alpha D x + \frac{\mu_m s x}{K_s + s} \tag{3}$$

$$\frac{ds}{dt} = D s_i - D s - k\frac{\mu_m s x}{K_s + s} \tag{4}$$

Validated enclosures are computed for this model in [6], where the model and the parameters are briefly described so we do not need to repeat the description here. The parameters α and D are exactly known, namely, $\alpha = 0.5$, $D = 0.36$, $k = 10.53$. The parameters μ_m and K_s are not exactly known. We have $p := (\mu_m, K_s) \in [1.19, 1.21] \times [7.09, 7.11] =: P$. The equations define a dynamical system on $\Omega = \mathbb{R}^2_+$ with two equilibria: the trivial $x = 0,\ s = s_i$ and the nontrivial

$$s = b := \frac{\alpha D K_s}{\mu_m - \alpha D}, \quad x = a := \frac{s_i - b}{\alpha k D}$$

which is positive for the stated values and ranges of the parameters. We will find a set in the basin of attraction of the nontrivial equilibrium by considering the system

$$\frac{du}{dt} = -\alpha D(a + u) + \frac{\mu_m (b + v)(a + u)}{K_s + b + v} \tag{5}$$

$$\frac{dv}{dt} = D s_i - D(b + v) - k\frac{\mu_m (b + v)(a + u)}{K_s + b + v} \tag{6}$$

The system (5)–(6) has equilibrium at the origin for all values of the parameters. In order to apply Theorem 6 we need to compute validated enclosures of the sets of solutions initiated in various neighborhoods of this equilibrium. Methods for constructing enclosures for the solutions of systems of ODEs is one of the major successes of Interval Analysis, see [4] for review of such methods most of which are based on the work of Lohner [3] as it is the case in [6]. Here we use simpler approach by first converting the system to a system which is monotone [5]. After some experimentation we found a set M with the properties required in Theorem 7. The figures below present the lower and upper bounds for u and v and show that (i) and (ii) of Theorem 7 are satisfied.

5 Conclusion

We propose a computer based method for proving stability and basin of attraction of an equilibrium. The idea of using a computer to provide rigorous mathematical proofs is not new any more as several well-known open problems in mathematics have been resolved in such a way. The method suggested here has become possible due to

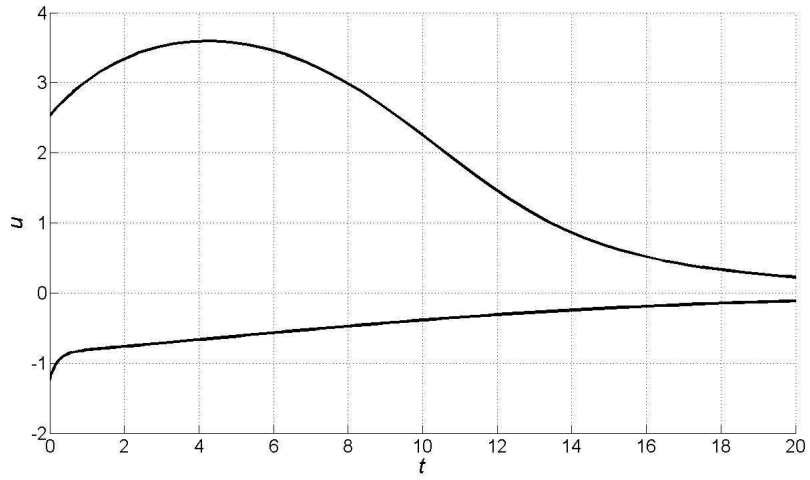

Lower and upper bounds for u.

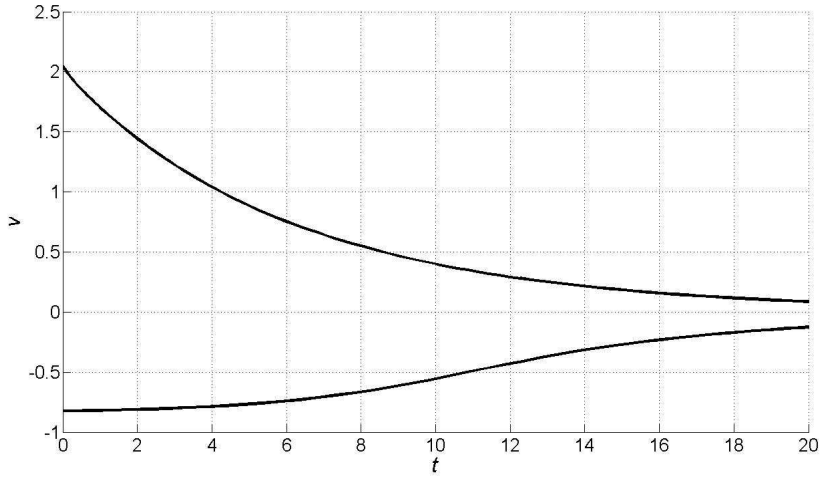

Lower and upper bounds for v.

the developments in computer arithmetic and interval analysis leading to computer programs providing validated enclosures for the solutions of systems of ODEs. It is quite clear that empirical search for a suitable set M in a high dimensional system requires a significant computational effort. However, now "the chips are cheap" and it seems natural to shift the burden of the technical proofs to computers.

References

[1] G. Bastin and D. Dochain, On-line Estimation and Adaptive Control of Bioreactors, Elsevier, Amsterdam, 1990.

[2] J. C. Kamgang and G. Sallet, Computation of threshold conditions for epidemiological models and global stability of the disease free equilibrium (DFE), *Math. Biosc.* **213** (2008), 1–12.

[3] R. J. Lohner, Computations of guaranteed enclosures for the solutions of ordinary initial and boundary value problems, In: J. Cash and I. Gladwell (eds), Computational Ordinary Differential Equations, Clarendon Press, Oxford, 1992, 425-436.

[4] Ned S. Nedialkov, Ken R. Jackson, and George F. Corliss, Validated Solutions of Initial Value Problems for Ordinary Differential Equations, Appl. Math. & Comp., 105 (1) (1999) pp. 21-68.

[5] H L Smith, Monotone Dynamical Systems, AMS, 1995.

[6] Y Lin, M Stadtherr, Validated solution of ODEs with parametric uncertainties, Proceedings of 16th European Symposium on Computer Aided Process Engineering and 9th International Symposium on Process Systems Engineering, and 9th International Symposium on Process Systems Engineering, Elsevier, 2006.

[7] A. M. Stuart and A. R. Humphries, *Dynamical systems and numerical analysis,* Cambridge University Press, New York, 1998.

Pricing Financial Derivatives on GPU

E. Atanassov, D. Dimitrov

Introduction

The financial option is a contract that gives the owner the right, but not the obligation, to buy or sell an asset at a set price on or before a given date. The problem of estimation the price of option(s) is one of the most important area in Financial Mathematics [24]. Pricing options, that are path dependent on the evolution of the prices requires precise simulation of stochastic processes that model the price of the underlying asset.

In 1972, Black and Scholes [7] published a paper, where they describe a model for pricing European options, assuming that the price is Brownian motion. This is the first standardized method for option pricing:

$$\frac{dS}{S} = rdt + \sigma dW_s,$$

where r is interest rate, σ is the volatility and dW_s is Brownian motion. There are several assumptions in the model but one of the most important is that the volatility is constant. Although this equation is one elegant mathematical representation of price evolution process, the assumption for constant volatility does not fit the real data from the markets.

Heston model

One more complex model for precise modelling was proposed by Steven Heston in 1993 [15]. Heston proposes model where the volatility is time dependent variable and follows a random process. Heston model contains two stochastic differential equations one for the price process and one for price variance:

$$dS_t = rS_t dt + \sqrt{\nu_t} S_t dW_s$$
$$d\nu_t = \kappa(\theta - \nu_t)dt + \sigma_\nu \sqrt{\nu_t} dW_\nu,$$

where S_t and ν_t are the price and its variance, W_t^s and W_t^v are correlated Brownian motions (with correlation ρ), ν_t is CIR [9] process and has long variance θ, κ is the rate at which the variance reverts to θ and σ_ν is the volatility of volatility.

There are various methods for simulation of the model but one of the most popular algorithms are based on the Monte Carlo approach [13]. In this work we considered several proposed numerical schemes for adequate simulation of the model and they can be categorized in two groups: schemes with bias and exact schemes. Euler-Maryuama, Lord Modification [19], Milstein [18], Kahl-Jackel [17] are schemes that are representatives of the biased schemes where there are two errors - from discretization of the continuous time process and the statistical Monte Carlo error. Andersen [3] scheme is representative of the exact schemes that uses the properties of the CIR process and the variance is sampled using it's exact distribution, so there is only

statistical Monte Carlo error.
Numerical Methods:
Euler-Maryama: The simplest method for solving SDEs.

$$S_t = S_s(1 + r\Delta t + \sqrt{V_t}Z_s\sqrt{\Delta t})$$
$$V_t = V_s + k\Delta t(\theta - V_s) + \sigma\sqrt{V_s}Z_v\sqrt{\Delta t}$$

Δt - time step;
$cor(Z_v, Z_s) = \rho$ - correlated random variables with normal distribution.
Lord Modification (Full Truncation): A scheme proposed by Roger Lord that aims to have better handling with the problems in Euler-Maryama.

$$log(S_t) = log(S_s) + [r - \frac{1}{2}f_4(V_s)]\Delta t + \sqrt{f_5(V_s)}Z_s\sqrt{\Delta t}$$
$$V_t = f_1(V_s) + k\Delta t(\theta - f_2(V_s)) + \sigma\sqrt{f_3(V_s)}Z_v\sqrt{\Delta t},$$

$f_i(x) = x$ for $x \geq 0$. Where for $f_i(x)$ are chosen : identity $f(x) = x$, absorption $f(x) = x^+$ or absolute value $f(x) = |x|$.
Milstein: A scheme with improved order of convergence.

$$S_t = S_s(1 + r\Delta t + \sqrt{V_t}Z_s\sqrt{\Delta t})$$
$$V_t = V_s + \kappa(\theta - V_s)\Delta t + \sigma\sqrt{V_s}Z_v + \frac{1}{4}\sigma^2(Z^2 - 1)\Delta t$$

Kahl-Jackel: Discretization for the Heston model using Milstein scheme for the variance process and alternative scheme for the price process.

$$\log(S_t) = \log(S_s) + (r - \frac{V_s + V_t}{4})\Delta t + \rho\sqrt{V_s}Z_v\sqrt{\Delta t}$$
$$+\frac{1}{2}(\sqrt{V_s} + \sqrt{V_t})(Z_s + \rho Z_v)\sqrt{\Delta t} + \frac{\rho\sigma\Delta t}{2}(Z_v^2 - 1)$$
$$V_t = \frac{V_s + \kappa\theta\Delta t + \sigma\sqrt{V_s}Z_v\sqrt{\Delta t} + \frac{1}{4}\sigma^2(Z^2 - 1)\Delta t}{1 + \kappa\Delta t}$$

the variance process always have positive values if $2\kappa\theta > \sigma$.
Andersen:
Andersen uses the system of SDEs in integral form and some of the properties of the variance process:

$$\begin{aligned} S(t) &= S(u)exp[r(t-u) - \frac{1}{2}\int_u^t V(s)ds + \rho\int_u^t \sqrt{V(s)}dW_v \\ &\quad +\sqrt{1-\rho^2}\int_u^t \sqrt{V(s)}dW_s] \\ V(t) &= V(u) + \kappa\theta(t-u) - k\int_u^t V(s)ds + \sigma_v\int_u^t \sqrt{V(s)}dW_v. \end{aligned}$$

Andersen Scheme: The algorithm is based on sampling the variance process using distributions which local moments match the original.

1. Generate a sample of V_t using distributions which local moments are the same as the original distribution;

2. Approximate the variance integral using drift interpolation:

$$\int_u^t V(u)du|V(s),V(t) \approx \Delta t[\gamma_1 V(s) + \gamma_2 V(t)]$$

   if $\gamma_1 = 1$ and $\gamma_2 = 0$ we have Euler type scheme

   if $\gamma_1 = \gamma_2 = 0.5$ we have predictor-corrector scheme;

3. Calculate10000) the price using the following equation:

$$\begin{aligned}\log S(t) &= \log S(s) + r\Delta t + K_0 + K_1 V(s) + K_2 V(t) + \\ &\quad \sqrt{K_3 V(s) + K_4 V(t)} Z_s,\end{aligned}$$

   where Z_s is random variable with normal distribution and K_i:

$$\begin{aligned}K_0 &= -\frac{\rho k\theta}{\sigma}\Delta t \\ K_1 &= \gamma_1 \Delta t \left(\frac{k\rho}{\sigma} - \frac{1}{2}\right) - \frac{\rho}{\sigma} \\ K_2 &= \gamma_2 \Delta t \left(\frac{k\rho}{\sigma} - \frac{1}{2}\right) + \frac{\rho}{\sigma} \\ K_3 &= \gamma_1 \Delta t (1-\rho^2) \\ K_4 &= \gamma_2 \Delta t (1-\rho^2).\end{aligned}$$

Numerical Results

Numerical schemes were implemented to work on GPU using NVidia CUDA framework [10]. This architecture allows the GPU processor to be turned into highly parallel multi-core system capable of executing hundreds of parallel threads. The CUDA topology is based on grouping the threads in blocks and run them parallel, in our case the most efficient scenario was to use 256 blocks with 256 threads that allowed us to execute 65536 threads at one call of the gpu function (the kernel function). In this scenario every thread is simulating one path from the Monte Carlo algorithm and in the quasi-random case use the coordinates of one point from 2M-dimensional quasi-sequence as source of random numbers(M is the number of time intervals). All of the schemes are implemented using the standard CURAND - pseudo-random number generator and generators for Sobol'(with Owen scrambling[21])[22][5][14][20] and modified Halton (proposed by Atanassov) sequences [4][6][16]. For test case it was chosen a example of European option[8] with period 1 year and the following parameters:

$$r = 3.19\%, \kappa = 6.21, \theta = 0.019, \sigma_v = 0.61, \rho = -0.7, S_0 = 100, V_0 = 0.010201.$$

In Table 1 is shown the error using CURAND generator and different schemes using the example European option parameters.

Intervals	EM	Lord	Milstein	Kahl-Jackle	Andersen
250	0.8640	0.8679	0.0541	0.0477	0.0382
500	0.5740	0.5582	0.0313	0.0244	0.0245
750	0.4392	0.4165	0.0155	0.0132	0.0109
1000	0.3440	0.3658	0.0104	0.0113	0.0074

Table 1: Results for the absolute error using CURAND pseudo-random number generator

EM	Lord	Milstein	Kahl-Jackel	Andersen
60.02	62.75	66.08	53.79	25.38

Table 2: Average time acceleration in times for CPU vs GPU

In Table 2 is shown the average acceleration in times for the schemes using the standard pseudo-random generators on CPU and GPU.
In Table 3 is shown the absolute error for small number of time steps using the Andersen scheme with different random number generators.

Paths	CURAND	Sobol	Halton
256	0.599679	0.228454	0.129998
512	0.238047	0.181489	0.084110
1024	0.131617	0.085438	0.041280
2048	0.088686	0.012982	0.016976

12 time steps

Paths	CURAND	Sobol	Halton
256	0.548801	0.233375	0.0999528
512	0.257233	0.161241	0.0731495
1024	0.173834	0.110316	0.0346040
2048	0.045946	0.024229	0.0112510

52 time steps

Table 3: Absolute error using Andersen scheme for small number of steps

Conclusion
As it is shown in the numerical results two important results are achieved. The first one is about up to 66 times speeding up of the schemes using NVidia GTX 295 with CUDA as a high-performance environment for simulations. The second one is that for small number of time steps using modified Halton quasi-random number sequence shows better accuracy than the CURAND and scrambled Sobol.
Acknowledgements This work was partially supported by the National Science Fund of Bulgaria under Contracts DO02-146/2008.

References

[1] Abate J. W. Whitt, , *"The Fourier-series method for inverting transforms of probability distributions."*, Queueing Systems 10(1), pp. 5-88, **1992**.

[2] Abramowitz M. I. A. Stegun, *"Handbook of Mathematical Functions with Formulas, Graphs, and Mathematical Tables"*, National Bureau of Standards , Washington DC., **1972**.

[3] Andersen Leif B. G. , *"Efficient simulation of the heston stochastic volatility model"*, **SSRN: http://ssrn.com/abstract=946405 , 2007**.

[4] Atanassov E., *" On the discrepancy of the Halton sequences"*, Mathematica Balkanica, Vol. 18,pp 15-31, **2004**.

[5] Atanassov E. A. Karaivanova S. Ivanovska, *"GPU-based generation of scrambled Sobol sequence"*, International Workshop on Mathematical Modelling and Scientific Computation,**2009**.

[6] Atanassov E. M. Durchova, *"Generating and Testing the Modified Halton Sequences"* , Numerical Methods and Applications, Springer-Verlag, LNCS 2542, pp 91-98, **2003**.

[7] Black F. M. Scholes, *"The pricing of options and corporate liabilities"*, Journal of Political Economy, 81(3), **1973**.

[8] Broadie M. O. Kaya, *"Exact simulation of stochastic volatility and other affine jump diffusion models."*, Operation Research, 54(2), **2006**.

[9] Cox J. J. Ingersoll A. Ross, *"A Theory of the Term Structure of Interest Rates"*, Econometrica 53, **1985**.

[10] CUDA , *"http://developer.nvidia.com/category/zone/cuda-zone"*

[11] Duffie D. P. Glynn, *"Efficient Monte Carlo estimation of security prices"*, Ann. Appl. Probab., 4(5) **1995**.

[12] Feller W., *"An Introduction to Probability Theory and Its Applications"*, Vol 2, 2nd edition John Wiley and Sons, New York, **1971**.

[13] Glasserman P., *"Monte Carlo Methods in Financial Engineering"*, Springer-Verlag, New York, **2003**.

[14] Gurov T. P. Whitlock, *"Investigation of the Sensitivity of the Monte Carlo Solution for the Barker-Ferry Equation with Sequential and Parallel Pseudo-Random Number Generators"*, Lecture Notes in Comp. Sci., Vol. 3039, Springer-Verlag, pp. 507-514, **2004**.

[15] Heston S., *"A closed-form solution of options with stochastic volatility with applications to bond and currency options"*, Rev. Financial Stud. 6(2), pp. 327-343, **1993**.

[16] Halton J., *"On the efficiency of certain quasi-random sequences of points in evaluating multi-dimensional integrals"*, Numer. math., 2 pp. 84-90, **1960**.

[17] KAHL C. P. JACKEL, *"Fast strong approximation Monte-Carlo schemes for SV models"*, Quantitative Finance, Taylor and Francis Journals, vol. 6(6), pages 513-536, **2005**.

[18] KLOEDEN P. E. PLATEN, *"Numerical Solution of Stochastic Differential Equations"*, Springer-Verlag, New York, **1992**.

[19] LORD R. KOEKKOEK AND D. VAN DIJK, *"A compariosn of biased simulation schemes for stochastic volatility models"*, Journal of Quantitative Finance, **2008**.

[20] NIEDERREITER H., *"Random Number Generation and Quasi-Monte Carlo Methods"*, SIAM Conf.Ser.Appl.Math.Vol.63 **1992**.

[21] OWEN A., *"Randomly permuted (t; m; s)-nets and (t; s)-sequences"*, MC and QMC Methods in Scientific Computing, pp 299-317, **1995**.

[22] SOBOL' I., *"The distribution of points in a cube and the accurate evaluation of integrals"*, Zh. Vychisl. Mat. i Mat. Phys., (7) 784-802, **1967**

[23] PASKOV S. J. TRAUB, *"Faster Valuation of Financial Derivatives"*, Journal of portfolio management, **1995**.

[24] WILMOTT P., *"Derivatives: The Theory and Practise of Financial Engineering"*, **1998**.

Cloud and Grid Computing: Security Aspects

E. Atanassov, T. Gurov, A. Karaivanova

1 Introduction

The Grid is a computational infrastructure which ensures transparent access to geographically and institutionally distributed computational resources and data. The Grid has been studied extensively during last two decades, here we refer to some works of Foster and Kesselman, and also to description of the largest grid (the EGEE grid) [1, 2, 3, 4]. Ian Foster and coauthors gave a three point checklist [4] to help determine what the Grid is, and what is not:

1. The Grid coordinates resources that are not subject to centralized control,
2. The Grid uses standard, open, general-purpose protocols and interfaces, and
3. The Grid delivers non-trivial qualities of service.

Recently, "Cloud" became very popular buzzword. Although Cloud Computing sounds like a new technology, it has intricate connection to Grid Computing paradigm. There is a little consensus on how to define the Cloud and here we accept the Foster definition in [5]: "*A large-scale distributed computing paradigm that is driven by economies of scale, in which a pool of abstracted, virtualized, dynamically-scalable, managed computing power, storage, platforms, and services are delivered on demand to external customers over the Internet.*"
In the same paper, [5], Foster et all compare Grid and Cloud and conclude that only point 3 from above checklist holds true for Cloud computing, but neither point 1 nor point 2 are valid for Clouds.
The common characteristics of Grid and Cloud are

- Utility computing
- Aggregation of heterogeneous resources
- Access transparency for the end user
- Re-configurability
- Service negotiation based on Service Level Agreements
- Capacity provisioned on demand
- Continuous availability
- Single sign on

This comparison of Cloud and Grid helps us understand the security issues which arise when using both of them as part of a scientific application.

2 Security aspects

We summarize below the types of authentication, authorization and accounting mechanisms that are used in Grids and Clouds.

2.1 Security management in Grids

The cornerstone of the security management in Grid is the notion of the so-called Virtual Organization (VO). Users are organized in Virtual Organisations, which share resources. Many institutions may provide the resources of the virtual organization and these resources become available to all members of the organization. It is important to note that only the biggest virtual organizations, comprising of thousands of scientists, define groups inside the virtual organization and enforce the division between members of these groups and the respective job priorities. It is important to note that in most practical cases a user of the VO has access to all the data files of the VO and can not only retrieve data, but also delete data, even if the file has been created by another user.

- Authentication is ensured mainly by X509 certificates. Other authentication mechanisms are also used. In some cases it is possible to use an identity provider to obtain an X509 certificate on-the-fly, thus allowing more decentralized management of the authentication process.
- Users sign proxies with their X509 certificate and use them to connect with services using https protocol or typical Grid protocols like GridFTP or SRM for data management or GRAM for job management.
- The Grid services may have finer-grained authorization mechanism, using groups and roles within the VO. This possibility is difficult to implement in practice because of the decentralized nature of deployment of Grid resources.

In Bulgaria IICT-BAS is responsible to issue certificates for BG scientists/students, operating the BG.ACAD Certification Authority - see http://ca.acad.bg. The same Grid certificates are used for other e-Science projects, e.g., PRACE1IP, PRACE2IP, HP-SEE. In some cases they are used to authenticate email or web servers.

2.2 Security management in Clouds

Access to Cloud infrastructure resources can be achieved with web, GUI or command line interfaces. Popular languages for development are *java, python, ruby*. Both Linux and Windows operating systems are supported as guest OS, as well as others. We should point out that the user effectively obtains administrator (root) access to the virtual machines launched over the cloud, which is not the case of Grid usage, where only local Unix user access can be obtained. Here we review the security models of the most popular Cloud service providers. Amazon cloud services [6] include:

- EC2 - Amazon Elastic Compute Cloud is a web service that provides resizable compute capacity in the cloud.
- S3 - Amazon Simple Storage Service provides a simple web services interface that can be used to store and retrieve data.

Access to Amazon cloud services is secured through use of:

- Access keys - used to make secure (signed) REST or Query protocol requests to any AWS service API
- X.509 certificates - make secure SOAP protocol requests to AWS service APIs.
- Key pairs - can be used to launch and then securely access your EC2 instances.

Many providers mimic the Amazon cloud model, sometimes using open source software. Some providers of cloud services follow a different model, where the user does not obtain administrative access to particular machine, but instead a whole scalable application environment is provided to them. This is the case of Google, for example. We should point out that the shared use of Cloud is not straightforward because of the lack of notion similar to the Virtual Organization. The Cloud paradigm allows for a layered approach, where for example one provider may provide added-value services to the customers using the infrastructure of another provider. In such cases the security model of the top-level provider may differ from those of the providers of the lower layers.

2.3 Interaction between Grid and Cloud

Due to the differences in the security mechanisms of Grids and Clouds it interesting to consider the most practical use cases for combining the use of Grid and Cloud resources for scientific computations. First of all, an infrastructure provider, e.g., a university, can use (lease) Cloud resources to provide Grid services for the users. It is technically feasible to provide the worker nodes for a Grid cluster using cloud resources. A small pool of Cloud-based Worker Nodes can provide QoS for jobs that are sensitive to waiting times Unfortunately, the requirement in some cases for proper forward and *backward* DNS resolution makes it a bit difficult to provide some service nodes for such cluster from Cloud resources. In any case, a user or VO can use the cloud to deploy service nodes, e.g., web servers, databases, especially if they are specific to a particular application that is not used by all the VO. Some of the Grid services may be efficiently put on the Cloud to benefit from the "elasticity" of Cloud service provisioning. For example, the so-called BDII is a service which would benefit from authomatic load-balancing.

3 Security threats and attack vectors and their mitigation

One of the main security threats on the Grid stem from the fact that users proxy certificates are sent to remote nodes, where they can be stolen, e.g., by a malicious user of the same cluster. Typically such a proxy is valid for 12 hours and provides access to most of the resources of the VO, as outlined above. On the worker nodes one usually employes a so-called limited proxy, which allows access to storage resources, but not the ability to launch jobs, thus limiting the impact of a potential breach. An unlimited proxy can be used to launch new jobs, but can be found on smaller number of machines with tighter security. Unfortunately, some virtual organizations have been granted the ability to create voms proxies with duration much larger than 24 hours, which means that the potential impact of a stolen proxy certificate will extend to several days. They are security mechanisms in place to react to such violations, for example using ARGUS nodes to ban malicious users or by revoking the user certificate, but they will not be started unless the problem has been discovered and reported. In the meantime the malicious user can attempt escalation of privileges on the nodes where he or she obtained access or tampter with the data or metadata of the virtual organization.
Now considering the case when a Grid application uses Cloud services, one should take into account that if cloud certificates and/or access keys are sent to remote Grid nodes, there is a danger that if they are stolen somebody will be able to do everything that the owner can do on the Cloud. Obviously the provider of an EC2-type service runs the risk of malicious users launching nodes which can be used to serve illicit content, control botnets or similar. Presumably the Cloud infrastructure providers ensure tight control and isolation between user's virtualized networks. However, investigation of security incidents is difficult due to the use of virtual machines.
Thus it is important that Grid jobs should not have access to the full cloud credentials of the users. This means that an extra level of redirection should be introduced to limit access, for example only to the necessary part of storage. This can be implemented as a broker service, launched on the cloud and answering to requests from the Grid jobs.
Unrelated applications should also be separated in terms of credentials and infrastructure used. Users must perform careful evaluation of the dangers of contagion should one part of the nodes participating in a given computation become compromised.

4 Conclusions and directions for future work

We can conclude from our investigation that the possibility of combining services or infrastructure resources from the Cloud with Grid resources and organization provides additional flexibility and substantial benefit to the demanding users and applications. The security issues that arise should be addressed firstly by infrastructure operators and Grid and Cloud middleware developers to provide for the necessary isolation

and control. We believe that the introduction of "Grid-Cloud brokerage" services that can translate between Grid and Cloud credentials and ensure limitations on the kinds of requests that can be issued between the Grid and Cloud parts of the scientific application thus effecitively reducing the exposure of the users to the inherent security risks and providing certain guarantees about the worst possible damage that may happen in case of security breach.

Acknowledgements. This work was partially supported by the National Science Fund of Bulgaria under Contracts DO02-146/2008 and DVCP02/1 CoE Super CA++.

References

[1] I. Bird, B. Jones, K. Kee, The organization and management of grid infrastructures, *IEEE Computer Society, Computer*, 2009, pp. 36-46, ISSN 0018-9162/09.

[2] J. Foster and C. Kesselmann: *The Grid: Blueprint for a New Computing Infrastructure*. Morgan Kaufmann, 1999.

[3] J. Foster, C. Kesselmann and S. Tuecke: The Anatomy of the Grid. *International Journal of Supercomputer Applications*, **15(3)**, 2001.

[4] I. Foster, What is the grid? A three Point Checklist, July 2002.

[5] Ian Foster, Yong Zhao, Ioan Raicu, Shiyong Lu, Cloud Computing and Grid Computing 360-Degree Compared, IEEE

[6] http://aws.amazon.com - Amazon Web Services

Singular Solutions of Cross-coupled EPDiff Equations: Waltzing Peakons and Compacton Pairs

Colin J. Cotter, Darryl D. Holm, Rossen I. Ivanov and James R. Percival

1. EPDiff equations. Let us define an one-parametric group of diffeomorphisms of $\mathbb{R}^n$ with elements that satisfy

$$\frac{\partial \mathbf{X}(\mathbf{x},t)}{\partial t} = \mathbf{u}(\mathbf{X}(\mathbf{x},t),t), \qquad \mathbf{X}(\mathbf{x},0) = \mathbf{x}, \tag{1}$$

or $\dot{X} = u \circ X$ with $\mathbf{x} \in \mathbb{R}^n$, $t \in \mathbb{R}$, $X \in \mathrm{Diff}(\mathbb{R}^n)$. Let us consider motion in $\mathbb{R}^n$ with a velocity field $u = \dot{X} \circ X^{-1}$; $\mathbf{u}(\mathbf{x},t)$: $\mathbb{R}^n \times \mathbb{R} \to \mathbb{R}^n$ and define a momentum variable $\mathbf{m} = Q\mathbf{u}$ for some (inertia) operator Q (for example the Helmholtz operator $Q = 1 - \partial_i\partial_i = 1 - \Delta$, where $\partial_i = \frac{\partial}{\partial x^i}$). Let us further define a Lagrangian

$$L[\mathbf{u}] = \frac{1}{2}\int \mathbf{m}\cdot\mathbf{u}\ \mathrm{d}^n\mathbf{x}. \tag{2}$$

Since the velocity $\mathbf{u} = u^i\partial_i \in \mathrm{Vect}(\mathbb{R}^n)$ is a vector field, $\mathbf{m} = m_i \mathrm{d}x^i \otimes \mathrm{d}^n\mathbf{x}$ is a $n+1$-form density, we have a natural right-invariant bilinear form

$$\langle \mathbf{m}, \mathbf{u}\rangle = \int \mathbf{m}\cdot\mathbf{u}\ \mathrm{d}^n\mathbf{x}. \tag{3}$$

The Euler-Poincaré equation for the geodesic motion in this case is [6, 5]

$$\frac{d}{dt}\frac{\delta L}{\delta \mathbf{u}} + \mathrm{ad}^*_{\mathbf{u}}\frac{\delta L}{\delta \mathbf{u}} = 0, \qquad \mathbf{u} = G * \mathbf{m}, \tag{4}$$

where G is the Green function for the operator Q. The corresponding Hamiltonian is

$$H[\mathbf{m}] = \langle \mathbf{m}, \mathbf{u}\rangle - L[\mathbf{u}] = \frac{1}{2}\int \mathbf{m}\cdot G * \mathbf{m}\ \mathrm{d}^n\mathbf{x}, \tag{5}$$

and the equation in Hamiltonian form ($\mathbf{u} = \frac{\delta H}{\delta \mathbf{m}}$) is

$$\frac{\partial \mathbf{m}}{\partial t} = -\mathrm{ad}^*_{\frac{\delta H}{\delta \mathbf{m}}}\mathbf{m}. \tag{6}$$

The left Lie algebra of vector fields is $[\mathbf{u},\mathbf{v}] = -(u^k(\partial_k v^p) - v^k(\partial_k u^p))\partial_p$. For an arbitrary vector field $\mathbf{v}$ one can write [6]

$$\begin{aligned}
\langle \mathrm{ad}^*_{\mathbf{u}}\mathbf{m}, \mathbf{v}\rangle &= \langle \mathbf{m}, \mathrm{ad}_{\mathbf{u}}\mathbf{v}\rangle = \langle \mathbf{m}, [\mathbf{u},\mathbf{v}]\rangle \\
&= -\langle m_l \mathrm{d}x^l \otimes \mathrm{d}^n\mathbf{x}, (u^k(\partial_k v^p) - v^k(\partial_k u^p))\partial_p\rangle \\
&= -\int m_p(u^k(\partial_k v^p) - v^k(\partial_k u^p))\mathrm{d}^n\mathbf{x} \\
&= \int v^p(u^k(\partial_k m_p) + m_p(\partial_k u^k) + m_k(\partial_p u^k))\mathrm{d}^n\mathbf{x} \\
&= \langle((\mathbf{u}\cdot\nabla)m_p + \mathbf{m}\cdot\partial_p\mathbf{u} + m_p\mathrm{div}\mathbf{u})\mathrm{d}x^p \otimes \mathrm{d}^n\mathbf{x}, \mathbf{v}\rangle,
\end{aligned}$$

and therefore (6) has the form, known as *EPDiff equation*:

$$\frac{\partial m_p}{\partial t} + (\mathbf{u}\cdot\nabla)m_p + \mathbf{m}\cdot\partial_p\mathbf{u} + m_p\mathrm{div}\mathbf{u} = 0. \tag{7}$$

Due to the invariance of the Hamiltonian under the right action of the group $\mathrm{Diff}(\mathbb{R}^n)$ there is a momentum conservation law according to the Noether's Theorem (which can be verified directly with (1)) :

$$m_i(\mathbf{X}(\mathbf{x},t),t)\partial_j X^i(\mathbf{x},t)\det\Big(\frac{\partial\mathbf{X}}{\partial\mathbf{x}}\Big) = m_j(x,0), \tag{8}$$

where $\Big(\frac{\partial\mathbf{X}}{\partial\mathbf{x}}\Big)_{ij} = \frac{\partial X^i}{\partial x^j}$ is the Jacobian matrix.
The Lie-Poisson bracket is

$$\begin{aligned}\{A,B\}(\mathbf{m}) &= \langle\mathbf{m},[\frac{\delta A}{\delta\mathbf{m}},\frac{\delta B}{\delta\mathbf{m}}]\rangle \\ &= -\int m_i\Big(\frac{\delta A}{\delta m_k}\partial_k\frac{\delta B}{\delta m_i} - \frac{\delta B}{\delta m_k}\partial_k\frac{\delta A}{\delta m_i}\Big)\mathrm{d}^n\mathbf{x}.\end{aligned} \tag{9}$$

When $n=1$ the algebra (9), associated with the bracket is the algebra of vector fields on the circle. This algebra admits a generalization with a central extension, which is the famous Virasoro algebra [8, 6]. In two dimensions, $n=2$, the algebra, associated with the bracket is the algebra of vector fields on a torus [1].
2. Singular solutions. The Camassa-Holm (CH) equation [2] can be considered as a member of the family of EPDiff equations in $n=1$ dimension [5]:

$$m_t + 2u_x m + u m_x = 0, \qquad m = u - u_{xx}. \tag{10}$$

The CH equation possesses the so-called N-peakon solution in the form

$$u(x,t) = \frac{1}{2}\sum_{i=1}^{N} p_i(t)\exp(-|x-x_i(t)|), \tag{11}$$

provided p_i and x_i evolve according to the following system of ordinary differential equations:

$$\dot{x}_i = \frac{\partial H}{\partial p_i}, \qquad \dot{p}_i = -\frac{\partial H}{\partial x_i}, \tag{12}$$

where the Hamiltonian is $H = \frac{1}{4}\sum_{i,j=1}^{N} p_i p_j\exp(-|x_i - x_j|)$. The momentum is singular,

$$m(x,t) = \sum_{i=1}^{N} p_i(t)\delta(x - x_i(t)), \tag{13}$$

it defines the so-called singular momentum map, [5]. CH is an integrable equation and is very well studied - see e.g. the review article [4].

The singular momentum map (13) suggests the following measure-valued singular momentum solution Ansatz for the $n-$dimensional solutions of the EPDiff equation:

$$\mathbf{m}(\mathbf{x},t) = \sum_{a=1}^{N} \int \mathbf{P}^a(s,t)\,\delta\big(\,\mathbf{x} - \mathbf{Q}^a(s,t)\,\big)\mathrm{d}s.$$

These singular momentum solutions, called "diffeons", [7] are vector density functions supported in $\mathbb{R}^n$ on a set of N surfaces (or curves) of codimension $(n-k)$ for $s \in \mathbb{R}^k$ with $k < n$. They may, for example, be supported on sets of points (vector peakons, $k = 0$), one-dimensional filaments (strings, $k = 1$), or two-dimensional surfaces (sheets, $k = 2$) in three dimensions.

3. Cross coupled CH equations and waltzing peakons. The Lagrangian for cross coupled CH (CCCH) is [3]

$$l(u,v) = \int_{\mathbb{R}} (uv + u_x v_x)\ \mathrm{d}x.$$

The corresponding two-component EP equations in 1D on $\mathbb{R}$ are

$$\partial_t m = -\operatorname{ad}^*_{\delta h/\delta m} m = -(vm)_x - m v_x \quad \text{with} \quad v := \frac{\delta h}{\delta m} = K * n,$$

$$\partial_t n = -\operatorname{ad}^*_{\delta h/\delta n} n = -(un)_x - n u_x \quad \text{with} \quad u := \frac{\delta h}{\delta n} = K * m.$$

with $K(x,y) = \frac{1}{2}e^{-|x-y|}$ being the Green function of the Helmholtz operator. The CCCH Hamiltonian is

$$h(n,m) = \int_{\mathbb{R}} n\, K * m\ \mathrm{d}x = \int_{\mathbb{R}} m\, K * n\ \mathrm{d}x.$$

This Hamiltonian system has **two-**component singular momentum maps

$$m(x,t) = \sum_{a=1}^{M} m_a(t)\,\delta(x - q_a(t)), \qquad n(x,t) = \sum_{b=1}^{N} n_b(t)\,\delta(x - r_b(t)).$$

The total momentum of CCCH is conserved, namely

$$\partial_t\,(u+v) + \partial_x\big(uv + K * (2uv + u_x v_x)\big) = 0.$$

4. Peakon solutions of the cross-flow equations. The CCCH equations are deformations of CH that support two different types of peakons, with velocities

$$u(x,t) = \tfrac{1}{2}\sum_{a=1}^{M} m_a(t)\,e^{-|x-q_a(t)|}\,, \qquad v(x,t) = \tfrac{1}{2}\sum_{b=1}^{N} n_b(t)\,e^{-|x-r_b(t)|}\,, \tag{14}$$

and momenta,

$$m(x,t) = \sum_{a=1}^{M} m_a(t)\,\delta(x - q_a(t))\,, \qquad n(x,t) = \sum_{b=1}^{N} n_b(t)\,\delta(x - r_b(t))\,. \tag{15}$$

The $2M+2N$ variables (q_a, m_a), $a = 1, \ldots, M$, and (r_b, n_b), $b = 1, \ldots, N$, are governed by the Hamilton's canonical equations for the Hamiltonian function,

$$H = \tfrac{1}{2} \sum_{a,b=1}^{M,N} m_a(t) n_b(t) e^{-|q_a(t) - r_b(t)|}\,, \tag{16}$$

namely,

$$\dot{q}_a(t) \;=\; \frac{\partial H}{\partial m_a} = \tfrac{1}{2} \sum_{b=1}^{N} n_b(t) e^{-|q_a(t) - r_b(t)|} = v(q_a(t), t)\,, \tag{17}$$

$$\dot{r}_b(t) \;=\; \frac{\partial H}{\partial n_b} = \tfrac{1}{2} \sum_{a=1}^{M} m_a(t) e^{-|q_a(t) - r_b(t)|} = u(r_b(t), t)\,, \tag{18}$$

for the positions of the peakons, and

$$\dot{m}_a(t) \;=\; -\frac{\partial H}{\partial q_a} = \tfrac{1}{2} m_a \sum_{b=1}^{N} n_b \operatorname{sgn}(q_a - r_b) e^{-|q_a(t) - r_b(t)|} = -\, m_a \left.\frac{\partial v}{\partial x}\right|_{x=q_a}, \tag{19}$$

$$\dot{n}_b(t) \;=\; -\frac{\partial H}{\partial r_b} = -\tfrac{1}{2} n_b \sum_{a=1}^{M} m_a \operatorname{sgn}(q_a - r_b) e^{-|q_a(t) - r_b(t)|} = -\, n_b \left.\frac{\partial u}{\partial x}\right|_{x=r_b} \tag{20}$$

for their canonical momenta. Conserved quantities include the energy H and the total momentum $\sum_a (m_a + n_a)$.

5. The coupled peakon pair. The simplest possible case is $M = N = 1$. Introducing the new variables $X = \frac{q+r}{2}$, $Y = q - r$, respectively the mean position of the peaks and their separation distance. The evolution equations in terms of the new variables are

$$\dot{X} = \frac{(m+n)}{4} e^{-|Y|}, \qquad \dot{Y} = \frac{n-m}{2} e^{-|Y|}.$$

Thus we can define the behavior of the exponential function of the absolute separation of the peaks,

$$\frac{\mathrm{d}}{\mathrm{d}t} e^{|Y|} = \operatorname{sgn}(Y) \frac{n-m}{2}, \tag{21}$$

From (19) - (20)

$$\dot{m} = -\dot{n} = \operatorname{sgn}(Y) \frac{mn}{2} e^{-|Y|} = \operatorname{sgn}(Y) E,$$

where $E = H|_{t=0}$ is the (constant) value of the Hamiltonian, that is to say the total energy of the coupled pair. Differentiating (21) again with respect to time gives

$$\frac{\mathrm{d}^2}{\mathrm{d}t^2} \left(e^{|Y|} \right) = -\operatorname{sgn}^2(Y)\, E + 2\delta(Y)\, (n-m)^2\,.$$

On integrating for a particular signature of $Y|_{t=0} = Y_0 \neq 0$,

$$e^{|Y|} = -\frac{1}{2} m_0 n_0 e^{-|Y_0|} t^2 + \frac{1}{2} \operatorname{sgn}(Y_0)\, (n_0 - m_0)\, t + e^{|Y_0|},$$

where

$$m_0 = m|_{t=0}\,, \quad n_0 = n|_{t=0} \quad Y_0 = Y|_{t=0}\,.$$

If m_0 and n_0 have the same signature then eventually we will have $|Y| = 0$, regardless of the value of $|Y_0|$. Thus, when m_0 and n_0 share the same signature the half period of their "waltzing" motion can be found by setting $Y_0 = 0$ and looking for when $e^{|Y|}$ attains unity, namely $t = 2\frac{n_0 - m_0}{n_0 m_0}$. It will be noted that at this time

$$m|_{t=2\frac{m_0-n_0}{m_0 n_0}} = m_0 + m_0 n_0 \left(\frac{m_0 - n_0}{m_0 n_0}\right) = n_0,$$

and similarly

$$n|_{t=2\frac{m_0-n_0}{m_0 n_0}} = m_0,$$

so that the two types of peakons do indeed exchange momentum amplitudes over a half cycle, see Fig. 1. The explicit solutions as well as other examples with waltzing peakons and compactons are given in [3].

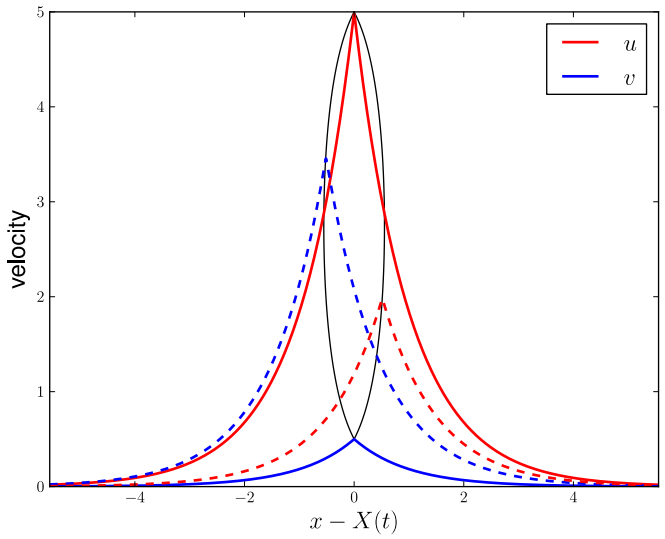

Figure 1: Plot showing velocity fields of a peakon-peakon pair with $m_0 = 5$, $n_0 = 0.5$, $l_0 = 0$ (solid lines). The dotted path indicates the subsequent path of the two peaks in the frame travelling at the particles mean velocity $\dot{X} = \frac{\dot{q}+\dot{r}}{2}$. For these initial conditions the total period for one orbit of the cycle is $T = 3.6$. Also shown is the form of the two peakons at subsequent times $t = 0.45 + 1.8n$, $n \in \mathbb{Z}$

6. Cross-coupled EPDiff in higher dimensions. The straightforward generalization to higher dimensions is

$$l = \int (\mathbf{u}\cdot\mathbf{v} + (\nabla\mathbf{u})\cdot(\nabla\mathbf{v}))\,\mathrm{d}^n x,$$

$$\frac{d\mathbf{m}}{dt} = -\mathrm{ad}^*_{\delta\mathbf{l}/\delta\mathbf{m}}\mathbf{m} = -\mathbf{v}\cdot\nabla\mathbf{m} - (\nabla\mathbf{v})^T\cdot\mathbf{m} - \mathbf{m}\,\mathrm{div}\,\mathbf{v},\ \mathbf{m} = \mathbf{u} - \Delta\mathbf{u},$$

$$\frac{d\mathbf{n}}{dt} = -\mathrm{ad}^*_{\delta\mathbf{l}/\delta\mathbf{n}}\mathbf{n} = -\mathbf{u}\cdot\nabla\mathbf{n} - (\nabla\mathbf{u})^T\cdot\mathbf{n} - \mathbf{n}\,\mathrm{div}\,\mathbf{u},\ \mathbf{n} = \mathbf{v} - \Delta\mathbf{v}.$$

Numerical studies in $n = 2$ dimensions show that the waltzing pairs also appear in higher dimensions. In the case with rotational symmetry the two concentric waves ($\mathbf{u}$ and $\mathbf{v}$) have "waltzing" fronts and also rotate with respect to each other.

Acknowledgements. The work of R.I. is supported by the Science Foundation of Ireland (SFI), under Grant No. 09/RFP/MTH2144.

References

[1] V. Arnold and B. Khesin, *Topological Methods in Hydrodynamics* (Springer Verlag, New York, 1998).

[2] R. Camassa and D. Holm, An Integrable Shallow Water Equation with Peaked Solitons, *Phys. Rev. Lett.* **71** (1993) 1661–1664; ArXiv: patt-sol/9305002.

[3] C. Cotter et al., Waltzing peakons and compacton pairs in a cross-coupled Camassa-Holm equation, *J. Phys. A: Math. Theor.* **44** (2011) 265205 (28pp).

[4] D. Holm and R. Ivanov, Smooth and peaked solitons of the Camassa-Holm equation and applications, *J. Geom. Symmetry Phys.* **22** (2011) 13–49.

[5] D. Holm, J. Marsden, in *The breadth of symplectic and Poisson geometry, Progr. Math.* **232**, (Birkhäuser, Boston, MA, 2005).

[6] D. Holm, J. Marsden and T. Ratiu, The Euler-Poincaré Equations and Semidirect Products with Applications to Continuum Theories *Adv. Math.* **137**, 1–81 (1998).

[7] D. Holm and M. Staley, Wave Structure and Nonlinear Balances in a Family of Evolutionary PDEs, *SIAM J. Appl. Dyn. Syst.* **2** (2003) 323–380.

[8] G. Misiołek, Conjugate points in the Bott-Virasoro Group and the KdV equation *Proceedings of the AMS* **125** (1997) 935–940.

GOES project - Good on Emergency Situation

Nina Dobrinkova, Valentin Marinov

1 Intorduction

The web mapping or sometimes referred to as Web GIS has advanced to great extends in the later years. Cartography was restricted to few companies and organizations because of the difficulties in processing and managing the geographic data both on a specific hardware and software. Nevertheless with the occurrence of more reliable and extensive geographic web services, this is not a privilege anymore to a specific group of professionals, but a more affordable and accessible solution to everyone with the necessary technical skills and enough know-how in the GIS area.
Nowadays it is a common thing to rely on a web service or a web application to view, collect and manage geographical information. The fact that GIS data is distributed over the Internet has reduced the need for a specific software and hardware for showing it. These services offer a lot more than just visualization of geographical objects, but rather a way to manage oneâĂŹs own collection of objects, do GIS analysis and search among a rich array of specially categories POI's(Points Of Interest).

2 Google Maps, OpenStreetMaps and other major GIS web applications

The most serious step in popularization of Web GIS has been done by Google. In 2004 they released a new product called Google Maps. It heavily utilizes JavaScript and the Ajax technology, thus providing the user with an almost desktop like experiencing, while using the web application. The map is scrollable through the use of a mouse or a keyboard, or even in recent years with the vast usage of tablets through touch commands. This functionality resembles very much a natural scrolling of a geographical map but the user does not need to have a desktop application installed and there is no need to download any additional data or install plugins.
Other features of the Google Maps application include finding a specific location by address or name, or showing the nearest geographic objects to a point. Perhaps the most powerful functionality of the web application is finding directions between two or more points. The routing algorithm provided by the Google Maps team is currently one of the fastest in a GIS web application.
Another very useful features of the Google Maps application are the tools to add additional objects on the map that are related to the user itself. These are own POIs, routes or polygons. This allows not only for collecting and organizing objects with own semantics, but also sharing this new information with other users. Given the huge success of the Google Maps application, others have decided to implement their own solution. These are Yahoo! Maps, Bing Maps, Yandex Maps, BGMaps.com etc.

Perhaps the most famous one among them is the publicly available, free and open source project OpenStreetMaps.
OpenStreetMap is a free editable map of the whole world. It allows the user to view, edit and use geographical data in a collaborative way from anywhere on Earth. OpenStreetMap is created and maintained entirely by the users. This project relies heavily on crowd-sourcing. In comparison with other GIS web applications that are a product of a company and may require paying for a particular service or feature, the OpenStreetMap is a project without the idea of a profit. It is a way to offer free and open-source mapping solution to the web, without any legal or technical restrictions. OpenStreetMap offers the same features like the other alternatives in its scope. However the implementation of some of the features is still not that advanced or or sophisticated. These features are mainly related to the user interaction with the map or that some of the tools present in other web maps solutions are missing here. Still it surpasses them in its openness to the users and their ability to import or export data, either with GPS tracks or POI's or geographic areas.
`http://wiki.openstreetmap.org/wiki/Main_Page`

2.1 GIS Web Application Programming Interface (API)

The most important part of the web GIS applications mentioned so far is that they provide a form of an Software Development Kit (SDK) consisting of a library part with the respective Application Programming Interface (API) and web services available through predefined interfaces. As can be expected from proprietary services, they are not free for a commercial use or user logins. However OpenStreetMap is still freely available.The API's capabilities are:

- Create and manage a simple web map
- Manage tiles and sources of tiles
- Manage features and addons of the map - zooming, scrolling, mouse events, etc.
- Create and manage map layers
- Add, edit or remove POI's from the map
- Draw geo-aware geometry figures - lines, polylines (routes), polygons (areas)
- Change the appearance of POIs or other objects on the map
- Managing geographical data
- Searching (through web services) and displaying GIS data
- Importing, displaying and exporting GPS tracks - usually .gpx files
- Manage geo Data Base data

All of these features are supported by the Web API's, where searching in the GIS databases may result in different objects, i.e. the search depends on the objects they contain and the search algorithm they utilize.The web services that are used for searching and fetching geographical objects may be either SOAP or REST based. The results could be in XML or JSON formats. The JSON format is the preferred one due to its many advantages in simplicity and quantity, thus providing better performance and less traffic. Having such powerful tools, creating and managing GIS driven applications has become more affordable and easy for developers, which reflected to providing better end user tools.
Developers without extended knowledge of GIS systems are utilizing this technology through the abstraction of API's. This is the best option for integrating GIS aware modules in an applications that need to display and/or manage geographical information. Thus the need for a dedicated servers and software solutions has been left to the consumers of the service. There preprocessors of todays GIS web applications were mostly created by companies with a focus on GIS systems. Such vendors are Intergraph, ESRI, NetCad and other smaller companies. Some of their early implementations are still supported and updated. The basic difference between them is the nature of client-server interaction.
Ajax-based applications are usually referred to as fat clients. The client has a more extended knowledge of how the application works. This may become a very disturbing security issue, especially with the case of web applications. The client, which may as well be referred to as the online user, gets a hold of a more complete collection of GIS data. For the major vendors of GIS data this is a potential security breach as they manage this data and provide it for a profit, but if it is supplied to the client without any restrictions it becomes available to everyone for free or very small amount of money. Therefore it is very important to be aware of the provided data to the user. There is also the so called slim approach where the basic API's are integrated and less security options are available.
`http://code.google.com/intl/bg/apis/maps/index.html`

2.2 Plugin based implementations

More advanced solutions for providing a RIA GIS for terrain usage is based on the solution with implementation of the plugin-based technology. Such technologies are Adobe Flash, Microsoft Silverlight, Java, etc. This approach, although has its own drawbacks about the security issues of the Ajax-based web applications. Such solutions include the ESRIâĂŹs ArcGIS Explorer online and other companies that are not directly involved in the GIS area like InfoSoft, Telerik etc.
The main downside of such a solution is that the user is required to install a plugin in order to run the application with his/her browser. With this requirement the nature of the application is actually shifted from its web nature and the browser becomes simply the medium to update the application with the new version. In its core this has become a desktop solution. These applications are very feature-rich and provide excellent user friendly approach, but their implementation usually relies

on appropriate environment, not on standards, which makes them costly. This is a problem in cases that the platform is not updated or is not supported anymore. In such cases the Web GIS application is useless.
`http://www.nn4d.com/site/global/build/partner_mapping_apis/p_partner_mapping_apis.jsp`

3 GOES (Good On Emergency Situation) project

The project GOES has been financially supported by the Civil Protection Financial Instrument of Directorate General - ECHO, which covers three main aspects of civil protection activities in the framework of the European Union:prevention, preparedness and response.
The GOES project aims to increase preparedness, awareness and maximum cooperation between public authorities of different member states through quick and effective information. The partner consortium is between the three counties: Spain, Italy and Bulgaria, where the cities of Valencia, Ancona and Sofia will implement the new system into their civil protection departments.
The authorities involved in the project proposal agree that an inadequate response to emergency situations is often the result of disorganization, delays or deficiencies in communication between local actors involved in various capacities in prevention and emergency management. From this reflection comes the project GOES which aims to create a network that collects daily all relevant information on road conditions related to any criticisms and suggestions on alternative routes. The network will convey this information to the regional civil protection structures and to the main network in order to promptly inform citizens. The system for collecting and transmitting data should be based on standardized and automated procedures to exchange across the partner territories. Once this connection has been created it may also be used to convey other information coming from the whole territory, not only from the roads.
GOES aims to create a network that collects daily all relevant information on road conditions related to any criticisms and suggestions on alternative routes. The network will convey this information to the regional civil protection structures and to the main network in order to promptly inform citizens. The system for collecting and transmitting data should be based on standardized and automated procedures to exchange across the partner territories. Once this connection has been created it may also be used to convey other information coming from the whole territory, not only from the roads. The figure 1 is illustrating the system architecture planned to be developed in the framework of the project.

3.1 Main Objectives of the project

The main objectives of the project cover:

- Optimizing systems for collecting and transmitting information concerning the civil protection particularly on natural disasters that have a negative impact on the feasibility of the roads.

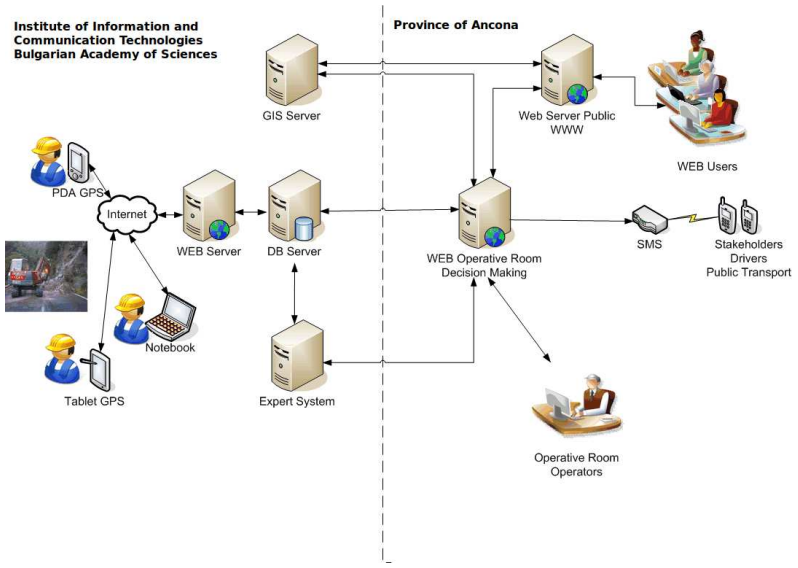

Figure 1: Graphical representation of the architecture of the GOES system

- To increase preparedness on emergency situation and give an adequate response to emergency situations.
- To improve cooperation between public authorities of different member states through quick and effective information and involving operators, stakeholders and population from the territories of the partnership.
- To Create a network that collects daily all relevant information on road conditions.
- Creating a database of the natural disasters which impact on the feasibility of the road.

3.2 The planned outcomes of the project

- A preliminary study of the different ways of organizing services, traffic and information management in order to increase the knowledge about the different ways of organizing services in the territories covered by the road test and understand the management mode of information concerning the roads' navigability in normal and emergency situations.
- A design of a standardized system among the partners for the receipt, sorting and transmission of information on disasters relevant for the roads navigability.
- raining of road and civil protection workers.

4 Conclusions

The project is going to be implemented in the Sofia municipality Civil Protection department with the development works established in the IICT-BAS. The used technology will be based on the openstreets approach with Web GIS databases for the incomming data from the mobile teams, which will be the main end users of the final developed system.

5 Acknowledgements

The paper has been supported by GOES (Good On Emergency Situation) project, grant agreement reference n° 070401/2010/579105/SUB/C4.

Influence of the Parameter R on ACO Start Strategies

Stefka Fidanova and Pencho Marinov

1 Introduction

Metaheuristic methods are general tools for solving hard (from computational point of view) optimization problems. Most of them use ideas coming from nature. Ant Colony Optimization is one of the most successive metaheuristic method. Idea for it comes from real ant behavior and their collective intelligence. The ability of ant colonies to form paths for carrying food is rather fascinating. The problem is solved collectively by the whole colony. This ability is explained by the fact that ants communicate in an indirect way by laying trails of pheromone. The higher the pheromone trail within a particular direction, the higher the probability of choosing this direction.
The ACO algorithm uses a colony of artificial ants that behave as cooperative agents in a mathematical space where they are allowed to search and reinforce pathways (solutions) in order to find the optimal ones. The problem is represented by graph and the ants walk on the graph to construct solutions. The solutions are represented by paths in the graph. After the initialization of the pheromone trails, the ants construct feasible solutions, starting from random nodes, and then the pheromone trails are updated. At each step the ants compute a set of feasible moves and select the best one (according to some probabilistic rules) to continue the rest of the tour. The structure of the ACO algorithm is shown by the pseudo-code below. The transition probability $p_{i,j}$, to choose the node j when the current node is i, is based on the heuristic information $\eta_{i,j}$ and the pheromone trail level $\tau_{i,j}$ of the move, where $i, j = 1, \ldots, n$.

$$p_{i,j} = \frac{\tau_{i,j}^a \eta_{i,j}^b}{\sum_{k \in Unused} \tau_{i,k}^a \eta_{i,k}^b},$$

where *Unused* is the set of unused nodes of the graph. The higher the value of the pheromone and the heuristic information, the more profitable it is to select this move and resume the search. In the beginning, the initial pheromone level is set to a small positive constant value τ_0; later, the ants update this value after completing the construction stage. ACO algorithms adopt different criteria to update the pheromone level.
The pheromone trail update rule is given by:

$$\tau_{i,j} \leftarrow \rho \tau_{i,j} + \Delta \tau_{i,j},$$

where ρ models evaporation in the nature and $\Delta \tau_{i,j}$ is the new added pheromone which is proportional to the quality of the solution.
As other metaheuristics, ACO algorithm is applied on hard combinatorial optimization problems coming from real life and industry. It is unpractical to apply exact

```
Ant Colony Optimization
Initialize number of ants;
Initialize the ACO parameters;
while not end-condition do
        for k=0 to number of ants
            ant k choses start node;
            while solution is not constructed do
                    ant k selects higher probability node;
            end while
        end for
        Update-pheromone-trails;
end while
```

Figure 1: Pseudocode for ACO

methods or traditional numerical methods on this kind of problems, because they need huge amount of computational resources, time and memory. Examples of optimization problems are Traveling Salesman Problem [6], Vehicle Routing [7], Minimum Spanning Tree [5], Multiple Knapsack Problem [4], etc.
The aim of this paper is analysis of the influence of the parameter R on the ACO algorithm behavior.

2 Subset Estimations

The essential part of ACO algorithm is starting from random node when ants create solutions. It is a kind of diversification of the search and leads to using small number of ants, which means less computational resources. But for some problems, especially subset problems, it is important from which node the search process starts. For example if an ant starts from node which does not belong to the good solution, probability to construct it is zero. Therefore we divide the set of nodes of the graph of the problem to subset, we estimate every subset how good and how bed is to start from it, after we offer several start strategies keeping in some extent the random start. Let the graph of the problem has m nodes. We divide the set of nodes on N subsets. There are different ways for dividing. Normally, the nodes of the graph are randomly enumerated. An example for creating of the nodes subsets, without loss of generality, is: the node number one is in the first subset, the node number two is in the second subset, etc. the node number N is in the $N-th$ subset, the node number $N+1$ is in the first subset, etc. Thus the number of the nodes in the subsets are almost equal. We introduce estimations $D_j(i)$ and $E_j(i)$ of the node subsets, where $i \geq 2$ is the number of the current iteration. $D_j(i)$ shows how good is the j^{th} subset and $E_j(i)$ shows how bad is the j^{th} subset. $D_j(i)$ and $E_j(i)$ are weight coefficients of $j-th$ node subset $(1 \leq j \leq N)$.

$$D_j(i) = \frac{i.D_j(i-1) + F_j(i)}{i},$$
$$E_j(i) = \frac{i.E_j(i-1) + G_j(i)}{i},$$

where $i \geq 1$ is the current process iteration and for each j $(1 \leq j \leq N)$:

$$F_j(i) = \begin{cases} \frac{f_{j,A}}{n_j} & \text{if } n_j \neq 0 \\ F_j(i-1) & \text{otherwise} \end{cases}, \tag{1}$$

$$G_j(i) = \begin{cases} \frac{g_{j,B}}{n_j} & \text{if } n_j \neq 0 \\ G_j(i-1) & \text{otherwise} \end{cases}, \tag{2}$$

$f_{j,A}$ is the number of the solutions among the best $A\%$, $g_{j,B}$ is the number of the solutions among the worst $B\%$, where $A + B \leq 100$, $i \geq 2$ and

$$\sum_{j=1}^{N} n_j = n, \tag{3}$$

where n_j $(1 \leq j \leq N)$ is the number of solutions obtained by ants starting from nodes subset j, n is the number of ants. Initial values of the weight coefficients are: $D_j(1) = 1$ and $E_j(1) = 0$. With this estimation we take in to account the information from previous iterations as well as the information from current iteration. The information from previous iterations have lass influence in the estimation because we divide to the number of iteration. The balance between the influence of the previous iterations and the last is important. At the beginning when the current best solution is far from the optimal one, some of the node subsets can be estimated as good. If the influence of the last iteration is too high then information for good and bad solutions from previous iterations is ignored, which can distort estimation too. We try to use the experience of the ants from previous iteration to choose the better starting node. Other authors use this experience only by the pheromone, when the ants construct the solutions [3]. Let us fix threshold E for $E_j(i)$ and D for $D_j(i)$, than we construct several strategies to choose start node for every ant, the threshold E increases every iteration with $1/i$ where i is the number of the current iteration:

1 If $E_j(i)/D_j(i) > E$ then the subset j is forbidden for current iteration and we choose the starting node randomly from $\{j \mid j \text{ is not forbidden}\}$;

2 If $E_j(i)/D_j(i) > E$ then the subset j is forbidden for current simulation and we choose the starting node randomly from $\{j \mid j \text{ is not forbidden}\}$;

3 If $E_j(i)/D_j(i) > E$ then the subset j is forbidden for K_1 consecutive iterations and we choose the starting node randomly from $\{j \mid j \text{ is not forbidden}\}$;

4 Let $r_1 \in [R, 1)$ is a random number. Let $r_2 \in [0, 1]$ is a random number. If $r_2 > r_1$ we randomly choose node from subset $\{j \mid D_j(i) > D\}$, otherwise we randomly chose a node from the not forbidden subsets, r_1 is chosen and fixed at the beginning.

5 Let $r_1 \in [R, 1)$ is a random number. Let $r_2 \in [0, 1]$ is a random number. If $r_2 > r_1$ we randomly choose node from subset $\{j \mid D_j(i) > D\}$, otherwise we randomly chose a node from the not forbidden subsets, r_1 is chosen at the beginning and increase with r_3 every iteration.

Where $0 \leq K_1 \leq$"number of iterations" is a parameter. If $K_1 = 0$, than strategy 3 is equal to the random choose of the start node. If $K_1 = 1$, than strategy 3 is equal to the strategy 1. If $K_1 =$"maximal number of iterations", than strategy 3 is equal to the strategy 2. R is a parameter which shows the probability the ants to start from "good" node subset. When $R = 0.5$ the probability to start from "good" node subset is two times higher. When the value of R decreases the probability to start from "good" node subset increases and when the value of R increases the probability to start from "good" node subset decreases.
We can use more than one strategy for choosing the start node, but there are strategies which can not be combined. We distribute the strategies into two sets: $St1 = \{strategy1,\ strategy2,\ strategy3\}$ and $St2 = \{strategy4,\ strategy5\}$. The strategies from same set can not be used at once. Thus we can use strategy from one set or combine it with strategies from the other set. Exemplary combinations are ($strategy1$), ($strategy2$; $strategy5$), ($strategy3$; $strategy4$). When we combine strategies from $St1$ and $St2$, first we apply the strategy from $St1$ and according it some of the regions (node subsets) become forbidden, and after that we choose the starting node from not forbidden subsets according the strategy from $St2$

3 Computational Results

We test the ideas for controlled start on MKP. MKP is a real world problem and is a representative of the class of subset problems. The MKP has numerous applications in theory as well as in practice. It also arises as a subproblem in several algorithms for more complex problems and these algorithms will benefit from any improvement in the field of MKP. The following major applications can be mentioned: problems in cargo loading, cutting stock, bin-packing, budget control and financial management. The computational experience of the ACO algorithm is shown using 10 MKP instances from "OR-Library" available within WWW access at **http://people.brunel.ac.uk/mastjjb/jeb/orlib/**, with 100 objects and 10 constraints. The parameters are fixed as follows: $\rho = 0.5$, $a = 1$, $b = 1$, number of used ants is 20, $A = 30$, $B = 30$, $D = 1.5$, $E = 0.5$, $K_1 = 5$, $r_3 = 0.01$. The values of ACO parameters (ρ, a, b) are from [4] and experimentally is found that they are best for MKP. The tests are run with 1, 2, 4, 5 and 10 nodes within the nodes subsets. The values of the parameter R are as follows $\{0.1, 0.2, 0.3, 0.4, 0.5, 0.6, 0.7, 0.8, 0.9\}$ For every experiment, the results

Table 4: Influence of parameter R

R	0.1	0.2	0.3	0.4	0.5	0.6	0.7	0.8	0.9
Random	28	28	28	28	28	28	28	28	28
strat. 1	78	78	78	78	78	78	78	78	78
strat. 2	82	82	82	82	82	82	82	82	82
strat. 3	80	80	80	80	80	80	80	80	80
strat. 4	84	80	81	78	**87**	83	82	81	78
strat. 5	84	81	82	80	82	80	80	77	79
strat. 1-4	80	82	79	83	83	84	82	84	81
strat. 1-5	84	83	85	81	82	82	82	84	84
strat. 2-4	82	83	80	86	81	85	82	83	80
strat. 2-5	84	79	80	82	83	81	83	84	84
strat. 3-4	83	82	80	**87**	82	86	83	83	80
strat. 3-5	83	79	80	80	81	81	83	84	84

are obtained by performing 30 independent runs, then averaging the fitness values. The computational time which takes start strategies is negligible with respect to the computational time which takes solution construction.
The problem which arises is how to compare the achieved solutions by different strategies and different node-devisions. Therefore the difference (interval) d between the worst and best average result for every problem is divided to 10. If the average result for some strategy, node devision and R is in the first interval with borders the worst average result and worst average plus $d/10$ it is appreciated with 1. If it is in the second interval with borders the worst average plus $d/10$ and worst average plus $2d/10$ it is appreciated with 2 and so on. If it is in the 10th interval with borders the best average minus $d/10$ and the best average result, it is appreciated with 10. Thus for a test problem the achieved results for every strategy, every nodes devision and every R is appreciated from 1 to 10. After that is summed the rate of all test problems for every strategy, every nodes devision and R. So the rate of the strategies/node-devision and R becomes between 10 and 100, because the benchmark problems are 10. It is mode of result classification, ranking.
For all values of the parameter R the best rate according node devision is when there is only one node in node-subsets. So we put in the table the rate of the start strategies when the node subsets consist one node, with bold is the best rate.
Regarding the table we observe that the best rate is when $R = 0.4$ and $R = 0.5$, or when the probability to start from "good" node subsets is two times higher than to start from others. When the value of R decreases the probability to start from "good" subsets increases and when the value of R increases the probability to start from "good" subsets decreases. When the value of the R is too small the probability to start from subset which is not estimated as good is too small and the diversification of the search decrease, therefore the ranking is low in this case. When the value of R is close to 1, the probability to start from "good" subsets is too small. Thus the intensification of the search around good solution decrease and therefore the ranking

is low in this case. When $R = 0.4$ or $R = 0.5$ there is good balance between diversification and intensification. The parameter R affects only Strategy 4 and Strategy 5 and combinations with them.

4 Conclusion

In this paper we address on influence analysis of the parameter R of start strategies on the ACO algorithm applied on MKP. We vary the value of the parameter R in the interval $(0, 1)$. We found that the good balance between intensification and diversification of the search process achieves better results, thus the best values are $R = 0.4$ and $R = 0.5$.In a future we will focus on parameter settings which manage the starting procedure. We will investigate on influence of the parameters to algorithm performance.

Acknowledgments: This work has been partially supported by the Bulgarian National Scientific Fund under the grants DID 02/29-"Modeling Processes with fixed development rules" and DTK 02/44-"Effective Monte Carlo Methods for large-scale scientific problems".

References

[1] Bonabeau E., Dorigo M., Theraulaz G., Swarm Intelligence: From Natural to Artificial Systems, New York,Oxford University Press, 1999.

[2] Dorigo M., Gambardella L.M., Ant Colony System: A Cooperative Learning Approach to the Traveling Salesman Problem. IEEE Transactions on Evolutionary Computation 1,53-66,1997.

[3] Dorigo M., Stutzle T., Ant Colony Optimization, MIT Press, 2004.

[4] Fidanova S., Evolutionary Algorithm for Multiple Knapsack Problem, Int. Conference Parallel Problems Solving from Nature, Real World Optimization Using Evolutionary Computing, ISBN No 0-9543481-0-9,Granada, Spain, 2002.

[5] Reiman M., Laumanns M., A Hybrid ACO algorithm for the Capacitated Minimum Spanning Tree Problem, In proc. of First Int. Workshop on Hybrid Metahuristics, Valencia, Spain, 2004, 1-10.

[6] Stutzle T. Dorigo M., ACO Algorithm for the Traveling Salesman Problem, In K. Miettinen, M. Makela, P. Neittaanmaki, J. Periaux eds., Evolutionary Algorithms in Engineering and Computer Science, Wiley, 163-183, 1999.

[7] Zhang T., Wang S., Tian W., Zhang Y., ACO-VRPTWRV: A New Algorithm for the Vehicle Routing Problems with Time Windows and Re-used Vehicles based on Ant Colony Optimization, Sixth International Conference on Intelligent Systems Design and Applications, IEEE press, 2006, 390-395.

Some Computational Aspects of Harmonic Interpolation Via Radon Projections

Irina Georgieva, Clemens Hofreither

1 Introduction

The Radon transform, named after Johann Radon who studied it in the early twentieth century, is the theoretical foundation for tomography methods for shape reconstruction of objects with non-homogeneous density. These methods were intensively studied in the 1960s and continue to find many applications in medicine, electronic microscopy, geology, plasma investigations, finding defects in nuclear reactors, etc. From the mathematical point of view, the problem is to recover a multivariate function using information given as line integrals of the unknown function.
An idea suggested by B. Bojanov is to incorporate additional knowledge about the function to be recovered into approximation methods. It is to be expected that this can improve the accuracy of the approximation while reducing the amount of input data required as well as the computational effort. In applications, such problem-specific knowledge is often provided in the form of a partial differential equation which the unknown satisfies.
In the present work, we concern ourselves with the simple case where the unknown is harmonic, i.e., satisfies the Laplace equation $\Delta u = u_{xx} + u_{yy} = 0$. This elliptic partial differential equation is important both as a model problem as well as in actual applications, like heat transport, diffusion problems or Stokes flow of incompressible fluids.
We consider an algebraic method for reconstruction of harmonic functions via a finite number of values of its Radon projections. More precisely, for given values of some Radon projections, we seek a harmonic polynomial which matches these data exactly.

2 Preliminaries

Let $I(\theta, t)$ denote a chord of the unit circle at angle $\theta \in [0, 2\pi)$ and distance $t \in (-1, 1)$ from the origin. The chord $I(\theta, t)$ is parameterized by

$$s \mapsto (t\cos\theta - s\sin\theta, t\sin\theta + s\cos\theta)^\top, \qquad \text{where } s \in (-\sqrt{1-t^2}, \sqrt{1-t^2}). \tag{1}$$

Definition 1. *Let $f(x, y)$ be a real-valued bivariate function in the unit disk in $\mathbb{R}^2$. The* Radon projection $\mathcal{R}_\theta(f; t)$ *of f in direction θ is defined by the line integral*

$$\mathcal{R}_\theta(f; t) := \int_{I(\theta,t)} f(\mathbf{x})\, d\mathbf{x} = \int_{-\sqrt{1-t^2}}^{\sqrt{1-t^2}} f(t\cos\theta - s\sin\theta, t\sin\theta + s\cos\theta)\, ds.$$

Johann Radon [11] showed in 1917 that a differentiable function f is uniquely determined by the values of its Radon transform,

$$f \;\mapsto\; \big\{\mathcal{R}_\theta(f;t) \,:\, -1 \le t \le 1,\; 0 \le \theta < \pi\big\}.$$

The problem of recovery of a polynomial from a finite number of values of its Radon transform may be viewed as a bivariate interpolation problem where the traditional point values are replaced by the means over chords of the unit circle. Many mathematicians studied problems of this class in the past few decades, among them Marr [10], Hakopian [9], Bojanov [1], and Xu [2]. Other works in which recovery of bivariate polynomials based on Radon projections was considered are [7, 8, 5, 6, 4].

3 Description of the method

Assume that we know *a priori* that the function to be interpolated is harmonic. Then it seems natural to work in the space $\mathcal{H}_n$ of real bivariate harmonic polynomials of total degree at most n, which has dimension $2n+1$. Let a set of chords of the unit circle $\mathcal{I} = \{I_1, I_2, \ldots, I_{2n+1}\}$ be given. Furthermore, to each chord $I \in \mathcal{I}$ a given value $\gamma_I \in \mathbb{R}$ is associated. Then, the aim is to find a harmonic polynomial $p \in \mathcal{H}_n$ such that

$$\int_I p(\mathbf{x})\, d\mathbf{x} = \gamma_I \qquad \forall I \in \mathcal{I}. \tag{2}$$

Here the given values γ_I are the chord integrals corresponding to an unknown harmonic function u. The hope is that then p approximates u reasonably well.
We call $\mathcal{I}$ *regular* if the interpolation problem (2) has a unique solution for all given values $\{\gamma_I\}$.
The regular schemes which we work with were constructed with the help of methods from symbolic computation [3], and we briefly present them below.

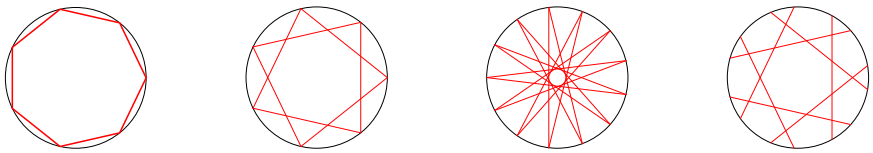

Figure 1: Regular schemes according to Theorem 1.

Theorem 1 ([3]). *Let the chords $\mathcal{I}$ be given by $I_m = I(\theta_m, t)$, where the angles θ_m are equally spaced over the unit circle $(0, 2\pi)$ and $t \in (0,1)$ is not a zero of any Chebyshev polynomial of the second kind $U_1, \ldots, U_n$. Then the interpolation problem (2) has a unique solution in $\mathcal{H}_n$ for any given data $\{\gamma_I\}$.*

In fact, in [3], arbitrarily spaced angles θ_m were admitted, however in the present work we stick with equally spaced chords. Some possible configurations which satisfy the assumptions of Theorem 1 are shown in Figure 1.

The proof uses the following basis of the harmonic polynomials,

$$\phi_0(x,y) = 1, \quad \phi_{k,1}(x,y) = \mathrm{Re}(x+\mathbf{i}y)^k, \quad \phi_{k,2}(x,y) = \mathrm{Im}(x+\mathbf{i}y)^k,$$

which is equal, in polar coordinates, to

$$\phi_{k,1}(r,\theta) = r^k \cos(k\theta), \quad \phi_{k,2}(r,\theta) = r^k \sin(k\theta).$$

We have shown the following analogue to Marr's formula [10] in the harmonic case.

Lemma 1. *The Radon projections of the basis harmonic polynomials satisfy*

$$\int_{I(\theta,t)} \phi_{k,1}\, d\mathbf{x} = \frac{2}{k+1}\sqrt{1-t^2}U_k(t)\cos(k\theta),$$
$$\int_{I(\theta,t)} \phi_{k,2}\, d\mathbf{x} = \frac{2}{k+1}\sqrt{1-t^2}U_k(t)\sin(k\theta).$$

Under the assumption of constant $t_m = t$, we can use this lemma to derive the following representation of the system matrix corresponding to (2): $A = CD$, where

$$C = \begin{pmatrix} 1 & \cos(\theta_1) & \sin(\theta_1) & \cos(2\theta_1) & \sin(2\theta_1) & \dots & \cos(n\theta_1) & \sin(n\theta_1) \\ 1 & \cos(\theta_2) & \sin(\theta_2) & \cos(2\theta_2) & \sin(2\theta_2) & \dots & \cos(n\theta_2) & \sin(n\theta_2) \\ \vdots & \vdots & \vdots & \vdots & \vdots & \ddots & \vdots & \vdots \\ 1 & \cos(\theta_{2n}) & \sin(\theta_{2n}) & \cos(2\theta_{2n}) & \sin(2\theta_{2n}) & \dots & \cos(n\theta_{2n}) & \sin(n\theta_{2n}) \\ 1 & \cos(\theta_{2n+1}) & \sin(\theta_{2n+1}) & \cos(2\theta_{2n+1}) & \sin(2\theta_{2n+1}) & \dots & \cos(n\theta_{2n+1}) & \sin(n\theta_{2n+1}) \end{pmatrix},$$
$$D = \mathrm{diag}(\alpha_0, \alpha_1, \alpha_1, \dots, \alpha_n, \alpha_n)$$

with the column factors $\alpha_k = \frac{2}{k+1}\sqrt{1-t^2}U_k(t) > 0$.
The matrix C is the same as for the one-dimensional problem of interpolation with a trigonometric polynomial of degree n in $[0, 2\pi]$ at the points $\{\theta_1, \dots, \theta_{2n+1}\}$. We use the fact that C is invertible if and only if the angles θ_m are pairwise distinct to show that A is invertible in this case.

4 Inversion of the linear system

For the equally spaced angles $\theta_m = \frac{2\pi m}{2n+1}$ and $t \in (0,1)$ such that $U_k(t) \neq 0$ for all $k \in \{0, \dots, n\}$, we use the orthogonality of the columns of C to derive the explicit inverse

$$A^{-1} = \mathrm{diag}(\beta_0, \beta_1, \beta_1, \dots, \beta_n, \beta_n)C^\top,$$

where the row factors

$$\beta_k = \begin{cases} \frac{1}{2(2n+1)}(\sqrt{1-t^2})^{-1} = \frac{1}{2n+1}\alpha_k^{-1}, & k = 0, \\ \frac{k+1}{2n+1}(\sqrt{1-t^2}U_k(t))^{-1} = \frac{2}{2n+1}\alpha_k^{-1}, & k \geq 1 \end{cases}$$

serve to normalize the orthogonal system formed by the columns of C.
Note that the action of the matrix $C^\top$ is essentially a discrete Fourier transform of the given data. This suggests an efficient algorithm for the solution of the linear system: using a suitable Fast Fourier Transform (FFT), we can compute the coefficients of the interpolating polynomial in slightly worse than linear ($\mathcal{O}(n)$) time. Having such a quasi-optimal solution method available is invaluable for practical large-scale problems.

5 Condition number

With the use of the explicit formula for A^{-1}, it is not difficult to compute the singular values of both A and A^{-1}. This allows us to obtain a uniform bound for the spectral condition number of A, to be precise,

$$\kappa_2(A) \leq 2\sqrt{2},$$

again under the assumption of equally spaced angles and constant t. The significance of this result is that the method is very stable with respect to errors in the input data, i.e., noise in the given measurements results in an error which is of the same order of magnitude. Indeed, our numerical examples confirm this.

6 Numerical Example

We test our method on a function which is given by the harmonic extension of the quadratic spline $f(\theta)$, $-\pi \leq \theta \leq \pi$, where θ is the angle on the unit circle.

$$f(\theta) = \begin{cases} -\frac{1}{2}(\theta + \frac{\pi}{2})(\theta + \frac{3}{2}\pi), & -\pi \leq \theta < -\frac{\pi}{2}, \\ \frac{1}{2}(\theta - \frac{\pi}{2})(\theta + \frac{\pi}{2}), & -\frac{\pi}{2} \leq \theta < \frac{\pi}{2}, \\ -\frac{1}{2}(\theta - \frac{\pi}{2})(\theta - \frac{3}{2}\pi), & \frac{\pi}{2} \leq \theta < \pi. \end{cases}$$

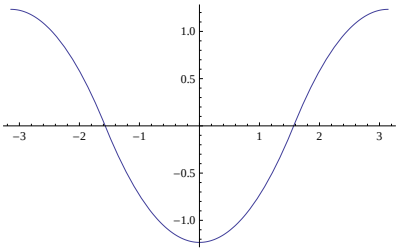

Note that $f(\theta)$ is a periodic C^1-function with discontinuous second derivative. The resulting harmonic function u has the series representation (in polar coordinates)

$$u(r,\theta) = \sum_{k=1}^{\infty} (-1)^k r^{2k-1} \frac{4\cos((2k-1)\theta)}{(2k-1)^3\pi}.$$

For our chords $\mathcal{I}$, we choose the edges of a regular $(2n+1)$-sided convex polygon (cf. Figure 1, first picture). Figure 2 shows the relative L_2-errors for varying degree n of the interpolating polynomial. The last column of the table displays the ratio between

n	relative L_2 error	rate
2	$2.97973 \cdot 10^{-2}$	—
4	$6.08456 \cdot 10^{-3}$	4.90
8	$9.26954 \cdot 10^{-4}$	6.56
16	$1.23962 \cdot 10^{-4}$	7.47
32	$1.58587 \cdot 10^{-5}$	7.82

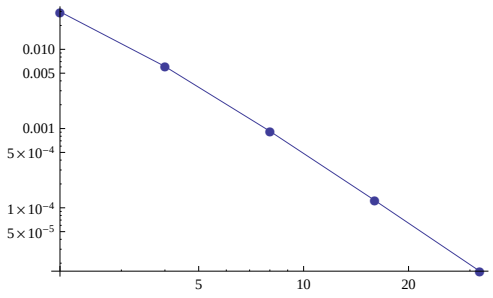

Figure 2: Relative L_2 errors for varying degree n, with log-log-plot

successive errors. This rate of convergence approaches 8 and thus suggests that the interpolation error is of the order $\mathcal{O}(n^{-3})$.
Previous experiments for recovery of functions which are C^∞ in the closed unit disk have shown exponential convergence [3].

7 Acknowledgments

The authors acknowledge the support by Bulgarian National Science Fund, Grant DMU 03/17. The research of the first author was also supported by Bulgarian National Science Fund, Grant DDVU 0230/11. The research of the second author was funded by the Austrian Science Fund (FWF): W1214-N15, project DK04.

References

[1] B. Bojanov and I. Georgieva. Interpolation by bivariate polynomials based on Radon projections. *Studia Math.*, 162:141–160, 2004.

[2] B. Bojanov and Y. Xu. Reconstruction of a bivariate polynomial from its Radon projections. *SIAM J. Math. Anal.*, 37:238–250, 2005.

[3] I. Georgieva, C. Hofreither, C. Koutschan, V. Pillwein, and T. Thanatipanonda. Harmonic interpolation based on Radon projections along the sides of regular polygons. 2011. Submitted. Also available as Technical Report 2011-12 in the series of the DK Computational Mathematics Linz, `https://www.dk-compmath.jku.at/publications/dk-reports/2011-10-20/view`.

[4] I. Georgieva, C. Hofreither, and R. Uluchev. Interpolation of mixed type data by bivariate polynomials. In G. Nikolov and R. Uluchev, editors, *Constructive Theory of Functions, Sozopol 2010: In memory of Borislav Bojanov*, pages 93–107. Prof. Marin Drinov Academic Publishing House, Sofia, 2012. Also available as Technical Report 2010-14 in the series of the DK Computational Math-

ematics Linz, https://www.dk-compmath.jku.at/publications/dk-reports/2010-12-10/view.

[5] I. Georgieva and S. Ismail. On recovering of a bivariate polynomial from its Radon projections. In B. Bojanov, editor, *Constructive Theory of Functions, Varna 2005*, pages 127–134. Marin Drinov Academic Publishing House, Sofia, 2006.

[6] I. Georgieva and R. Uluchev. Smoothing of Radon projections type of data by bivariate polynomials. *J. Comput. Appl. Math.*, 215:167–181, 2008.

[7] I. Georgieva and R. Uluchev. Surface reconstruction and Lagrange basis polynomials. In I. Lirkov, S. Margenov, and J. Waśniewski, editors, *Large-Scale Scientific Computing 2007*, pages 670–678, Berlin, Heidelberg, 2008. Springer-Verlag.

[8] I. Georgieva and R. Uluchev. On interpolation in the unit disk based on both Radon projections and function values. In I. Lirkov, S. Margenov, and J. Waśniewski, editors, *Large-Scale Scientific Computing 2009*, pages 747–755, Berlin, Heidelberg, 2010. Springer-Verlag.

[9] H. Hakopian. Multivariate divided differences and multivariate interpolation of Lagrange and Hermite type. *J. Approx. Theory*, 34:286–305, 1982.

[10] R. Marr. On the reconstruction of a function on a circular domain from a sampling of its line integrals. *J. Math. Anal. Appl.*, 45:357–374, 1974.

[11] J. Radon. Über die Bestimmung von Funktionen durch ihre Integralwerte längs gewisser Mannigfaltigkeiten. *Ber. Verch. Sächs. Akad.*, 69:262–277, 1917.

Visualization Tool of Sensitivity Study Results

Rayna Georgieva and Sofiya Ivanovska

1 Introduction

Sensitivity analysis (SA) has an important twofold role: for mathematical models verification and/or improvement, and/or on the other hand, for a reliable interpretation of experts of the main effect, the interaction and higher-order interaction effect of input parameters on the model output. A possible definition of sensitivity analysis is given in [8]: *the study of how uncertainty in the output of a model (numerical or otherwise) can be apportioned to different sources of uncertainty in the model input.*

The general procedure for sensitivity analysis can be described in the following steps presented on Figure 1 [11]:

- definition of probability distributions for the parameters under study,
- generation of samples according to the defined probability distributions using a sampling strategy,
- sensitivity analysis of the output variance in relation to the variation of the inputs.

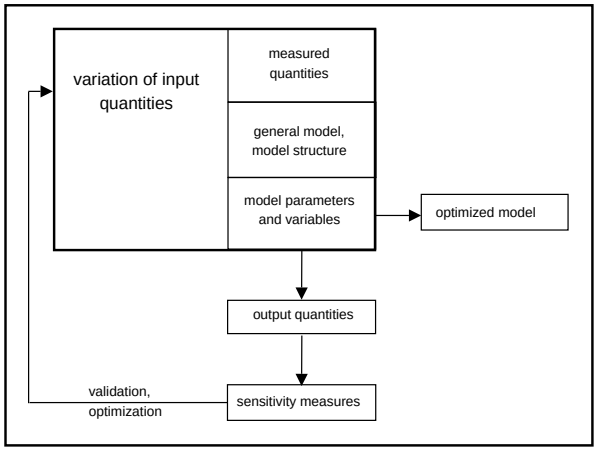

Figure 1: General procedure for sensitivity analysis.

Variance-based sensitivity analysis is an useful tool for an advanced study of relations between the input parameters of a model, output results and internal mechanisms regulating the system under consideration. They deliver global, quantitative and

model-independent sensitivity measures and are efficient of the computational point of view. Its computational cost for estimating all first-order and total sensitivity measures is proportional to the sample size and the number of input parameters.

The aim of the current work is development of a visualization tool to present sensitivity study results about ozone concentration levels due to variation of chemical rates in the large-scale mathematical model for remote transport of air pollutants (**Uni**fied **D**anish **E**ulerian **M**odel, UNI-DEM[2], [12]).

2 Numerical Methods

Various variance-based techniques for global sensitivity analysis have been applied to study the sensitivity of ozone concentrations according to variations of rates of some chemical reactions. The input data analised has been obtained during runs of the mathematical model for remote transport of air pollutants UNI-DEM. The Sobol method is one of the most often used variance-based methods [9]. An important advantage of this method is that it allows to compute not only the first-order indices, but also indices of a higher-order in a way similar to the computation of the main effects. The problem of providing global sensitivity analysis applying Sobol approach (and its modifications [8, 10]) consists in evaluating total sensitivity indices, and in particular Sobol global sensitivity indices of corresponding order. It represents a problem of multidimensional integration.

Several sensitivity analysis techniques and efficient Monte Carlo approaches have been developed and applied to compute sensitivity indices for the UNI-DEM model of remote transport of air pollutants [1, 2, 3, 4]. A number of numerical tests have been performed to study and compare efficiency of these approaches:

- variance-based approaches for sensitivity analysis - Sobol approach, extended Fourier Amplitude Sensitivity Test (eFAST),
- Monte Carlo algorithms (adaptive algorithm [3], algorithm based on Sobol quasirandom sequences (MCA-MSS, [2]), approach for very small sensitivity indices [10]),
- random number generators
  - SIMD-oriented Fast Mersenne Twister pseudorandom number generator [7, 13],
  - quasirandom number generator of Sobol sequences (an algorithm with Gray code implementation and sets of direction numbers proposed by Joe and Kuo [5]),

[2]UNI-DEM has been developed at the Danish National Environmental Research Institute (http://www2.dmu.dk/AtmosphericEnvironment/DEM/), at present - National Centre for Environment and Energy (NERI), Aarhus University.

- software packages
  - R language and environment for statistical computing [15],
  - SIMLAB [16].

The algorithms under consideration are tested numerically for computing sensitivity measures for UNI-DEM model to study sensitivity of ozone concentration according to variation of chemical rates. A comparison with several scrambling approaches (mainly based on Owen scrambling, [6]) also has been done. All algorithms mentioned above are efficient and converge with the expected rate of convergence. It is important to notice that the Monte Carlo algorithm MCA-MSS based on modified Sobol sequences gives similar rates of the relative error in comparison with scrambling approaches. But there are many cases when MCA-MSS has essential advantages. It holds especially for small in values sensitivity indices. The latter case is crucial to provide reliable sensitivity analysis.

Specifying the most important chemical reactions for the model output the specialists from various applied fields (chemistry, physics) may obtain valuable information for an improvement of the model and thus it will lead to an increase of reliability and robustness of predictions.

3 Description of the Visualization Tool

The current tool shown on Figure 2 is constructed to present sensitivity study done for the influence of chemical reaction rates on the variability of the ozone concentrations in the mathematical model UNI-DEM describing remote transport of air pollutants.

The visualization tool has been developed using GUI Builder in Matlab [14]. Its user-friendly menu allows different random number generators, Monte Carlo approaches and sensitivity analysis strategies to be selected in order to visualize corresponding results. Description of the mathematical model under consideration as well as of the algorithms applied is available (see Figure 2). Various results of first-order and total sensitivity indices obtained with MATLAB, R Package, and SIMLAB software, as well as of relative errors and computational times calculated applying numerical approaches mentioned in Section 2 are available (Figure 3).

Acknowledgment

The numerical results presented by the visualization tool have been obtained in a joint work with Prof. Ivan Dimov, Dr. Tzvetan Ostromsky, and Prof. Zahari Zlatev.

This work is partly supported by the Bulgarian NSF Grants DTK 02/44/2009 and DO 02-215/2008.

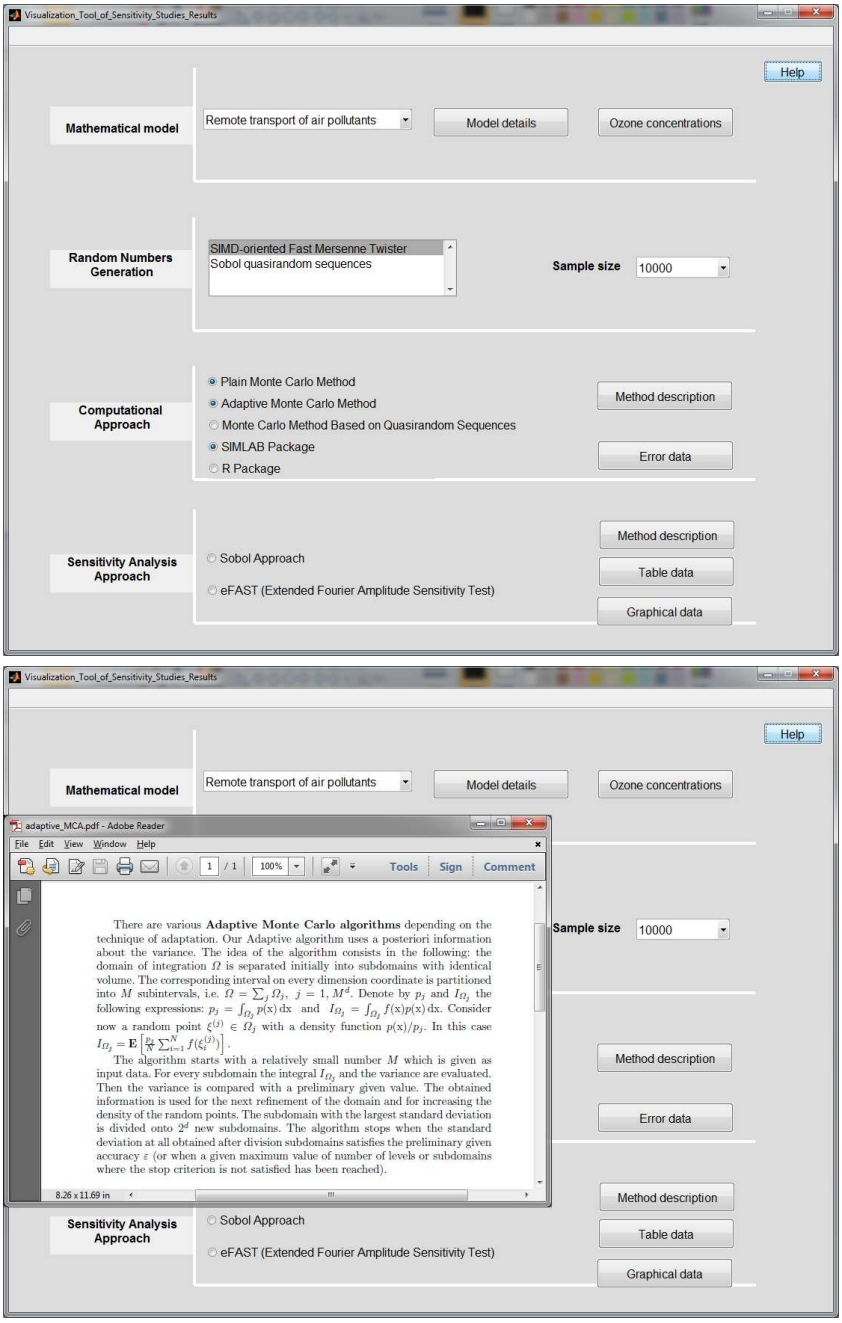

Figure 2: General view of the visualization tool. An example with description of a computational approach.

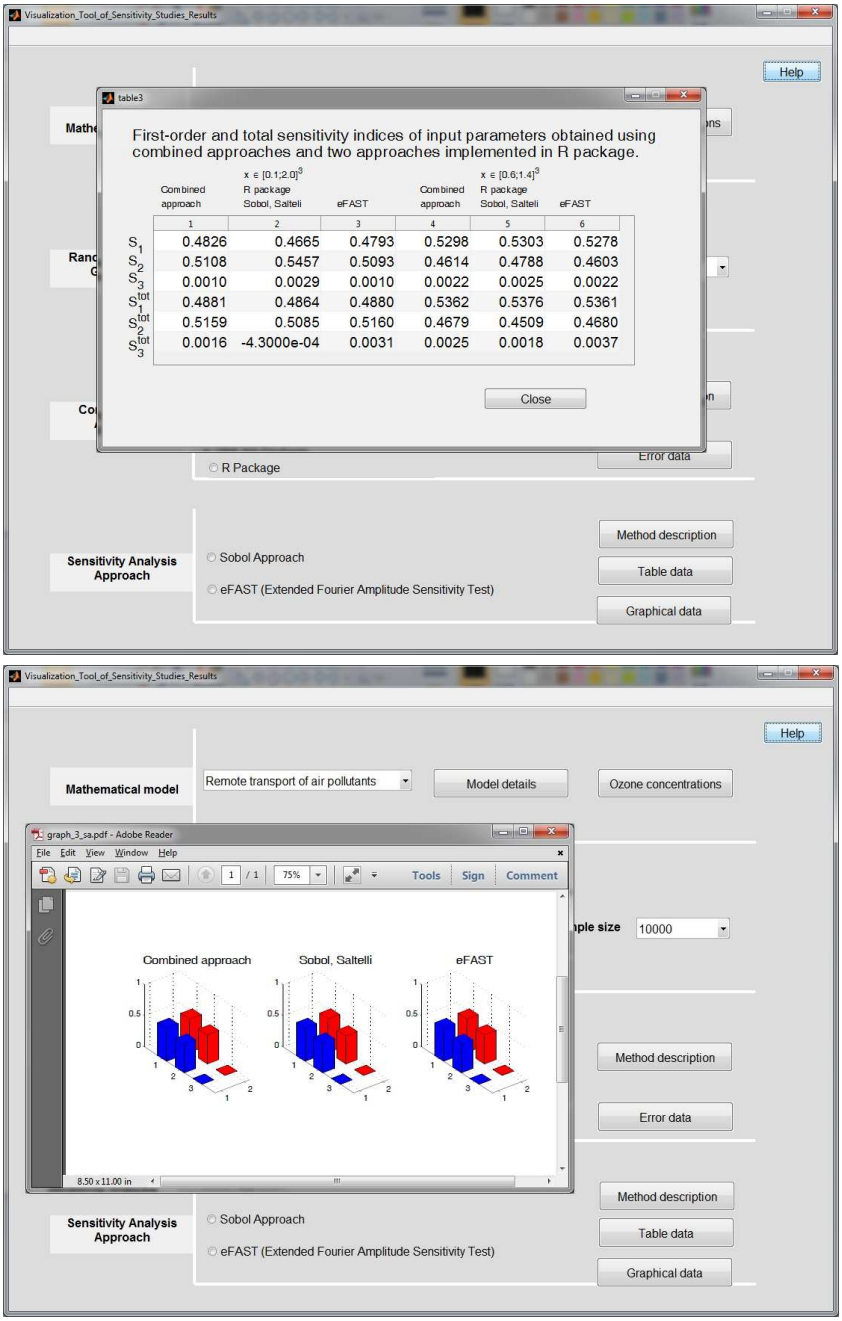

Figure 3: Examples of numerical results presented in a table and a figure.

References

[1] I.T. Dimov, R. Georgieva, Tz. Ostromsky. Monte Carlo Sensitivity Analysis of an Eulerian Large-scale Air Pollution Model. *Reliability Engineering & System Safety*, Elsevier (accepted). Doi: 10.1016/j.ress.2011.06.007.

[2] I.T. Dimov, R. Georgieva. Monte Carlo Method for Numerical Integration based on Sobol's Sequences. - In: Proceeding of NMA'10. LNCS **6046** (2011), 50–59. Springer. ISSN: 0302-9743.

[3] I.T. Dimov, R. Georgieva. Monte Carlo Adaptive Technique for Sensitivity Analysis of a Large-scale Air Pollution Model. - In: Proceeding of LSSC'09. LNCS **5910** (2010), 387–394. Springer. ISSN: 978-3-642-12534-8.

[4] I.T. Dimov, R. Georgieva, S. Ivanovska, Tz. Ostromsky, Z. Zlatev. Studying the Sensitivity of Pollutants Concentrations Caused by Variations of Chemical Rates. *Journal of Computational and Applied Mathematics* **235** (2010), 391-402.

[5] S. Joe, F.Y. Kuo. Constructing Sobol Sequences with Better Two-dimensional Projections. *SIAM J. Sci. Comput.* **30** (2008), 2635–2654.

[6] A. Owen, Randomly Permuted (t, m, s)-nets and (t, s)-sequences. Monte Carlo and Quasi-Monte Carlo Methods in Scientific Computing, 106 in Lecture Notes in Statistics: 299-317, 1995.

[7] M. Saito, M. Matsumoto. SIMD-oriented Fast Mersenne Twister: a 128-bit Pseudorandom Number Generator. - In: Proceeding of MCQMCM'06. Springer, 607–622 (2008).

[8] A. Saltelli, M. Ratto, T. Andres, F. Campolongo, J. Cariboni, D. Gatelli, M. Saisana, S. Tarantola. *Global Sensitivity Analysis. The Primer*. John Wiley & Sons Ltd. (2008). ISBN: 978-0-470-05997-5.

[9] I. M. Sobol'. Global Sensitivity Indices for Nonlinear Mathematical Models and Their Monte Carlo Estimates. *Mathematics and Computers in Simulation* **55 (1-3)** (2001), 271–280.

[10] I. Sobol', E. Myshetskaya. Monte Carlo Estimators for Small Sensitivity Indices. *Monte Carlo Methods and Applications* **13 (5-6)** (2007), 455–465.

[11] V. Schwieger. Variance-based Sensitivity Analysis for Model Evaluation in Engineering Surveys. - In: Proceeding of INGEO 2004 and FIG Regional Central and Eastern European Conference on Engineering Surveying, Bratislava, Slovakia (2004).

[12] Z. Zlatev, I.T. Dimov. *Computational and Numerical Challenges in Environmental Modelling*. Elsevier, Amsterdam (2006).

[13] http://www.math.sci.hiroshima-u.ac.jp/~m-mat/MT/emt.html.

[14] http://www.mathworks.com/.

[15] http://www.r-project.org/.

[16] http://simlab.jrc.ec.europa.eu/.

On the 6-wave equations related to the $\mathfrak{g}_2$ algebra. Minimal sets of scattering data.

V. S. Gerdjikov

Abstract

Here we briefly analyze the 6-wave equations related to the exceptional $\mathfrak{g}_2$ algebra. We demonstrate several inequivalent $\mathbb{Z}_2$-reductions and formulate the minimal sets of scattering data of the relevant Lax operator.

1 Introduction

The integrability of the N-wave equations has been discovered [13] and studied extensively [13, 12, 9, 3, 11] during the 1970'ies. Later it was been shown that N-wave equations can be related to each simple Lie algebra [1, 2, 7]. It was of special interest also to study their reductions [4, 5, 6] using the Mikhailov's reduction group [10].
The aim of the present paper is to explore deeper the 6-wave equations related to the exceptional $\mathfrak{g}_2$ algebra. It is only natural to with the compatibility condition of the operators L and M:

$$\begin{aligned} L\psi &\equiv i\frac{d\psi}{dx} + U(x,t,\lambda)\psi(x,t,\lambda) = 0, \\ M\psi &\equiv i\frac{d\psi}{dt} + V(x,t,\lambda)\psi(x,t,\lambda) = 0, \end{aligned} \tag{1}$$

where

$$\begin{aligned} U(x,t,\lambda) = [J, q(x,t)] - \lambda J, \qquad V(x,t,\lambda) = [I, q(x,t)] - \lambda I \\ q(x,t) = \sum_{\alpha\in\Delta_+} (q_\alpha(x,t)E_\alpha + p_\alpha(x,t)E_{-\alpha}), \end{aligned} \tag{2}$$

and the Cartan elements $J = 3a_1H_1 + a_2H_2$ and $I = 3b_1H_1 + b_2H_2$. We assume that q_α and p_α are smooth complex-valued functions and E_α and H_j, $j = 1, 2$ are the Cartan-Weyl basis of the exceptional $\mathfrak{g}_2$ algebra, see the Appendix. The NLEE

$$i\left[I, \frac{\partial q}{\partial x}\right] - i\left[J, \frac{\partial q}{\partial t}\right] + [[J, q], [I, q(x,t)]] = 0. \tag{3}$$

is a system of 12 equations; the first 6 of them take the form:

$$\begin{aligned}
i(2a_1-3a_2)\frac{\partial q_{10}}{\partial t}-i(2b_1-3b_2)\frac{\partial q_{10}}{\partial x}+\kappa(p_{01}q_{11}-2q_{21}p_{11}+p_{21}q_{31})=0,\\
i(a_1-2a_2)\frac{\partial q_{01}}{\partial t}-i(b_1-2b_2)\frac{\partial q_{01}}{\partial x}-\kappa(p_{10}q_{11}-p_{31}q_{32})=0,\\
i(a_1-3a_2)\frac{\partial q_{11}}{\partial t}-i(b_1-3b_2)\frac{\partial q_{11}}{\partial x}+\kappa(q_{01}q_{10}+2q_{21}p_{10}-p_{21}q_{32})=0,\\
ia_1\frac{\partial q_{21}}{\partial t}-ib_1\frac{\partial q_{21}}{\partial x}+\kappa(p_{11}q_{32}+2q_{11}q_{10}+p_{10}q_{31})=0,\\
i(a_1-a_2)\frac{\partial q_{31}}{\partial t}-i(b_1-b_2)\frac{\partial q_{31}}{\partial x}-\kappa(q_{10}q_{21}+p_{01}q_{32})=0,\\
ia_2\frac{\partial q_{32}}{\partial t}-ib_2\frac{\partial q_{32}}{\partial x}-\kappa(q_{21}q_{11}-q_{01}q_{31})=0,
\end{aligned}\tag{4}$$

where $\kappa=a_1b_2-b_1a_2$ and the indices ij correspond to the root $i\alpha_1+j\alpha_2$, see eq. (7) below. The other 6 equations are obtained from (4) by interchanging q_{ij} and p_{ij}. The 6-wave equations are obtained from (4) by imposing the typical reduction $p_\alpha=\pm q^*_\alpha$. The equations (3) are Hamiltonian ones with Hamiltonian $H_{6\mathrm{w}}=H_0+H_{\mathrm{int}}$:

$$\begin{aligned}
H_0&=\frac{i}{2}\int_{-\infty}^{\infty}dx\ \sum_{\alpha>0}\alpha(I)\left(q_\alpha\frac{\partial p_\alpha}{\partial x}-p_\alpha\frac{\partial q_\alpha}{\partial x}\right),\\
H_{\mathrm{int}}&=-2\kappa\int_{-\infty}^{\infty}dx\ \left(p_{32}(q_{21}q_{11}-q_{01}q_{31})+p_{10}(2q_{21}p_{11}-q_{31}p_{21}-q_{11}p_{01})\right.\\
&\quad\left.-q_{32}(p_{21}p_{11}-q_{01}q_{31})-q_{10}(2p_{21}q_{11}-p_{31}q_{21}-p_{11}q_{01})\right).
\end{aligned}\tag{5}$$

The typical reduction is not the only one that can be imposed on (4). Below we will show other reductions and will discuss the spectral properties of the Lax operator.

2 Preliminaries: The Lie algebra $\mathfrak{g}_2$

The root system of $\mathfrak{g}_2$ is given in fig. 2. The Cartan-Weyl basis satisfies the commutation relations [8]:

$$[H,E_\alpha]=\alpha(H)E_\alpha,\qquad [E_\alpha,E_\beta]=N_{\alpha,\beta}E_{\alpha+\beta},\qquad [E_\alpha,E_{-\alpha}]=H_\alpha.\tag{6}$$

where $E_{-\alpha}=(E_\alpha)^T$. The simple roots and the positive roots are given by:

$$\begin{aligned}
&\alpha_1=\frac{1}{3}(e_1-e_2+2e_3),\qquad &&\alpha_2=e_2-e_3\\
&\alpha_1=10,\qquad &&\alpha_2=01,\qquad &&\alpha_1+\alpha_2=11,\\
&2\alpha_1+\alpha_2=21,\qquad &&3\alpha_1+\alpha_2=31,\qquad &&3\alpha_1+2\alpha_2=32.
\end{aligned}\tag{7}$$

The root 32 is the maximal root of $\mathfrak{g}_2$; its height is $3+2=5$.
The Weyl group is generated by the reflections S_{α_1} and S_{α_2} where by definition $S_\alpha\vec{x}=\vec{x}-\frac{2(\vec{x},\alpha)}{(\alpha,\alpha)}\alpha$. Explicitly the Cartan-Weyl basis for the typical 7-dimensional representation of $\mathfrak{g}_2$ is given in the appendix.

3 Reductions of the 6-wave equations

The Mikhailov's reduction group [10] is a finite group acting on the Lax pair by:

$$C_k(L(\Gamma_k(\lambda))) = \eta_k L(\lambda), \qquad C_k(M(\Gamma_k(\lambda))) = \eta_k M(\lambda). \tag{8}$$

Here $C_k \in \mathrm{Aut}\ \mathfrak{g}$ and $\Gamma_k(\lambda) \in \mathrm{Conf}\,\mathbb{C}$ are the images of g_k and $\eta_k = 1$ or -1 depending on the choice of C_k. Since G_R is a finite group then for each g_k there exist an integer N_k such that $g_k^{N_k} = \mathbb{1}$. In what follows we consider several different realizations of $\mathbb{Z}_2$ reduction groups. Using this method one can classify all inequivalent $\mathbb{Z}_2$-reductions of the N-wave equations [4, 5, 6].

Example 1. *$C_1 = w_0$. $C_1(U^*(x,t,\eta\lambda^*)) + U(x,t,\lambda) = 0$ and $\eta = \pm 1$. This gives:*

$$a_1^* = \eta a_1, \quad a_2^* = \eta a_2, \quad b_1^* = \eta b_1, \quad b_2^* = \eta b_2; \quad p_\alpha = -\eta q_\alpha^* \tag{9}$$

Example 2. *$\Sigma^{-1}U^\dagger(x,t,\eta\lambda^*)\Sigma - U(x,t,\lambda) = 0$, $\eta = \pm 1$ where Σ belongs to the Cartan subgroup and equals $\Sigma = \mathrm{diag}\,(s_1 s_2, s_1, s_2, 1, 1/s_2, 1/s_1, 1/(s_1 s_2))$. Then all Cartan elements become real (purely imaginary) for $\eta = 1$ ($\eta = -1$) and*

$$\begin{aligned} &p_{10} = -\frac{\eta}{s_2} q_{10}^*, && p_{01} = -\frac{\eta}{s_1} q_{01}^*, && p_{11} = -\frac{\eta}{s_1} q_{11}^*, \\ &p_{21} = -\frac{\eta}{s_1 s_2} q_{21}^* \quad , && p_{31} = -\frac{\eta}{s_1 s_2^2} q_{31}^*, && p_{32} = -\frac{\eta}{s_1^2 s_2} q_{32}^*, \end{aligned} \tag{10}$$

In the particular case $s_1 = s_2 = 1$ we obtain one of the typical reductions.

Example 3. *$C_3 = S_{\alpha_1}$. $C_3(U^*(x,t,\eta\lambda^*)) + U(x,t,\lambda) = 0$ and $\eta = \pm 1$. Then:*

$$\begin{aligned} &a_2 = a_1 - \eta a_1^*, && b_2 = b_1 - \eta b_1^*, && q_{31} = \eta q_{01}^*, && p_{10} = \eta q_{10}^*, \ q_{21} = \eta q_{11}^*, \\ &q_{32}^* = \eta q_{32}, && p_{31} = \eta p_{01}^*, && p_{21} = \eta p_{11}^*, && p_{32}^* = \eta p_{32}. \end{aligned} \tag{11}$$

so we obtain a 7–wave system with 2 real and 5 complex waves.

Example 4. *$C_4 = S_{\alpha_2}$. $C_4(U^*(x,t,\eta\lambda^*)) + U(x,t,\lambda) = 0$ and $\eta = \pm 1$. Then:*

$$\begin{aligned} &a_1 = \frac{a_2 - \eta a_2^*}{3}, && b_1 = \frac{b_2 - \eta b_2^*}{3}, && q_{11} = -\eta q_{10}^*, && p_{01} = \eta q_{01}^*, && q_{21}^* = -\eta q_{21}, \\ &q_{32} = \eta q_{31}^*, && p_{11} = -\eta p_{10}^*, && p_{21}^* = -\eta p_{21}, && p_{32} = \eta p_{31}^*. \end{aligned} \tag{12}$$

so we obtain another 7–wave system with 2 real and 5 complex waves.

4 The minimal sets of scattering data of L

The Jost solutions are introduced by:

$$\lim_{x\to\infty} \psi(x,t,\lambda) e^{i\lambda J x} = \mathbb{1}, \qquad \lim_{x\to-\infty} \phi(x,t,\lambda) e^{i\lambda J x} = \mathbb{1}, \tag{13}$$

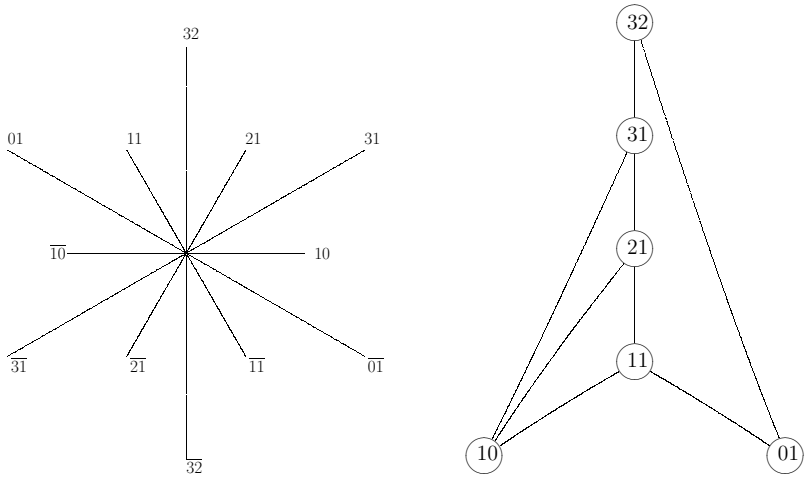

Figure 1: The root system of G_2 (left panel) and the decay scheme of the G_2 6-wave interactions with typical reduction (right panel).

Next we introduce the scattering matrix $T(t,\lambda)$ and its Gauss decomposition:

$$T(\lambda,t) \equiv \hat{\psi}\phi(x,t,\lambda) = T^- D^+ \hat{S}^+ = T^+ D^- \hat{S}^- \tag{14}$$

where $S^\pm$, $T^\pm$, $D^\pm$ are the Gauss factors and $\hat{X} \equiv X^{-1}$. Skipping the details we construct the fundamental analytic solutions (FAS) of L:

$$\chi^\pm(x,t,\lambda) = \phi(x,t,\lambda)S^\pm(t,\lambda) = \psi(x,t,\lambda)T^\mp(t,\lambda)D^\pm(\lambda). \tag{15}$$

As a consequence of this construction there follows that $D^\pm(\lambda)$ are generating functionals of the integrals of motion.
Next instead of solving the inverse scattering problem for the operator L, we use the fact that the FAS $\chi^\pm(x,t,\lambda)$ satisfy a Riemann-Hilbert problem. Introducing $\xi^\pm(x,t,\lambda) = \chi^\pm(x,t,\lambda)e^{-i\lambda Jx}$ we find that

$$\begin{gathered}\xi^+(x,t,\lambda) = \xi^-(x,t,\lambda)G(x,t,\lambda), \qquad G(x,t,\lambda) = e^{-i\lambda Jx}\hat{S}^- S^+ e^{i\lambda Jx}, \\ \lim_{\lambda\to\infty} \xi^\pm(x,t,\lambda) = \mathbb{1}.\end{gathered} \tag{16}$$

We also mention that each of the reductions can easily be extended to the FAS, $T(t,\lambda)$ and its Gauss factors $S^\pm(t,\lambda)$, $T^\pm(t,\lambda)$ and $D^\pm(\lambda)$. Taking the example 1 with $\eta = 1$ and $J^* = J$ we have:

$$\begin{aligned}\xi^{+,*}(x,t,\lambda^*) &= C_1(\xi^-(x,t,\lambda)), & S^{+,*}(t,\lambda^*) &= C_1(S^-(t,\lambda)), \\ T^{+,*}(t,\lambda^*) &= C_1(T^-(t,\lambda)), & D^{+,*}(\lambda^*) &= C_1(D^-(\lambda)).\end{aligned} \tag{17}$$

Finally we formulate the main result in this paper.

Proposition 1. *Let the potential $q^*(x,t) = C_1(q)$ be such that L has no discrete eigenvalues. Then we can introduce two minimal sets of scattering data, that determine uniquely both the scattering matrix $T(t,\lambda)$ and the potential $q(x,t)$ given by:*

$$\mathcal{T}_1 \equiv \{s^+_\alpha(t,\lambda), \quad \alpha \in \Delta_+\}, \qquad \mathcal{T}_2 \equiv \{t^+_\alpha(t,\lambda), \quad \alpha \in \Delta_+\}, \tag{18}$$

where the coefficients $s^+_\alpha(t,\lambda)$ and $t^+_\alpha(t,\lambda)$ determine the Gauss factors $S^+(t,\lambda)$ and $T^+(t,\lambda)$, see eq. (21) below.

Proof 1. *The fact that L has no discrete eigenvalues means that $\xi^+(x,t,\lambda)$ are regular solutions of the RHP. Using eq. (17) from $\mathcal{T}_1$ (resp. $\mathcal{T}_2$) we recover $S^\pm(t,\lambda)$ (resp. $T^\pm(t,\lambda)$) and the sewing function $G(x,t,\lambda)$. It determines uniquely the regular solutions $\xi^\pm(x,t,\lambda)$. Next we analyze their asymptotics for $x \to \infty$ (resp. for $x \to -\infty$). This allows us to show that $\mathcal{T}_1$ (resp. $\mathcal{T}_2$) determines uniquely $D^\pm(\lambda)$ and $T^\pm(t,\lambda)$ (resp. $S^\pm(t,\lambda)$) and, as a consequence, $T(t,\lambda)$. It remains to show how one recovers the potential $q(x,t)$. Using the canonical normalization of the RHP and the Zakharov-Shabat theorem (see [11, 1]) we find that:*

$$[J, q(x,t)] = \lim_{\lambda\to\infty} \lambda(J - \xi^+(x,t,\lambda) J \hat{\xi}^+(x,t,\lambda)). \qquad \square. \tag{19}$$

5 Conclusions

We analyzed several reductions of the 6-wave equations related to the exceptional $\mathfrak{g}_2$ algebra. The system describes a complicated cascade of 3-wave interactions (see fig. 1). Next we constructed the Gauss factors of the scattering matrix and showed that they can be used to construct the minimal sets of scattering data for L.

A Cartan Weyl basis of $\mathfrak{g}_2$ and the Gauss factors

Here we provide explicitly the first fundamental 7-dimensional representation of G_2 along with some additional properties.

$$H_{10} = \frac{1}{3}(\mathcal{E}_{11} - \mathcal{E}_{22} + 2(\mathcal{E}_{33} - \mathcal{E}_{55}) + \mathcal{E}_{66} - \mathcal{E}_{77}), \quad H_{01} = \mathcal{E}_{22} - \mathcal{E}_{33} + \mathcal{E}_{55} - \mathcal{E}_{66}.$$

$$\begin{aligned} E_{10} &= \mathcal{E}_{12} - \mathcal{E}_{67} + \sqrt{2}(\mathcal{E}_{34} - \mathcal{E}_{45}), & E_{01} &= \mathcal{E}_{23} - \mathcal{E}_{56}, \\ E_{11} &= \mathcal{E}_{13} - \mathcal{E}_{57} - \sqrt{2}(\mathcal{E}_{24} - \mathcal{E}_{46}), & E_{31} &= \mathcal{E}_{15} - \mathcal{E}_{37}, \\ E_{21} &= \mathcal{E}_{25} - \mathcal{E}_{36} + \sqrt{2}(\mathcal{E}_{14} - \mathcal{E}_{47}), & E_{32} &= \mathcal{E}_{16} - \mathcal{E}_{27}, \end{aligned} \tag{20}$$

Here $(\mathcal{E}_{km})_{sn} = \delta_{ks}\delta_{mn}$. The Gauss factors, introduced in (14) take the form:

$$S^\pm(\lambda,t) = \exp\left(\sum_{\alpha\in\Delta_+} s^\pm(\lambda,t) E_{\pm\alpha}\right), \quad T^\pm(\lambda,t) = \exp\left(\sum_{\alpha\in\Delta_+} t^\pm(\lambda,t) E_{\pm\alpha}\right), \tag{21}$$

References

[1] Gerdjikov V. S., *Generalised Fourier Transforms for the Soliton Equations. Gauge Covariant Formulation.* Inverse Problems **2** (1986) 51–74.

[2] Gerdjikov V. S., *Algebraic and Analytic Aspects of N-wave Type Equations.* Contemporary Mathematics **301** (2002) 35-68.

[3] V. S. Gerdjikov, P. P. Kulish. *The generating operator for the $n\times n$ linear system.* Physica D **3D** (1981) 549–564.

[4] V. S. Gerdjikov, G. G. Grahovski, N. A. Kostov. *Reductions of N-wave interactions related to low-rank simple Lie algebras. I: $\mathbb{Z}_2$- reductions.* **nlin.SI/0006001**; J. Phys. A: Math & Gen. **34**, 9425-9461 (2001).

[5] V. S. Gerdjikov, G. G. Grahovski, R. I. Ivanov, N. A. Kostov. *N-wave interactions related to simple Lie algebras. $\mathbb{Z}_2$- reductions and soliton solutions.* **nlin.SI/0009034**. Inverse Problems **17**, 999-1015 (2001).

[6] V. S. Gerdjikov, G. G. Grahovski. *Reductions and real forms of hamiltonian systems related to N-wave type equations.* **nlin.SI/0009035**; Balkan Phys. Lett. BPL (Proc. Suppl.), BPU-4, pp.531-534 (2000).

[7] V. S. Gerdjikov, G. Vilasi, A. B. Yanovski. *Integrable Hamiltonian Hierarchies. Spectral and Geometric Methods* Lecture Notes in Physics **748**, Springer Verlag, Berlin, Heidelberg, New York (2008). ISBN: 978-3-540-77054-1.

[8] Helgasson, S, Differential geometry, Lie groups and symmetric spaces Academic Press 1978.

[9] D.J. Kaup, A. Reiman, and A. Bers. *Space-Time Evolution of Nonlinear Three-Wave Interactions in an Homogeneous Medium.* Rev. Mod. Phys. **51**, 275–310 (1979).

[10] Mikhailov A. V. *On the Integrability of Two-dimensional Generalization of the Toda Lattice*, Lett. in Jour. of Exper. and Theor. Phys. **30** (1979) 443–448;
Mikhailov A V. *The reduction problem and the inverse scattering problem.* Physica D, **3D**, no. 1/2, 73–117 (1981).

[11] V. E. Zakharov, S. V. Manakov, S. P. Novikov, L. P. Pitaevskii. *Theory of solitons: the inverse scattering method.* (Plenum, N.Y.: Consultants Bureau, 1984).

[12] Shabat A B. Inverse scattering problem for a system of differential equations. Functional Annal. & Appl. **9**, n.3, 75–78 (1975);
Shabat A B. *The inverse scattering problem.* Diff. Equations **15**, 1824–1834 (1979) (In Russian).

[13] V. E. Zakharov, S. V. Manakov. The exact theory of resonanse wave packet interactions in nonlinear media. INR preprint, Novosibirsk, (1974); JTEPh **69** (1975) 1654–1673.

Quasi-Monte Carlo Approach for Solving BVPs

Aneta Karaivanova and Todor Gurov

1 Motivation

Quasi-Monte Carlo (QMC) methods offer higher precision and faster convergence for integrals and some kinds of integral equation. Some of the advantages of QMC are:

- Improved convergence (in practice the log factor is not observed);
- Can be either completely deterministic or include some randomness;
- Some families of sequences can be tuned to a particular application;
- Scrambling provides a way of combining the advantages of Monte Carlo and quasi-Monte Carlo methods, offering automatic error estimation;
- Faster generation than pseudo-random numbers;
- Amenable to parallel implementation;
- The spread of computational grids makes the parallelization properties of the MC and QMC algorithms important for the practical implementation.

The use of QMC methods for BVPs is studied in many papers. Here we refer to quasi-Monte Carlo variants of three Monte Carlo algorithms: grid-walk, walk-on-spheres and walk-on-balls, [7, 8]. The first one uses a discretization of the problem on a mesh and solves the linear algebraic system which approximates the original problem. The second two methods use an integral representation of the problem which leads to a *Random Walk on Spheres* (WoS) or to a *Random Walk on Balls* (WoB) method. Different strategies for using quasirandom sequences are proposed and tested in order to generate quasirandom walks on grids, spheres, and balls. The QMC methods preserve the advantages of the Monte Carlo for solving problems in complicated domains, and show slightly better rates of convergence for QMC methods. Additionally, the Walk-on-Balls method has been extensively studied in [7, 8] using scrambled sequences and c.u.d. sequences. In this work we present numerical results for Walk-on-Spheres (WoS) using scrambled sequences.

2 The Monte Carlo Approach

Let $G \subset \mathbf{R}^d$ be a bounded domain with boundary ∂G. We consider the boundary value problem

$$Lu \equiv \sum_{|\alpha| \leq 2m} a_\alpha(x) D^\alpha u(x) = -f(x), \qquad x \in G, \tag{1}$$

$$u(x) = \varphi(x), \qquad x \in \partial G\,, \tag{2}$$

where L is an arbitrary elliptic operator in $\mathbf{R}^d$ of order $2m$, $a_\alpha(x) \in C^\infty(\mathbf{R}^d)$, and the function $f(x)$ belongs to the Banach space $\mathbf{X}(G)$. Assume that $f(x)$, $\varphi(x)$, and the boundary ∂G satisfy conditions ensuring that the solution of the problem (1), (2) exists and is unique. We study Monte Carlo algorithms for calculating linear functionals of the solution of the problem (1), (2)

$$J(u) = (h, u) = \int_G u(x)h(x)dx, \tag{3}$$

where $h \in \mathbf{X}^*(G)$ ($\mathbf{X}^*(G)$ is the conjugate functional space to $\mathbf{X}(G)$).

For many applications $\mathbf{X} = \mathbf{L}_1$ and thus $\mathbf{X}^* = \mathbf{L}^\infty$, or $\mathbf{X} = \mathbf{X}^* = \mathbf{L}_2$.

Suppose we can rewrite (1), (2) as

$$u = Ku + f. \tag{4}$$

Then we consider the sequence of functions $u_1, u_2, ...$, defined by the recursion

$$u_{k+1} = Ku_k + f, \;\; k = 1, 2, \ldots \tag{5}$$

The formal solution of (4) is the truncated von Neuman series

$$u_{k+1} = f + Kf + \cdots + K^{k-1}f + K^k u_0, \qquad k > 0\,, \tag{6}$$

where K^k is the k-th iterate of K.
The truncation error of (6) is

$$u_k - u = K^k(u_0 - u). \tag{7}$$

Our approaches (Walk-on=Grid, Walk-on-Spheres, and Walk-on-Balls) correspond to two special cases of the linear operator K: (i) K is a matrix and u and f are vectors; (ii) K is an ordinary integral transform

$$Ku = \int_G k(x, y)u(y)dy\,. \tag{8}$$

To estimate the functional (3) via a MCM[1], we construct random walks using h to select initial spatial coordinates for each random walk, and the kernel $k(x, y)$, suitably normalized, to decide between termination and continuation of each random walk, and to determine the location of next point. There are numerous ways to accomplish this.

Consider the following **r**andom **v**ariable (RV) whose mathematical expectation is equal to $J(u)$, [5]:

$$\theta[h] = \frac{h(\xi_0)}{\pi(\xi_0)} \sum_{j=0}^{\infty} Q_j f(\xi_j), \tag{9}$$

[1]We develop the solution in a Neumann series under the condition $||K^{n_0}|| < 1$ for some $n_0 \geq 1$

where $Q_0 = 1$; $Q_j = Q_{j-1}\dfrac{k(\xi_{j-1},\xi_j)}{p(\xi_{j-1},\xi_j)}, j = 1, 2, \ldots$. Here $\xi_0, \xi_1, \ldots$ is a Markov chain (random walk) in the domain G with initial probability density $\pi(x)$ and transition probability density $p(x, y)$. The latter is equal to the normalized integral equation kernel.

The Monte Carlo estimate of $J(u) = E[\theta]$ is

$$J(u) = E[\theta] \approx \frac{1}{N}\sum_{s=1}^{N}\{\theta_{k_s}\}_s, \tag{10}$$

where $\{\theta_{k_s}\}_s$ is the s-th realization of the RV θ on a Markov chain with length k_s, and N is the number of Markov chains (random walks) realized. The statistical error is $err_N \approx \sigma(\theta)N^{-\frac{1}{2}}$ where $\sigma(\theta)$ is the standard deviation of our statistic, θ.

In case K is the matrix $L = \{l_{ij}\}$, we construct the following r.v.:

$$\theta[h] = \frac{h_{k_0}}{p_0}\sum_{\nu=0}^{\infty} Q_\nu f_{k_\nu} \ , \tag{11}$$

where

$$Q_0 = 1; \qquad Q_\nu = Q_{\nu-1}\frac{l_{k_{\nu-1},k_\nu}}{p_{k_{\nu-1},k_\nu}}, \qquad \nu = 1, 2, \ldots$$

and $k_0, k_1, \ldots$ is a Markov chain on the elements of the matrix L constructed by using initial probability p_0 and transition probability $p_{k_{\nu-1},k_\nu}$ for choosing the next element $l_{k_{\nu-1},k_\nu}$ of the matrix L.

3 Quasi-Random Walks

Here we discuss how to construct a quasi-MCM for the problem considered here.
Error bounds arising in the use of quasi-MCMs for integral equations is based on Chelson's estimates, [3]. Below Chelson's results are rewritten in terms related to our particular problem:

$$\left| u(\xi_0) - \frac{1}{N}\sum_{1}^{N}\theta_s^*(\xi_0)\right| \le V(\theta^*)\ D_N^*(Q) \tag{12}$$

where Q is a sequence of quasirandom vectors in $[0, 1)^{dT}$, d is the number of QRNs in one step of a random walk, T is the maximal number of steps in a single random walk, and θ^* corresponds to θ for the random walk $\xi_0, \xi_1, \ldots, \xi_{k_\varepsilon}$ generated from Q by a one-to-one map. Space precludes more discussion of the work of Chelson, but the reader is referred to the original for clarification, [3].
This digestion of Chelson's results is the integral equation analog of the Koksma-Hlawka inequality. It ensures convergence, but it's rate is very pessimistic due to the high dimension of the quasirandom sequence.

The effectiveness of quasi-MCMs has some important limitations. First of all, quasi-MCMs may not be directly applicable to certain simulations, due to correlations between points of the quasirandom sequence. This problem can be overcome in many cases by scrambling of the QRNs used. However, as the resulting integral is often of very high dimensional, this leads to a second limitation as the improved accuracy of quasi-MCMs applied to integrals is generally lost in very high dimensions.

In the MCM described in this paper, a random walk is a trajectory

$$\xi_0 \to \xi_1 \to \ldots \to \xi_{k_\varepsilon},$$

where ξ_0 is the initial point and the transition probability from ξ_{j-1} to ξ_j is $p(\xi_{j-1}, \xi_j)$. Using quasirandom sequences in this problem is not so simple. One possible approach is to use k_ε-dimensional sequence for random walk on spheres or grid, and $k_\varepsilon(1 + 3S_0^{-1}) \approx 7k_\varepsilon$- dimensional sequence for random walk on balls, with length N for N random walks. Here k_ε is the length of a Markov chain and S_0 is the efficiency of the *Acceptance-rejection method* used in Walk-On-Balls method. Here we interpret the trajectory as a point in $G \times \ldots \times G = G^{i+1}$, and the density of this point is:

$$p_i(\xi_0, \xi_1, \ldots \xi_i) = p(\xi_0, \xi_1) \ldots p(\xi_{i-1}, \xi_i). \tag{13}$$

The difficulty here is that the dimension of such a sequence is very high (several hundreds for RWB) and, consequently, the discrepancy of such a high dimensional quasirandom sequence is approximately that of a pseudorandom sequence and therefore provides no improvement over ordinary MCMs.
In [7] and [8] the QMC variant of ROW has been considered and two variants have been proposed - an algorithm that uses c.u.d. sequences and an algorithm that uses a special case of the scrambled Halton sequences. The results are very good. In this work we continue with application of scrambled quasirandom sequences for solving Poisson equation.

4 Numerical Tests and Conclusion

We consider the following Poisson equation:

$$\frac{1}{2}\Delta u(\mathbf{x}) = -(1 - \frac{r^2}{2})e^{-r^2/2} \tag{14}$$

with the boundary conditions $u(r, 0) = e^{-r^2/2}$, $u(r, -3\pi/2) = -r^{1/3} + e^{-r^2/2}$, and $u(1, \theta) = \sin(\theta/3) + e^{-1/2}$.
The known analytic solution is

$$u(r, \theta) = r^{1/3} \sin(\theta/3) + e^{-r^2/2}. \tag{15}$$

Here we use a k_ε-dimensional sequence with length N for N random walks, where k_ε is the length of the Markov chain (see Figure 1). The maximum dimension is around 100 and the average dimension about 14.

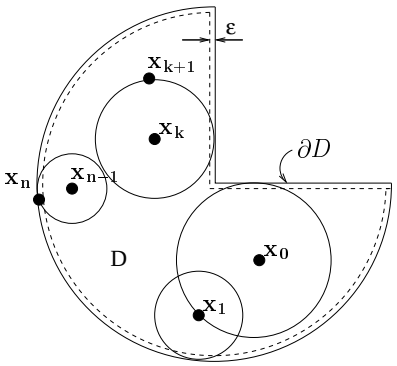

Figure 1: Modified WOS. $\mathbf{x_0}$, $\mathbf{x_1}$, ..., $\mathbf{x_k}$, ..., $\mathbf{x_n}$ are a series of discrete jumps of a Brownian trajectory which terminates on absorption in the ϵ-absorption layer.

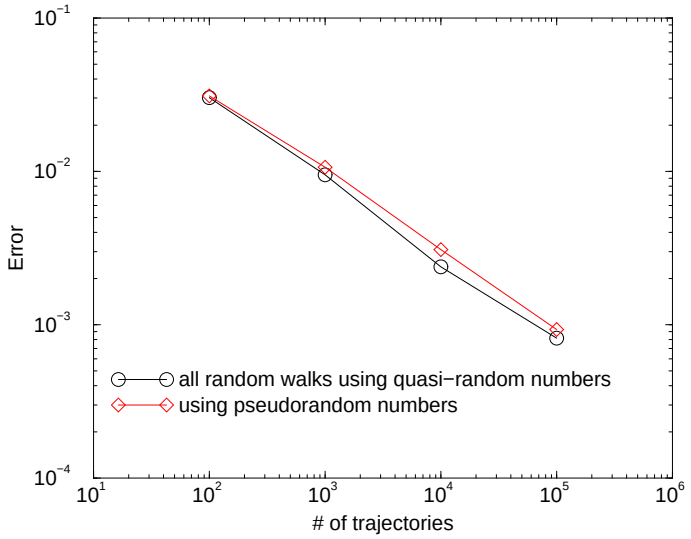

Figure 2: Error versus number of trajectories for MCM and quasi-MCM using Niederreiter sequence.

Although the numerical tests show very small improvement in accuracy using scrambled quasirandom sequences (see Fig. 2), the actual benefit is the decreased computational time and readiness for parallel and distributed implementation.

Acknowledgements. This work has been supported by the National Science Fund of Bulgaria under grant DO02-146/2008.

References

[1] R. E. Caflisch, Monte Carlo and quasi-Monte Carlo methods, Acta Numerica, 7: 1–49, 1998.

[2] S. Chaudhary, Acceleration of Monte Carlo Methods using Low Discrepancy Sequences, Dissertation, University of California, Los Angeles, 2004.

[3] P. Chelson, Quasi-Random Techniques for Monte Carlo Methods, Ph.D. dissertation, The Claremont Graduate School, 1976.

[4] B. Elepov, G. Mikhailov, To the theory of Monte Carlo estimations connected with random walk on spheres, Sib. mat. journal, Vol. 36, No.3:543–550, 1995 (in Russian).

[5] S.M. Ermakov, G.A. Mikhailov, Statistical Modeling, Nauka, Mosow, 1982.

[6] S. Ermakov, V. Nekrutkin, V. Sipin, Random Processes for solving classical equations of the mathematical physics, Nauka, Moscow, 1984.

[7] A. Karaivanova, H. Chi, T. Gurov, Quasi-random walks on balls using c.u.d., Lecture Notes in Computer Science, Vol. 4310 . Springer-Verlag, Berlin Heidelberg New York (2007) 165–172.

[8] A. Karaivanova, H. Chi, T. Gurov, Error Analysis of Quasirandom Walks on Balls, MIPRO/GVS 2009, ISBN 978-953-233-044-1, pp. 285-289.

[9] A. Karaivanova, M. Mascagni, N. Simonov, Solving BVPs using quasirandom walks on the boundary, Lecture Notes in Computer Science, Vol. 2907. Springer-Verlag, Berlin Heidelberg New York (2004) 162–169.

[10] M. Mascagni, A. Karaivanova, C. Hwang, Quasi-Monte Carlo Methods for Elliptic BVPs, Monte Carlo and Quasi-Monte Carlo Methods 2002, Springer, (H. Niederreiter, Ed.):345-356.

Positivity Preserving Numerical Methods for Haptotaxis Models

Mikhail K. Kolev, Miglena N. Koleva, Lubin G. Vulkov

1 Introduction

The application of mathematical and computational methods in biosciences is a challenging and promising area of research. In particular, during the last several decades mathematics has been widely applied to model such complex processes as viral infections and cancer development and progression. We consider the following reaction-diffusion-haptotaxis model problem

$$\begin{aligned} \frac{\partial n}{\partial t} &= d_n \frac{\partial^2 n}{\partial x^2} - \gamma \frac{\partial}{\partial x}\left(n \frac{\partial f}{\partial x} \right) + H_1(n,f), \\ \frac{\partial f}{\partial t} &= -\eta m f + H_2(n,f), \\ \frac{\partial m}{\partial t} &= d_m \frac{\partial^2 m}{\partial x^2} - \beta m + H_3(n,f). \end{aligned} \tag{1}$$

The unknown functions $n = n(x,t)$, $f = f(x,t)$, $m = m(x,t)$ depend on the space variable x (the distance from the centre of the tumour) belonging to the scaled domain $\overline{\Omega} = [0,1]$ of tissue and time t; d_n, γ, η, d_m and β are given positive constants. The system (1) describes interactions between cancer cells (their density is denoted by the function n), extracellular matrix (its density is denoted by the function f), and matrix degradative enzymes (their concentration is denoted by the function m).
This system is a part of a more general model of cancer invasion proposed by Anderson et al.[1] and developed later in a series of papers (see for example [2]). Various modifications of the model have been numerically investigated in [6, 10]. Numerical methods for solutions of Keller-Segel chemotaxis systems has been proposed in [3, 5, 12], see also references therein.
The system (1) will be solved numerically at the boundary conditions

$$\frac{\partial n}{\partial x}(0,t) = \frac{\gamma}{d_n} n(0,t) \frac{\partial f}{\partial x}(0,t), \quad \frac{\partial m}{\partial x}(0,t) = 0, \quad n(1,t) = 0, \quad m(1,t) = 0, \tag{2}$$

and initial conditions

$$n(x,0) = n_0(x), \quad f(x,0) = f_0(x), \quad m(x,0) = m_0(x), \quad n_0, f_0, m_0 \geq 0, \ \not\equiv 0. \tag{3}$$

The solutions to the considered advection-diffusion-reaction equations describe concentrations or densities of molecular or cellular populations, these physical quantities are necessarily non-negative. Therefore, the solutions of the model are also non-negative. However, standard numerical integration methods using finite difference or

finite element discretizations do not guarantee the non-negativity of the numerical solutions.
Here we will develop efficient, positivity preserving numerical methods for the model problem (1)-(3), with $H_1(n,f) = H_2(n,f) = 0$, $H_3(n,f) = \alpha n$, where $\alpha > 0$ is a given constant.

2 Numerical methods

Let N is a positive number and $h = 1/N$. In the interval $[0,1]$ we define the uniform mesh $\overline{\omega}_h = \{x_i = ih,\ i = 0,\dots,N\}$ and grid points over $[0,T]$, given by $t^{k+1} = t^k + \tau_k$, $k = 0,1,2,\dots$, $t^0 = 0$. In the discrete space, the approximations of $n(x_i,t^k)$, $m(x_i,t^k)$, $f(x_i,t^k)$ and $\frac{\partial f}{\partial x}(x_i,t^k)$ are denoted by n_i^k, m_i^k, f_i^k and $f_{xi}^{\ k}$, respectively. A second order approximation of $f_{xi}^{\ k}$, $i = 0,1,\dots,N$ is defined by

$$f_{x0}^{\ k} = \frac{f_0^k - 3f_1^k + 2f_2^k}{h},\quad f_{xi}^{\ k} = \frac{f_{i+1}^k - f_{i-1}^k}{2h},\quad f_{xN}^{\ k} = -\frac{f_N^k - 3f_{N-1}^k + 2f_{N-2}^k}{h}. \quad (4)$$

Let $n_i^k \geq 0$, $m_i^k \geq 0$ and $f_i^k \geq 0$, $i = 0,\dots,N$ are known. In order to find n_i^{k+1}, m_i^{k+1} and f_i^{k+1} in such a way that allows us to avoid treating a large system of equations, we solve consecutively and separately the following Discrete Problems (DP).
DP 1. Find n_i^{k+1}, $i = 0,\dots,N$ from the following discrete scheme

$$\begin{aligned}
&\mathcal{L}_0(n_0^{k+1}, n_1^{k+1}) = \mathcal{F}_0(n_0^k, n_1^k, f_0^k, f_1^k),\\
&\mathcal{L}_i(n_{i\pm1}^{k+1}, n_i^{k+1}) = \mathcal{F}_i(n_{i\pm1}^k, n_i^k, f_{i\pm1}^k, f_i^k), \quad i = 1,\dots,N-1,\\
&n_N^{k+1} = 0.
\end{aligned}$$

DP 2. For n_i^{k+1}, $i = 0,\dots,N$ computed in DP 1, find m_i^{k+1} from the system

$$\begin{aligned}
&\left(\frac{1}{\tau_k} + \frac{2d_m}{h^2} + \beta\right) m_0^{k+1} - \frac{2d_m}{h^2} m_1^{k+1} = \frac{1}{\tau_k} m_0^k + \alpha n_0^{k+1},\\
&\left(\frac{1}{\tau_k} + \frac{2d_m}{h^2} + \beta\right) m_i^{k+1} - \frac{d_m}{h^2}(m_{i+1}^{k+1} + m_{i-1}^{k+1}) = \frac{1}{\tau_k} m_i^k + \alpha n_i^{k+1},\quad i = 1,\dots,N-1,\\
&m_N^{k+1} = 0.
\end{aligned}$$

DP 3. For m_i^{k+1}, $i = 0,\dots,N$ computed in DP 2, find f_i^{k+1} solving the system

$$\left(\frac{1}{\tau_k} + \eta m_i^{k+1}\right) f_i^{k+1} = \frac{1}{\tau_k} f_i^k, \quad i = 0,\dots,N.$$

Further we present three numerical methods (Methods I - III) for solving the model problem (1)-(3), which differ only by the operators $\mathcal{L}_i$ and $\mathcal{F}_i$, $i = 0,\dots,N$ in DP 1. Methods I,II are based on the flux-limited van Leer technique [5, 7]. The limiter Φ of the flux is a nonlinear function of neighboring fluxes that defines a high order accurate oscillation-free scheme on the base of low order positive one. For the solution

of the corresponding explicit-implicit DP1, the property: if $n_i^k \geq 0$, then $n_i^{k+1} \geq 0$ is guaranteed, under a time step restriction. Method III is a development of the idea presented in [4] for advection-diffusion-reaction equations. In this case, DP1 is a fully explicit and the property: if $n_i^k > 0$, then $n_i^{k+1} > 0$, is provided without restriction for the time step size, i.e. this method is unconditionally positive.

2.1 Method I

Let $F_{i+1/2}^k$ be a consistent approximation of the flux $n\frac{\partial f}{\partial x}$ at point $(x_{i+1/2}, t^k)$ and $\widetilde{f}_i^k = n_i^k f_{x_i}^{\ k}$. Then the first equation in (1) is approximated in space by the following semi-discrete, conservative scheme

$$\frac{n_i^{k+1} - n_i^k}{\tau_k} = d_n \frac{n_{i+1}^{k+1} - 2n_i^{k+1} + n_{i-1}^{k+1}}{h^2} - \frac{\gamma}{h}(F_{i+1/2}^k - F_{i-1/2}^k), \tag{5}$$

where $F_{i+1/2}^k$ is presented by two invariant forms, at this stage formally indicated only by the sign of $f_{x_i}^{\ k}$

$$F_{i+1/2}^k = \begin{cases} \widetilde{f}_i^k + \dfrac{1}{2}\Phi(r_{i+1/2}^k)(\widetilde{f}_i^k - \widetilde{f}_{i-1}^k), & \text{for } \ f_{x_i}^{\ k} \geq 0, \\ \widetilde{f}_{i+1}^k + \dfrac{1}{2}\Phi(r_{i+3/2}^{k\ -1})(\widetilde{f}_{i+1}^k - \widetilde{f}_{i+2}^k), & \text{for } \ f_{x_i}^{\ k} < 0, \end{cases} \tag{6}$$

$$r_{i+1/2}^k = \frac{\widetilde{f}_{i+1}^k - \widetilde{f}_i^k}{\widetilde{f}_i^k - \widetilde{f}_{i-1}^k}, \qquad \Phi(r) = \frac{|r| + r}{1 + |r|} \ \text{ (van Leer limiter [5])}, \tag{7}$$

where $\Phi(r)$ is Lipschitz continuous and continuously differentiable for all $r \neq 0$ and

$$\Phi(r) = 0, \ \text{ if } \ r \leq 0 \ \text{ and } \ 0 \leq \Phi(r) \leq \delta; \ \ \Phi(r) \leq 2r \ \text{ if } \ r > 0, \ \ \delta = 2. \tag{8}$$

Just as in [5], in real computations we add small positive number ($\sim 10^{-30}$) to both numerator and denominator of $r_{i+1/2}^k$ to avoid division by zero in uniform flow regions. To obtain a second order discretization for boundary conditions we apply the well known technique of involving fictitious grid nodes [11]. Thus, the corresponding operators in DP 1 become

$$\mathcal{L}_0 = \left(\tfrac{1}{\tau_k} + \tfrac{2d_n}{h^2}\right) n_0^{k+1} - \tfrac{2d_n}{h^2} n_1^{k+1}, \quad \mathcal{L}_i = \left(\tfrac{1}{\tau_k} + \tfrac{2d_n}{h^2}\right) n_i^{k+1} - \tfrac{d_n}{h^2}(n_{i+1}^{k+1} + n_{i-1}^{k+1}),$$
$$\mathcal{F}_0 = \tfrac{1}{\tau_k} n_0^k - \tfrac{2\gamma}{h} L_0^k, \quad \mathcal{F}_i = \tfrac{1}{\tau_k} n_i^k - \tfrac{\gamma}{h} L_i^k,$$

where the form of L_i^k, $i = 0, \ldots, N-1$ depends on the following cases

$$\text{case 1} : n_i^k > 0 \ \text{ and } \ f_{x_i}^{\ k} \geq 0 \ \text{ or } \ n_i^k = 0 \ \text{ and } \ f_{x_{i-1}}^{\ k} \geq 0,$$
$$\text{case 2} : n_i^k > 0 \ \text{ and } \ f_{x_i}^{\ k} < 0 \ \text{ or } \ n_i^k = 0 \ \text{ and } \ f_{x_{i+1}}^{\ k} \leq 0.$$

Namely, we have

$$L_0^k = \begin{cases} \widetilde{f}_0^k + \frac{1}{2}\Phi(r_{1/2}^k)(\widetilde{f}_0^k - \widetilde{f}_{-1}^k), & \text{if case 1 for } i=0, \\ \widetilde{f}_0^k + \left[1 - \frac{1}{2}\Phi(r_{3/2}^{k\,-1}) r_{3/2}^k\right](\widetilde{f}_1^k - \widetilde{f}_0^k), & \text{if case 2 for } i=0, \\ 0, & \text{otherwise,} \end{cases}$$

$$L_i^k = \begin{cases} \left[1 + \frac{1}{2}\Phi(r_{i+1/2}^k) - \frac{\Phi(r_{i-1/2}^k)}{2r_{i-1/2}^k}\right](\widetilde{f}_i^k - \widetilde{f}_{i-1}^k), & \text{if case 1, } i=1,\ldots,N-1, \\ \left[1 + \frac{1}{2}\Phi(r_{i+1/2}^{k\,-1}) - \frac{\Phi(r_{i+3/2}^{k\,-1})}{2r_{i+3/2}^{k\,-1}}\right](\widetilde{f}_{i+1}^k - \widetilde{f}_i^k), & \text{if case 2, } i=1,\ldots,N-1, \\ 0, & \text{otherwise,} \end{cases}$$

Here the terms in brackets $[\cdot]$ are always positive.
External solutions $\widetilde{f}_{-1}^k$ and $\widetilde{f}_{N+1}^k$ are computed by second order extrapolation formulae

$$\widetilde{f}_{-1}^k = 3\widetilde{f}_0^k - 3\widetilde{f}_1^k + \widetilde{f}_2^k \quad \text{and} \quad \widetilde{f}_{N+1}^k = 3\widetilde{f}_N^k - 3\widetilde{f}_{N-1}^k + \widetilde{f}_{N-2}^k. \tag{9}$$

Theorem 1. *Let $n_i^k \geq 0$, $i=0,\ldots,N$. If $\tau_k \leq h/(8\gamma\|\mathbf{f}_{\mathbf{x}}^k\|)$, $\|\mathbf{f}_{\mathbf{x}}^k\| = \max\limits_{0\leq i\leq N} |f_{x_i}^{\,k}|$, then there exist solution $n_i^{k+1} \geq 0$, $i=0,\ldots,N$ of DP 1 for Method I.*

The non-negativity of m_i^{k+1}, f_i^{k+1}, $i=0,\ldots,N$ follows directly, taking into account that $m_i^k \geq 0$ and the corresponding left hand side coefficient matrix in DP 2 is a M-matrix.

2.2 Method II

For this method, again the starting point is conservative scheme (5). We follow the same strategy as for the first method. The difference is in the implementation of the van Leer flux-limiter. Now, (6)-(8) are defined in terms of n and applied for $n_{i\pm1/2}^k$ in the approximation of $F_{i\pm1/2}^k = n_{i\pm1/2}^k f_{x\,i\pm1/2}^{\,k}$, $i=1,\ldots,N-1$, in dependence of the sign of $f_{x\,i\pm1/2}^{\,k}$, $f_{x\,i\pm1/2}^{\,k} = (\pm f_{i\pm1}^k \mp f_i^k)/h$. Moreover, at grid node x_i, $i=0,\ldots,N$ the approximation is constructed such that the coefficient in front of the unknown solutions at neighbourhood grid nodes (i.e. $n_{i\pm1}^k$) to be always *non-negative*.
Further, for simplicity we introduce the following notations: for an arbitrary value v_i^k of the mesh function v we set $v_i^{k,+} = \max\{0, v_i^k\}$, $v_i^{k,-} = \max\{0, -v_i^k\}$. The operators $\mathcal{L}_i$ and $\mathcal{F}_i$, $i=0,\ldots,N-1$ in DP 1 are the same as for Method I, but now L_i^k, $i=0,\ldots,N-1$ are given by

$$\begin{aligned} L_0^k &= f_{x\,1/2}^{\,k,+}\left[n_0^k + D_0^k\left(n_0^k - n_{-1}^k\right)\right] - f_{x\,1/2}^{\,k,-}[n_0^k + (1-D_1^k)(n_1^k - n_0^k)], \\ L_i^k &= f_{x\,i+1/2}^{\,k,+}[n_i^k + D_i^k(n_i^k - n_{i-1}^k)] - f_{x\,i+1/2}^{\,k,-}[n_i^k + (1-D_{i+1}^k)(n_{i+1}^k - n_i^k)] \\ &\quad - f_{x\,i-1/2}^{\,k,+}[n_i^k + (1-P_{i-1}^k)(n_{i-1}^k - n_i^k)] + f_{x\,i-1/2}^{\,k,-}[n_i^k + P_i^k(n_i^k - n_{i+1}^k)], \end{aligned}$$

where $D_i^k = \frac{1}{2}\Phi(s_{i+1/2}^k)$, $P_i^k = D_i^k / s_{i+1/2}^k$, and $0 \le D_i^k, P_i^k < 1$. Again we apply extrapolation formulae (9), but written for n, to eliminate external solutions n_{-1}^k and n_{N+1}^k.

Theorem 2. *Let $n_i^k \ge 0$, $i = 0, \ldots, N$. If $\tau_k \le h/(4\gamma \|\mathbf{f}_{\hat{\mathbf{x}}}^k\|)$, $\|\mathbf{f}_{\hat{\mathbf{x}}}^k\| = \max\limits_{0 \le i \le N-1} |f_{xi+1/2}^k|$, then there exist solution $n_i^{k+1} \ge 0$, $i = 0, \ldots, N$ of DP 1 for Method II.*

2.3 Method III

In order to construct unconditionally positive approximation we rewrite the flux in the first equation of (1) in the non-divergent form and then, for each $i = 1, ..., N-1$ we check the sign of the expressions representing the second-order accurate approximations to the first and second spatial derivatives of the obtained in the previous time step approximate solutions f_i^k, and depending on them choose appropriate approximations for n and $\frac{\partial n}{\partial x}$. The boundary conditions are treated similarly. This non-standard use of values at different time levels allows us to obtain the unconditionally positive explicit formulae for n_i^{k+1}, i.e. $\mathcal{L}_0 = n_0^{k+1}$, $\mathcal{L}_i = n_i^{k+1}$, $i = 1, \ldots, N-1$ and $\mathcal{F}_i$ depends on the sign of $f_{xxi}^k = (f_{i+1}^k - 2f_i^k + f_{i-1}^k)/h^2$ and f_{xi}^k given by (4)

$$\mathcal{F}_0 = \begin{cases} \dfrac{n_1^k}{1 + \frac{\gamma h}{d_n} f_{x0}^k}, & \text{if } f_{x0}^k \ge 0, \\ n_1^k - \dfrac{\gamma h}{d_n} f_{x0}^k n_0^k, & \text{if } f_{x0}^k < 0, \end{cases}$$

$$\mathcal{F}_i = \begin{cases} \dfrac{\frac{d_n}{h^2} n_{i+1}^k + \frac{1}{\tau_k} n_i^k + \left(\frac{d_n}{h^2} + \frac{\gamma}{h} f_{xi}^k\right) n_{i-1}^k}{\frac{1}{\tau_k} + \frac{2d_n}{h^2} + \frac{\gamma}{h} f_{xi}^k + \gamma f_{xxi}^k}, & \text{if } f_{xi}^k \ge 0 \text{ and } f_{xxi}^k \ge 0, \\ \dfrac{\left(\frac{d_n}{h^2} - \frac{\gamma}{h} f_{xi}^k\right) n_{i+1}^k + \frac{1}{\tau_k} n_i^k + \frac{d_n}{h^2} n_{i-1}^k}{\frac{1}{\tau_k} + \frac{2d_n}{h^2} - \frac{\gamma}{h} f_{xi}^k + \gamma f_{xxi}^k}, & \text{if } f_{xi}^k < 0 \text{ and } f_{xxi}^k \ge 0, \\ \dfrac{\frac{d_n}{h^2} n_{i+1}^k + \left(\frac{1}{\tau_k} - \gamma f_{xxi}^k\right) n_i^k + \left(\frac{d_n}{h^2} + \frac{\gamma}{h} f_{xi}^k\right) n_{i-1}^k}{\frac{1}{\tau_k} + \frac{2d_n}{h^2} + \frac{\gamma}{h} f_{xi}^k}, & \text{if } f_{xi}^k \ge 0 \text{ and } f_{xxi}^k < 0, \\ \dfrac{\left(\frac{d_n}{h^2} - \frac{\gamma}{h} f_{xxi}^k\right) n_{i+1}^k + \left(\frac{1}{\tau_k} - \gamma f_{xxi}^k\right) n_i^k + \frac{d_n}{h^2} n_{i-1}^k}{\frac{1}{\tau_k} + \frac{2d_n}{h^2} - \frac{\gamma}{h} f_{xi}^k}, & \text{if } f_{xi}^k < 0 \text{ and } f_{xxi}^k < 0. \end{cases}$$

3 Conclusions

Numerical experiments confirm that Methods I,II are second order accurate in space and preserve the non-negativity of the numerical solution under the resulting time step restrictions. Method III is first order accurate in space and unconditionally positive, but in contrast, the stability condition is much stronger.

The best precision is obtained by Method II and the convergence rate is better for Method I in comparison with Method II.
The detail description of Methods I-III can be found in our forthcoming papers [8, 9].

Acknowledgments. The second and third authors are supported by the Bulgarian Fund for Science under the Projects DID 02/37 from 2009.

References

[1] A.R.A. Anderson, M.A.I. Chaplain, E.L. Newman, R.i.C. Steele, A.M. Thompson, Mathematical modelling of tumour invasion and metastasis, Journal of Theoretical Medicine 2 (2000) 129-154.

[2] M.A.I. Chaplain, G. Lolas, Mathematical modelling of cancer invasion of tissue: dynamic heterogeneity, Networks and Heterogeneous Media 1(3) (2006) 399-439.

[3] A. Chertock, A. Kurganov, A second-order positivity preserving central-upwind scheme for chemotaxis and haptotaxis models, Numer. Math. 111 (2008) 169–205.

[4] B.M. Chen-Charpentier, H.V. Kojouharov, An unconditionally positivity preserving scheme for advection-diffusion reaction equations, Mathematical and Computer Modelling (2011) (in press). Available online 10 May 2011.

[5] A. Gerisch, D.F. Griffiths, R. Weiner,M.A.J. Chaplain, A Positive splitting method for mixed hyperbolicï£¡parabolic systems, Num. Meth. for PDEs 17(2) (2001) 152–168.

[6] A. Gerisch, J. G. Verwer, Operator splitting and approximate factorization for taxis-diffusion-reaction models, Appl. Numer Math. 42 (2002) 159–176.

[7] W. Hundsdorfer, B. Koren, M. van Loon, J.G. Verwer, A positive finite-difference advection scheme, J. of Comp. Phys. 117 (1995) 35–46.

[8] M. Kolev, M. Koleva, L. Vulkov, Two positivity preserving flux limited, second order numerical methods for a Haptotaxis model, submitted.

[9] M. Kolev, M. Koleva, L. Vulkov, An unconditionally positive preserving numerical scheme for models of tissue invasion and migration of tumour cells, submitted.

[10] M. Kolev, B. Zubik-Kowal, Numerical solutions for a model of tissue invasion and migration of tumour cells, *Computational and Mathematical Methods in Medicine* 2011 (2011) 16 pages, Article ID 452320, doi:10.1155/2011/452320.

[11] Samarskii A. A., The Theory of Difference Schemes, Marcel Dekker Inc, 2001.

[12] N. Saito, T. Suzuki, Notes on finite difference scheme to a parabolic-elliptic system modelling chemotaxis, Appl. Math. and Comp. 171 (2005) 72–90.

Receptor-Based Cellular Neural Network Models

Maya Markova

1 Dynamical behavior of the CNN model. Describing function approach.

We consider one-dimensional epithelial sheet of length L. We denote the concentration of ligands by $w(x,t)$, where x and t are space and time coordinates, with x increasing from 0 to L along the body column. The bound and free receptors densities are denoted by $u(,t)$ and $v(x,t)$ respectively. For simlicity we assume that all binding processes are governed by the law of mass action without saturation effects. The model is described by the following dynamical system:

$$\begin{aligned} \frac{\partial}{\partial t}u &= f_1(u,v,w) \\ \frac{\partial}{\partial t}v &= f_2(u,v,w) \\ \frac{\partial}{\partial t}w &= d\frac{\partial^2}{\partial x^2}w + f_3(u,v,w), \end{aligned} \tag{1}$$

where $u,v,w : [0,1] \times \mathbf{R}^+ \to \mathbf{R}^+$, functions $f_i, i = 1,2,3$ are nonnegative for nonnegative arguments and they have the following form:

$$f_1 = -a_1u + g_1(u,v) - buw + cv,$$

$$f_2 = -a_2v + buw - cv,$$

$$f_3 = -a_3w - buw + g_3(u,v) + cv,$$

$a_i > 0, i = 1,2,3$, $b,c > 0$. We will suppose that the functions $g_i, i = 1,3$ are of quadratic form, i.e. $g_i(u,v) = g_iu^2$. The model has biological interpretation for such functions [7]. a_1 is the rate of decay of free receptors, a_2 is the rate of decay of bound receptors and a_3 is the rate of decay of ligands, function g_1 defines the rate of production of new free receptors, function g_3 defines the rate of production of ligands, cv is the rate of dissociation of bound receptors, b is the rate os binding of ligands and free receptors and d is diffusion coefficient for ligands.
Most of the models of morphogenesis are reaction-diffusion models assuming the existence of diffusing substances [5,6]. Since some of the molecules, which take part in the morphogenetic processes, e.g. receptors or cells, do not diffuse, it is necessary to consider systems of reaction-diffusion equations coupled with ordinary differential equations. All considered receptor-based models consist of two subsystems of

reaction-diffusion equations and ordinary differential equations coupled via the nonlinear kinetics functions. In general, equations of our models can be represented in the form:

$$\begin{aligned} u_t^1 &= f_1(u^1, u^2), \\ u_t^2 &= D_+ \Delta u^2 + f_2(u^1, u^2), \\ \partial_n u^2 &= 0 \text{ in } \partial\Omega, \\ u^1(0,x) &= u_0^1(x), \\ u^2(0,x) &= u_0^2(x), \end{aligned}$$

where $\Omega \subset \mathbf{R}^N$ is a bounded region and D_+ is a diagonal matrix with positive coefficients. $u^1 : \Omega \times \mathbf{R}^+ \to \mathbf{R}^r$, $u^2 : \Omega \times \mathbf{R}^+ \to \mathbf{R}^{m-r}$, where r is the number of ordinary differential equations, and $m-r$ is the number of reaction-diffusion equations. f_1 and f_2 are smooth mappings, $f_1 : \mathbf{R}^m \to \mathbf{R}^r$, $f_2 : \mathbf{R}^m \to \mathbf{R}^{m-r}$.
As we mentioned above there are several ways to approximate the Laplacian operator in discrete space by a CNN synaptic law with an appropriate A-template [2]. In our case we will take one-dimensional discretized Laplacian template:

$$A : (1, -2, 1).$$

Therefore the CNN representation for our receptor-based model (1) will be the following:

$$\begin{aligned} \frac{du_j}{dt} &= -a_1 u_j + g_1 u_j^2 - b u_j w_j + c v_j \qquad (2) \\ \frac{dv_j}{dt} &= -a_2 v_j + b u_j w_j - c v_j \\ \frac{dw_j}{dt} &= -a_3 w_j + d(w_{j-1} - 2w_j + w_{j+1}) - \\ &- b u_j w_j + g_3 u_j^2 + c v_j, \end{aligned}$$

$1 \le j \le N$. The above equation is actualy ordinary differential equation which is identified as the state euqation of an autonomous CNN made of N cells. For the output of our CNN model we will take the standard sigmoid function [2].
In this section we will introduce an approximative method for studying the dynamics of CNN model (2), based on a special Fourier transform. The idea of using Fourier expansion for finding the solutions of PDEs is well known in physics. It is used to predict what spatial frequences or modes will dominate in nonlinear PDEs. In CNN literature this approach, has been developed for analyzing the dynamics of CNNs with symmetric templates [3,4].
In this paper we investigate the dynamic behavior of a CNN model (2) by use of Harmonic Balance Method well known in control theory and in the study of electronic oscillators [5] as describing function method. The method is based on the fact that

all cells in CNN are identical [2], and therefore by introducing a suitable double transform, the network can be reduced to a scalar Lur's scheme [7].
We shall study the dynamics and the stability properties of (2) by using the describing function method [5,7]. Applying the double Fourier transform:

$$F(s,z) = \sum_{k=-\infty}^{k=\infty} z^{-k} \int_{-\infty}^{\infty} f_k(t) exp(-st) dt,$$

to the CNN equation (2) we obtain:

$$\begin{aligned} sU &= -a_1 U + g_1 U^2 - bUW + cV \\ sV &= -a_2 V + bUW - cV \\ sW &= -a_3 W + d(z^{-1}W - 2W + zW) + \\ &+ g_3 U_b^2 UW + cV. \end{aligned} \tag{3}$$

Without loss of generality we can denote $N(U,V,W) = g_i U^2 - bUW + cV$ and then we obtain from (3):

$$\begin{aligned} U &= \frac{1}{s+a_1} N \\ V &= \frac{1}{s+a_2} N \\ W &= \frac{1}{s+a_3 - d(z^{-1} - 2 - z)} N. \end{aligned} \tag{4}$$

In the double Fourier transform we suppose that $s = i\omega_0$, and $z = exp(i\Omega_0)$, where ω_0 is a temporal frequency, Ω_0 is a spatial frequency.
According to the describing function method, $H(s,z) = \frac{s+a_1}{s+a_3-d(z^{-1}-2+z)}$ is the transform function, which can be presented in terms of ω_0 and Ω_0, i.e. $H(s,z) = H_{\Omega_0}(\omega_0)$.
We are looking for possible periodic state solutions of system (3) of the form:

$$X_{\Omega_0}(\omega_0) = X_{m_0} sin(\omega_0 t + j\Omega_0), \tag{5}$$

where $X = (U,V,W)$. According to the describing function method we take the first harmonics, i.e. $j = 0 \Rightarrow$

$$X_{\Omega_0}(\omega_0) = X_{m_0} sin\omega_0 t,$$

On the other side if we substitute $s = i\omega_0$ and $z = exp(i\Omega_0)$ in the transfer function $H(s,z)$ we obtain:

$$H_{\Omega_0}(\omega_0) = \frac{i\omega_0 + a_1}{i\omega_0 + a_3 - d(2cos\Omega_0 - 2)}. \tag{6}$$

According to (6) the following constraints hold:

$$\begin{aligned} \Re(H_{\Omega_0}(\omega_0)) &= \frac{X_{m_0}}{Y_{m_0}} \\ \Im(H_{\Omega_0}(\omega_0)) &= 0. \end{aligned} \tag{7}$$

Hence, we obtain the following constraints:

$$\begin{aligned} \omega_0 &= \frac{1}{a_3 - a_1 + d(2cos\Omega_0 - 2)} \\ X_{m_0} &= \frac{4}{\pi}[X_{m_0} Arcsin(\frac{1}{X_{m_0}}) + \\ &\quad \sqrt{1 - \frac{1}{X_{m_0}^2}}]. \end{aligned} \tag{8}$$

Suppose that our CNN model (2) is a finite circular array of N cells. For this case we have finite set of frequences:

$$\Omega_0 = \frac{2\pi k}{N}, \;\; 0 \leq k \leq N-1. \tag{9}$$

Thus (7), (8) and (9) give us necessary set of equations for finding the unknowns X_{m_0}, ω_0, Ω_0. As we mentioned above we are looking for a periodic wave solution of (3), therefore X_{m_0} will determine approximate amplitude of the wave, and $T_0 = \frac{2\pi}{\omega_0}$ will determine the wave speed.

Proposition 1. *CNN model (2) of the receptor-based system (16) with circular array of N cells has periodic state solutions $x_j(t)$ with a finite set of spatial frequences $\Omega_0 = \frac{2\pi k}{N}$, $0 \leq k \leq N-1$.*

Remark 1. For the Turing-type instability [9], the functions describing production of free receptors (f.r.) must depend on the density of f.r. and this dependence must be a power function of the order $\alpha + 1$, where $\alpha > 0$. Hence, Turing type patterns can occur if $g_1(u) = g_1 u^{\alpha+1}, \alpha > 0$. This function can depend also on the density of bound receptors (b.r.), but also it is critical here that it depends on the density of f.r. For numerical simulations the simplest function fulfilling the above condition is used, namely $g_1(u) = g_1 u^2$. To model the production rate of ligands (l.) g_3 we also take a function of the concentration of free receptors. In numerical simulations a function similar to g_1 is used $g_3(u) = g_3 u^2$.

2 Simulations and discussions

The following bifuraction diagrams are obtained for functions u, v, w.

We showed that Turing-type patterns can be obtained in a receptor-based CNN model. The Turing-type mechanism [9] is one of the simplest theories for the biological pattern formation. In models with such mechanism patterns can arise spontaneously. The parameters must be tightly controlled to obtain the instability at the desired point in parameter space. From the simulations it appears that the model (2) cannot exhibit a wave bifurcation. We carry out our simulations for the following set of parameters: $a_1 = 0.2$, $a_2 = 0.02$, $a_3 = 0.2$, $b = 0.7$, $g_1 = 1.466$, $g_3 = 2$, $c = 0.02672$. In summary, we showed that for the simplest receptor-based model consisting of 3 equations, Turing-type patterns can arise only if there is a self-enhancement of free

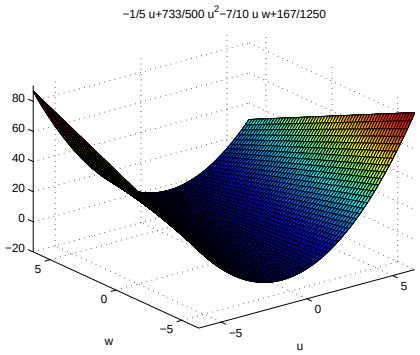

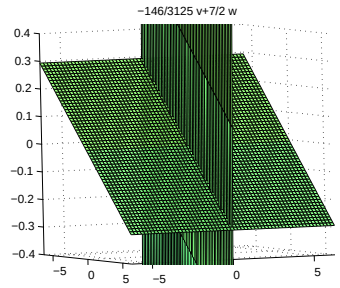

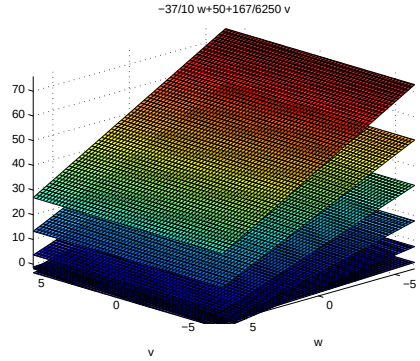

receptors. The final pattern strongly depends on the initial perturbation. There are two kinds of Turing-type patterns: 1).stationary patterns - in such case long-time solutions are stationary and spatially heterogeneous structures; 2). wave patterns- it is a supercritical Hopf bifurcation from a homogeneous solution to a stable periodic and nonconstant solution and the result is a pattern which oscillates in time.

References

[1] N.F.Britton, Reaction-Diffusion Equations and Their Applications to Biology, New York: Academic, 1986.

[2] L.O.Chua, L.Yang, "Cellular Neural Network: Theory and Applications", IEEE Trans. CAS, vol. 35, pp. 1257-1290, Oct. 1988.

[3] L.O.Chua, M.Hasler, G.S.Moschytz, J.Neirynsk, "Autonomous cellular neural networks: a unified paradigm for pattern formation and active wave propagation", IEEE Trans. CAS-I, vol. 42, N 10, pp. 559-577, Oct. 1995.

[4] R.Genesio, A.Tesi, F.Villoresi, "A frequency approach for analyzing and controlling chaos in nonlinear circuits", IEEE Trans. CAS-I, vol. 40, N 11, pp. 819-827, Nov. 1993.

[5] S.Heinze, B.Schweizer, "Creeping fronts in degenerate reaction-diffusion systems", to appear.

[6] F.Hoppensteadt,W.Jager, "Pattern formation by bacteria". In S.Levin, editor, Lecture Notes in Biomathematics:Biological Growth and Spread, pp. 69-81, Heidelberg, Springer-Verlag, 1980.

[7] A.I.Mees,Dynamics of Feedback Systems, London, England:Wiley, 1981.

[8] T.Roska, L.O.Chua, D.Wolf, T.Kozek, R.Tetzlaff, F.Puffer, "Simulating nonlinear waves and partial differential equations via CNN- Part I: Basic techniques", IEEE Trans. CAS-I, vol. 42, N 10, pp. 807-815, Oct. 1995.

[9] A.M.Turing, "The chemical basis of morphogenesis", Phil. Trans.Roy.Soc. B, 237:37-72, 1952.

The United Solution Set to 3D Linear System with Symmetric Interval Matrix

Evgenija D. Popova

1 Introduction

Consider the linear algebraic system

$$A(p)\cdot x \;=\; b(p), \qquad p=(p_1,\ldots,p_m)^\top, \tag{1}$$

$$a_{ij}(p) := a_{ij,0}+\sum_{\mu=1}^{m} a_{ij,\mu}p_\mu, \qquad b_i(p) := b_{i,0}+\sum_{\nu=1}^{m} b_{i,\mu}p_\mu, \tag{2}$$

$$a_{ij,\mu}, b_{i,\mu}\in\mathbb{R}, \qquad \mu=0,\ldots,m,\ i,j=1,\ldots,n.$$

The parameters p_μ, $\mu=1,\ldots,m$ are uncertain and varying within given intervals

$$p \;\in\; [p]=([p]_1,\ldots,[p]_m)^\top. \tag{3}$$

A set of solutions to (1)–(3), called *united parametric solution set*, is

$$\Sigma^p=\Sigma\left(A(p),b(p),[p]\right) \quad := \quad \{x\in\mathbb{R}^n \mid \exists p\in[p], A(p)x=b(p)\}\,. \tag{4}$$

Characterizing the solution set (4) by inequalities not involving the interval parameters is a fundamental problem useful for visualizing the solution set, exploring its properties and for computing componentwise boundaries. Apart from quantifier elimination, the only known general way of describing the parametric solution set is a lengthy and non-unique Fourier-Motzkin-type parameter elimination process presented in [1]. The special cases of symmetric and skew-symmetric solution sets

$$\Sigma_{sym} := \{x\in\mathbb{R}^n \mid Ax=b, A=A^\top, A\in[A], b\in[b]\}, \quad (A=-A^\top \text{ for } \Sigma_{skew})$$

are studied most exhaustively, see [1, 2] and the references given therein. Following a different approach than the Fourier-Motzkin-type parameter elimination, M. Hladík provided in [2] explicit descriptions of the symmetric and skew-symmetric solution sets which have the smallest, known by now, number of characterizing inequalities. Basing on an improved Fourier-Motzkin-type parameter elimination process [3, Theorem 3.1] and some sufficient conditions (proven therein) for detecting superfluous characterizing inequalities, here we study the parameter elimination process and its properties for linear parametric systems involving 3×3 symmetric matrix. The consideration answers the open question, see [1], about the uniqueness of the parameter elimination process for the symmetric solution set. The obtained explicit description of the 3D symmetric solution set involves two times less number of characterizing inequalities than that reported in [2].

Let $\mathbb{R}^n, \mathbb{R}^{n\times m}$ be the set of real vectors with n components and the set of real $n \times m$ matrices, respectively. A real compact interval is $[a] = [a^-, a^+] := \{a \in \mathbb{R} \mid a^- \leq a \leq a^+\}$. By $\mathbb{IR}^n, \mathbb{IR}^{n\times m}$ we denote the sets of interval n-vectors and interval $n \times m$ matrices, respectively. Define mid-point $\dot{a} := (a^- + a^+)/2$ and radius $\hat{a} := (a^+ - a^-)/2$. These functionals are applied to interval vectors and matrices componentwise.

Definition 1. A parameter p_μ, $1 \leq \mu \leq m$, is of 1st class *if it occurs in only one equation of the system (1).*

Definition 2. A parameter p_μ, $1 \leq \mu \leq m$, is of 2nd class *if it is involved in more than one equation of the system (1).*

The elimination of 2nd class parameters from two inequality pairs is studied in [3].

Theorem 1 ([3])**.** *For two arbitrary inequality pairs (α) and (β)*

$$f_{0,\lambda}(x) + \sum_{\mu=1}^{m+s} f_{\mu,\lambda}(x)p_\mu \quad \leq 0 \leq \quad f_{0,\lambda}(x) + \sum_{\mu=1}^{m+s} f_{\mu,\lambda}(x)p_\mu, \qquad \lambda \in \{\alpha, \beta\},$$

involving $m+s$ interval parameters p_μ such that $f_{\mu,\lambda}(x) \not\equiv 0$ for all $\lambda \in \{\alpha, \beta\}$, $\mu \in M$, $Card(M) = m$ and $f_{\mu,\lambda}(x) \not\equiv 0$ for exactly one $\lambda \in \{\alpha, \beta\}$, $\mu \in S$, $Card(S) = s$, the elimination of all parameters yields the inequalities

$$\left| f_{0,\lambda}(x) + \sum_{\mu=1}^{m+s} f_{\mu,\lambda}(x)\dot{p}_\mu \right| \quad \leq \quad \sum_{\mu=1}^{m+s} |f_{\mu,\lambda}(x)|\hat{p}_\mu, \qquad \lambda \in \{\alpha, \beta\} \tag{5}$$

$$\left| \Delta_{0,i}(x) + \sum_{\mu=1,\mu\neq i}^{m+s} \Delta_{\mu,i}(x)\dot{p}_\mu \right| \quad \leq \quad \sum_{\mu=1,\mu\neq i}^{m+s} |\Delta_{\mu,i}(x)|\hat{p}_\mu, \qquad i \in M, \tag{6}$$

where $\Delta_{u,v}(x) := f_{u,\alpha}(x)f_{v,\beta}(x) - f_{u,\beta}(x)f_{v,\alpha}(x)$.

The proof of Theorem 1 was constructive showing which combination of inequalities is superfluous/redundant[1] and with respect to which cross inequality.

Corollary 1 (constructive)**.** *For two inequality pairs $(\alpha), (\beta)$ involving the parameter p_1 in both inequality pairs and the parameter p_2 in only one, the elimination of p_1 generates the cross inequality (α, β) involving p_2. Then, in the elimination of p_2*

$\alpha \times (\alpha, \beta)$ *is* **superfluous** *to the inequality (β) if p_2 is involved in (α)*
$\beta \times (\alpha, \beta)$ *is* **superfluous** *to the inequality (α) if p_2 is involved in (β).*

The above cross inequalities are **redundant** *to (β), resp. (α), if more than one 2nd class or 1st class parameter have been eliminated before the elimination of p_2.*

[1] A cross inequality which is equivalent to another cross inequality is called superfluous, while a cross inequality which does not contribute to the boundary of the solution set is called redundant.

Corollary 2 (constructive). *For two inequality pairs $(\alpha),(\beta)$ involving the parameters p_1, p_2 in both inequality pairs, the elimination of p_1 generates the cross inequality*[2] *(α_1,β_1) involving p_2. Then the elimination of p_2 generates three more cross inequality pairs: $(\alpha_1,\beta_1)_2$, $\alpha_{1,2}\times(\alpha_1,\beta_1)_2$, $\beta_{1,2}\times(\alpha_1,\beta_1)_2$. The cross inequality pairs $\alpha_{1,2}(\alpha_1,\beta_1)_2/f_{1\alpha}(x)$ and $\beta_{1,2}(\alpha_1,\beta_1)_2/f_{1\beta}(x)$ (where $f_{1\alpha}(x)$, $f_{1\beta}(x)$ are the coefficient functions of p_1 in the inequalities (α), resp. (β)) are equivalent and therefore one of them is superfluous with respect to the other. The cross inequality pair $(\alpha_1,\beta_1)_2$ is either superfluous or redundant to $\alpha_{1,2}(\alpha_1,\beta_1)_2/f_{1\alpha}(x)$, resp. $\beta_{1,2}(\alpha_1,\beta_1)_2/f_{1\beta}(x)$ which yields only one active cross inequality (6) in the elimination of p_2 instead of 3.*

2 Parameter Elimination in 3D Symmetric System

Consider the the following slight generalization of the classical linear system with symmetric matrix, considered in [1, 2].

$$A(p)x = b(p), \qquad \text{where} \tag{7}$$

$$A(p) := A + B(q), \quad A = (a_{ij}) - \operatorname{diag}(a_{ii}) \in \mathbb{R}^{n\times n},\ A = A^\top \tag{8}$$

$$B(q) = B^{(0)} + \sum_{\nu=1}^{s} B^{(\nu)} q_\nu \in \mathbb{R}^{n\times n}, \quad b(q) = b^{(0)} + \sum_{\nu=1}^{s} b^{(\nu)} q_\nu \in \mathbb{R}^{n\times 1}, \tag{9}$$

$$q = (q_1,\dots,q_s) := (a_{11},\dots,a_{nn},q_{n+1},\dots,q_s), \tag{10}$$

every q_ν, $\nu = 1,\dots,s$, is involved in exactly one equation of the system and

$$p = (p_1,\dots,p_m) := (a_{12},\dots,a_{n-1,n},q_1,\dots,q_s), \qquad p \in ([p_1],\dots,[p_m]), \tag{11}$$

where $m = n(n-1)/2 + s$. The system (7)–(11) can contain in the diagonal elements of the matrix and in the right-hand side vector numerical values and an arbitrary but fixed number of 1st class parameters q_ν. We call this system *quasi-symmetric* and search for a description of its solution set by the improved Fourier-Motzkin-type elimination of parameters.

Consider a 3×3 quasi-symmetric system and assume that all 1st class parameters are eliminated from the trivial set of inequality pairs characterizing the solution set. Since all 1st class parameters behave the same way, without loss of generality we assume that each equation involves only one 1st class parameter q_i whose coefficient vector is $g_i(x)$, $i = 1,\dots,n$. Let $\mathcal{N} = \{1,2,3\}$ be the index set of the three characterizing inequality pairs. For any $i \in \mathcal{N}$ and $\mathcal{N}_i = \{1,\dots,n\}\setminus\{i\}$, the inequality pair (e_i) is

$$f_{i0}(x) + g_i(x)\dot{q}_i \mp |g_i(x)|\hat{q}_i + \sum_{j\in\mathcal{N}_i} x_j a_{ij} \ \le 0 \le \cdots, \tag{e_i}$$

where $f_{i0}(x) = A_{i\bullet 0}x - b_{i0}$ and "$\cdots$" denotes the whole expression in the left inequality with the bottom sign of $\mp$. For arbitrary $\alpha,\beta,\gamma \in \mathcal{N}$ we perform the elimination

[2] The subscript in the notation of the cross inequalities denotes which parameter is eliminated.

$a_{\alpha\beta}, a_{\alpha\gamma}, a_{\beta\gamma}$. The elimination of $a_{\alpha\beta}$ generates the following cross inequality pair

$$f_{\alpha 0}x_\alpha - f_{\beta 0}x_\beta + g_\alpha x_\alpha \dot{q}_\alpha - g_\beta x_\beta \dot{q}_\beta \mp |g_\alpha x_\alpha|\hat{q}_\alpha \mp |g_\beta x_\beta|\hat{q}_\beta + \sum_{j\in\mathcal{N}_\alpha\setminus\{\beta\}} x_\alpha x_j a_{\alpha j} - \sum_{j\in\mathcal{N}_\beta\setminus\{\alpha\}} x_\beta x_j a_{\beta j} \ \leq 0 \leq \cdots \qquad (e_{(\alpha,\beta)})$$

and updates the initial characterizing inequalities (e_α), (e_β) by combining the latter with the end-point inequalities for the parameter $a_{\alpha\beta}$.
The parameter $a_{\alpha\gamma}$ is involved in the updated inequality (e_α) and the inequalities $(e_\gamma), (e_{(\alpha,\beta)})$. So, in the elimination of $a_{\alpha\gamma}$ we have to consider all cross inequalities between these three inequality pairs. The cross between $(e_\alpha), (e_\gamma)$ gives

$$f_{\alpha 0}x_\alpha - f_{\gamma 0}x_\gamma + g_\alpha x_\alpha \dot{q}_\alpha - g_\gamma x_\gamma \dot{q}_\gamma \mp |g_\alpha x_\alpha|\hat{q}_\alpha \mp |g_\gamma x_\gamma|\hat{q}_\gamma + x_\alpha x_\beta \dot{a}_{\alpha\beta} \mp |x_\alpha x_\beta|\hat{a}_{\alpha\beta} + \sum_{j\in\mathcal{N}_\alpha\setminus\{\beta,\gamma\}} x_\alpha x_j a_{\alpha j} - \sum_{j\in\mathcal{N}_\gamma\setminus\{\alpha\}} x_\gamma x_j a_{\gamma j} \ \leq 0 \leq \cdots . \qquad (e_{(\alpha,\gamma)})$$

The cross between $(e_\alpha), (e_{(\alpha,\beta)})$ is redundant to (e_β) by the constructive Corollary 1. Eliminating $a_{\alpha\gamma}$, the cross between $(e_\gamma), (e_{(\alpha,\beta)})$ gives

$$f_{\gamma 0}x_\gamma - f_{\alpha 0}x_\alpha + f_{\beta 0}x_\beta + g_\gamma x_\gamma \dot{q}_\gamma - g_\alpha x_\alpha \dot{q}_\alpha + g_\beta x_\beta \dot{q}_\beta \mp |g_\gamma x_\gamma|\hat{q}_\gamma \mp |g_\alpha x_\alpha|\hat{q}_\alpha \mp |g_\beta x_\beta|\hat{q}_\beta + \sum_{j\in\mathcal{N}_\gamma\setminus\{\alpha\}} x_j x_\gamma a_{\gamma j} - \sum_{j\in\mathcal{N}_\alpha\setminus\{\beta,\gamma\}} x_\alpha x_j a_{\alpha j} + \sum_{j\in\mathcal{N}_\beta\setminus\{\alpha\}} x_\beta x_j a_{\beta j} \ \leq 0 \leq \cdots \quad (e_{\gamma_\alpha(\alpha,\beta)})$$

The parameter $a_{\beta\gamma}$ is involved in the inequalities $(e_\beta), (e_\gamma), (e_{(\alpha,\beta)}), (e_{(\alpha,\gamma)}), (e_{\gamma_\alpha(\alpha,\beta)})$. In the elimination of $a_{\beta\gamma}$ we have to consider all cross inequalities between these five inequality pairs updated by combining them with the end-point inequalities for $a_{\alpha\beta}$ and $a_{\alpha\gamma}$. The cross between $(e_\beta), (e_\gamma)$ gives

$$f_{\beta 0}x_\beta - f_{\gamma 0}x_\gamma + g_\beta x_\beta \dot{q}_\beta \mp |g_\beta x_\beta|\hat{q}_\beta - g_\gamma x_\gamma \dot{q}_\gamma \mp |g_\gamma x_\gamma|\hat{q}_\gamma + x_\alpha x_\beta a_{\beta\alpha} \mp |x_\alpha x_\beta|a_{\beta\alpha} - x_\alpha x_\gamma \dot{a}_{\gamma\alpha} \mp |x_\alpha x_\gamma|\hat{a}_{\gamma\alpha} + \sum_{j\in\mathcal{N}_\beta\setminus\{\alpha,\gamma\}} x_\beta x_j a_{\beta j} - \sum_{j\in\mathcal{N}_\gamma\setminus\{\alpha,\beta\}} x_\gamma x_j a_{\gamma j} \leq 0 \leq \cdots . \quad (e_{(\beta,\gamma)})$$

The cross between $(e_\beta), (e_{(\alpha,\beta)})$ is redundant to (e_α) by the constructive Corollary 1. Eliminating $a_{\beta\gamma}$, the cross between the updated $(e_\gamma), (e_{(\alpha,\beta)})$ gives

$$-f_{\gamma 0}x_\gamma - f_{\alpha 0}x_\alpha + f_{\beta 0}x_\beta - g_\gamma x_\gamma \dot{q}_\gamma - g_\alpha x_\alpha \dot{q}_\alpha + g_\beta x_\beta \dot{q}_\beta \qquad (e_{\gamma_\beta(\alpha\beta)})$$
$$\mp|g_\gamma x_\gamma|\hat{q}_\gamma \mp |g_\alpha x_\alpha|\hat{q}_\alpha \mp |g_\beta x_\beta|\hat{q}_\beta - 2x_\alpha x_\gamma \dot{a}_{\gamma\alpha} \mp 2|x_\alpha x_\gamma|\hat{a}_{\gamma\alpha}$$
$$- \sum_{j\in\mathcal{N}_\gamma\setminus\{\alpha,\beta\}} x_\gamma x_j a_{\gamma j} - \sum_{j\in\mathcal{N}_\alpha\setminus\{\beta,\gamma\}} x_\alpha x_j a_{\alpha j} + \sum_{j\in\mathcal{N}_\beta\setminus\{\alpha,\gamma\}} x_\beta x_j a_{\beta j} \ \leq 0 \leq \cdots .$$

Eliminating $a_{\beta\gamma}$, the cross between the updated $(e_\beta), (e_{(\alpha,\gamma)})$ gives

$$-f_{\beta 0}x_\beta - f_{\alpha 0}x_\alpha + f_{\gamma 0}x_\gamma - g_\beta x_\beta \dot{q}_\beta - g_\alpha x_\alpha \dot{q}_\alpha + g_\gamma x_\gamma \dot{q}_\gamma$$
$$\mp|g_\beta x_\beta|\hat{q}_\beta \mp |g_\alpha x_\alpha|\hat{q}_\alpha \mp |g_\gamma x_\gamma|\hat{q}_\gamma - 2x_\alpha x_\beta \dot{a}_{\alpha\beta} \mp 2|x_\alpha x_\beta|\hat{a}_{\alpha\beta} \qquad (e_{\beta_\gamma(\alpha\gamma)})$$
$$- \sum_{j\in\mathcal{N}_\beta\setminus\{\alpha,\gamma\}} x_\beta x_j a_{\beta j} - \sum_{j\in\mathcal{N}_\alpha\setminus\{\beta,\gamma\}} x_\alpha x_j a_{\alpha j} + \sum_{j\in\mathcal{N}_\gamma\setminus\{\alpha,\beta\}} x_\gamma x_j a_{\gamma j} \leq 0 \leq \cdots .$$

The cross between the updated $(e_\gamma), (e_{(\alpha,\gamma)})$ is redundant to (e_α) by Corollary 1. Eliminating $a_{\beta\gamma}$, the cross between the updated $(e_\beta), (e_{\gamma_\alpha(\alpha,\beta)})$ gives

$$\begin{gathered} f_{\beta 0}x_\beta - f_{\gamma 0}x_\gamma + f_{\alpha 0}x_\alpha + g_\beta x_\beta \dot{q}_\beta - g_\gamma x_\gamma \dot{q}_\gamma + g_\alpha x_\alpha \dot{q}_\alpha \\ \mp 3|g_\beta x_\beta|\hat{q}_\beta \mp |g_\gamma x_\gamma|\hat{q}_\gamma \mp |g_\alpha x_\alpha|\hat{q}_\alpha + 2x_\alpha x_\beta \dot{a}_{\alpha\beta} \mp 2|x_\alpha x_\beta|\hat{a}_{\alpha\beta} \\ + \sum_{j\in\mathcal{N}_\beta\setminus\{\alpha,\gamma\}} x_\beta x_j a_{\beta j} - \sum_{j\in\mathcal{N}_\gamma\setminus\{\alpha,\beta\}} x_j x_\gamma a_{\gamma j} + \sum_{j\in\mathcal{N}_\alpha\setminus\{\beta,\gamma\}} x_\alpha x_j a_{\alpha j} \ \leq 0 \leq \cdots . \end{gathered}$$

This inequality pair is superfluous to $(-1)(e_{\beta_\gamma(\alpha,\gamma)})$ if there are no 1st class parameters, or redundant to the latter otherwise (due to the extra positive term $2|g_\beta x_\beta|\hat{q}_\beta$). Analogously, eliminating $a_{\beta\gamma}$, we prove that the following cross inequalities are superfluous (if there are no 1st class parameters) or redundant (otherwise). The cross inequality pair between $(e_\gamma), (e_{\gamma_\alpha(\alpha,\beta)})$ is superfluous/redundant to $(-1)(e_{\gamma_\beta(\alpha,\beta)})$ by Corollary 2. The cross inequality pair between the updated $(e_{(\alpha,\beta)}), (e_{(\alpha,\gamma)})$ is superfluous/redundant to $(-1)(e_{(\beta,\gamma)})$. The cross inequality pair between $(e_{(\alpha,\beta)})$, $(e_{\gamma_\alpha(\alpha,\beta)})$ is superfluous/redundant to $(e_{\gamma_\beta(\alpha,\beta)})$ by Corollary 2. The cross inequality pair between $(e_{(\alpha,\gamma)})$, $(e_{\gamma_\alpha(\alpha,\beta)})$ is superfluous/redundant to $(e_{\beta_\gamma(\alpha,\gamma)})$.

Thus, for a 3-dimensional quasi-symmetric linear system (7)–(11), we proved above by Corollaries 1, 2 and by a direct evaluation that the improved Fourier-Motzkin-type parameter elimination of $a_{\alpha\beta}, a_{\alpha\gamma}, a_{\beta\gamma}$ yields 6 active characterizing cross inequalities

$$e_{(\alpha,\beta)},\ e_{(\alpha,\gamma)},\ e_{\gamma_\alpha(\alpha,\beta)},\ e_{(\beta,\gamma)},\ e_{\beta_\gamma(\alpha,\gamma)},\ e_{\gamma_\beta(\alpha,\beta)},$$

and 6 superfluous/redundant cross inequalities. The active characterizing cross inequalities are two times less than those reported in [2]. Since α, β, γ are taken arbitrary from the set $\{1, 2, 3\}$, for different orders of parameter elimination the active characterizing cross inequalities are the same (up to the order of their generation). Exchanging the order of inequalities or the order of parameter elimination we have

$$e_{(\alpha,\beta)} = -e_{(\beta,\alpha)} \tag{12}$$

$$e_{\gamma_\alpha(\alpha,\beta)} = \begin{cases} e_{\beta_\alpha(\alpha,\gamma)} & \text{if } \alpha < \gamma \\ -e_{\beta_\alpha(\gamma,\alpha)} & \text{if } \alpha > \gamma \end{cases} \tag{13}$$

$$e_{\gamma_\beta(\alpha,\beta)} \overset{(12)}{=} (-1)e_{\gamma_\beta(\beta,\alpha)} \overset{(13)}{=} \begin{cases} (-1)e_{\alpha_\beta(\beta,\gamma)} & \text{if } \beta < \gamma \\ e_{\alpha_\beta(\gamma,\beta)} & \text{if } \beta > \gamma. \end{cases} \tag{14}$$

Table 5: Elimination schema for the 2nd class parameters in a 3D system with symmetric matrix. Rows, labeled in the second column, represent the characterizing inequality pairs. The occurrence of the parameters is represented column-wise: "v" denotes the occurrence of a non-eliminated parameter in the corresponding inequality, "!" denotes the occurrence of an eliminated parameter, dashes denote lack of a corresponding parameter.

	ineqs	a_{12}	a_{13}	a_{23}	
	(1)	v	v	–	
	(2)	v	–	v	
el.par.:	(3)	–	v	v	superfluous ineqs
a_{12}	(1,2)	–	v	v	
a_{13}	(1,3)	!	–	v	
	$3_1(1,2)$	–	–	v	
					$1_3(1,2)$ by Corollary 1
a_{23}	(2,3)	!	!	–	
	$3_2(1,2)$	–	!	–	
					$3_2(1,3)$ by Corollary 1
					$3_2 \times 3_1(1,2)$ by Corollary 2
					$2_3(1,2)$ by Corollary 1
	$2_3(1,3)$	!	–	–	
					$2_3 \times 3_1(1,2) \overset{(13)}{\equiv} 2_3 \times 2_1(1,3)$ red. to $2_3(1,3)$
					$(1,2)_3 \times (1,3) \equiv 3_2 \times 3_1(1,2)$ red. to $3_2(1,2)$
					$(1,2)_3 \times 3_1(1,2)$ by Corollary 2

Acknowledgements. This work is partially supported by the Bulgarian National Science Fund under grant No. DO 02-359/2008.

References

[1] Alefeld G., Kreinovich, V., Mayer, G.: On the Solution Sets of Particular Classes of Linear Interval Systems, J. Comput. Appl. Math. 152, 1–15 (2003)

[2] Hladík, M., Description of Symmetric and Skew-Symmetric Solution Set, SIAM J. Matrix Anal. Appl. 30(2):509–521 (2008)

[3] Popova, E.: Explicit description of 2D parametric solution sets, BIT Numerical Mathematics, June 2011, DOI: 10.1007/s10543-011-0339-z

Edge of chaos in reaction- diffusion CNN models

Victoria Rashkova

1 Nature and application of the reaction-diffusion equation

Reaction- diffusion type equations are widely used to describe phenomena in different fields, as biology- Fisher model, FitzHugh- Nagumo nerve convection model, Vector-disease model, chemistry- Brusselator model, physics- Sine Gordon model, etc. Modulation equations play an essential role in the description of systems which exhibit patterns of nearly periodic nature. We shall study the Newel- Whitehead equation of the form:

$$\frac{\partial u}{\partial t} = \frac{\partial^2 u}{\partial x^2} + au - bu^3 \tag{1}$$

Spatial and spatio- temporal patterns occur widely in physics, chemistry and biology. In many cases, they seem to be generated spontaneously. These phenomena have motivated a great deal of mathematical modeling and the analysis of the resultant systems has led to a greater understanding of the underplaying mechanisms. Partial differential equations of diffusion type have long several as models for regulatory feedbacks and pattern formation. Such systems cause some difficulty since both existence and behavior of the solutions are difficult to establish. For this purpose we apply the Cellular Neural Networks (CNN) approach for studying the Newell- Whitehead models represented by equation (1). The dynamics of this model will be studied by using the describing function technique. It is known that some autonomous CNNs represent an excellent approximation to nonlinear partial differential equations (PDEs). The intrinsic space distributed topology makes the CNN able to produce real- time solutions of nonlinear PDEs. Consider the following well- known PDEs, generally referred to us in the literature as a reaction- diffusion equation:

$$\frac{\partial u}{\partial t} = f(u) + D\nabla^2 u \tag{2}$$

where $u \in R^N, f \in R^N, D$ is a matrix with the diffusion coefficient, and $\nabla^2 u$ is Laplacian operator in R^2. There are several ways to approximate the Laplacian operator in discrete space by a CNN synaptic law with an appropriate A- template. Consider CNN layer such that the state voltage of a CNN cell $u_j(t)$ at a grid point j is associated with $u(jh,t), h = \Delta x$. Therefore, an one- dimensional Laplacian template will be in the following form $A_1 = (1,-2,1)$ and the CNN model in this case is:

$$\frac{du_j}{dt} = (u_{j-1} - 2u_j + u_{j+1}) + au_j - bu_j^3, j = 1,...,n, n = M.M \tag{3}$$

We will introduce an approximative method for studying the dynamics of CNN model (3), based on a special Fourier transform. The idea of using Fourier expansion for finding the solution of PDFs is used to predict what spatial frequencies or models will dominate in nonlinear PDEs. In CNN literature this approach, has been developed for analyzing the dynamics of CNNs with symmetric templates.

2 CNN model of reaction-diffusion for Newell - Whitehead equation

We shall study the dynamics and the stability properties of (3) by using the describing function method. Applying the double Fourier transform:

$$F(s,z) = \sum_{k=-\infty}^{k=\infty} z^{-k} \int_{-\infty}^{\infty} f_k(t) \exp(-st) dt$$

To the CNN equation (1) we obtain:

$$sU = (z^{-1}U - 2U + zU) + aU - bU^3 \tag{4}$$

We denote $N(U) = aU - bU^3$ and then from (3) we obtain

$$U(s,z) = \frac{1}{s - (z^{-1} - 2 + z)} N(U(s,z)) \tag{5}$$

In the double Fourier transform we suppose that $s = i\omega_0$ and $z = exp(i\Omega_0)$ where ω_0 is a temporal frequency, Ω_0 is a spatial frequency. According to the describing function method, $H(s,z) = \frac{1}{s-(z^{-1}-2+z)}$ is the transform function, which can be presented in term of ω_0, Ω_0 as $H(s,z) = H_{\Omega_0}(\omega_0)$. We are looking for possible periodic state solutions of the system of the form:

$$U_{\Omega_0}(\omega_0) = U_{m_0} \sin(\omega_0 t + j\Omega_0) \tag{6}$$

Then we can approximate the output in the same way:

$$V_{\Omega_0}(\omega_0) = V_{m_0} \sin(\omega_0 t + j\Omega_0) \tag{7}$$

According to the describing function method we take the first harmonics, i.e. $j = 0$

$$U_{\Omega_0}(\omega_0) = U_{m_0} \sin \omega_0 t \tag{8}$$

$$V_{\Omega_0}(\omega_0) = V_{m_0} \sin \omega_0 t$$

We can find the amplitude V_{m_0} of the output:

$$V_{m_0} = \frac{1}{\pi} \int_{-\pi}^{\pi} N(U_{m_0} \sin \psi) \sin \psi d\psi = aU_{m_0} - \frac{3}{4} bU_{m_0}^3 \tag{9}$$

If we substitute $s = i\omega_0$ and $z = exp(i\Omega_0)$ in the transfer function $H(s,z)$ we obtain:

$$H_{\Omega_0}(\omega_0) = \frac{1}{i\omega_0 - 2\cos\Omega_0 + 2} \tag{10}$$

According to (10) the following constraint hold:

$$\Re(H_{\Omega_0}(\omega_0)) = \frac{U_{m_0}}{V_{m_0}} \tag{11}$$

$$\Im(H_{\Omega_0}(\omega_0)) = 0$$

Suppose that our CNN model (3) is a finite circular array of N cells. For this case we have finite set of frequencies:

$$\Omega_0 = \frac{2\pi k}{N}, 0 \leq k \leq N-1 \tag{12}$$

Thus (10),(11) and (12) give us equations necessary set of equations for finding the unknowns $U_{m_0}, \omega_0, \Omega_0$. As we mentioned above we are looking for a periodic wave solution of (4), therefore U_{m_0} will determine approximate amplitude, of the wave and $T_0 = \frac{2\pi}{\omega_0}$.will determine the wave speed.

Proposition 1. *CNN model (3) of the Newell- Whitehead equation (1) with circular array of N cells has periodic solutions $x_j(t)$ with a finite set of spatial frequencies (12).*

Let us know consider the nonlinear term of our CNN model in the form

$$g(c,u) = c - au + bu^3$$

We shall study the dynamics of $g(c,0)$ for different values of the parameter c in order to show the bifurcation diagram of our CNN model. For $c = 0$, equation it has stable orbit structure. The flow continues to have stable orbit structure for small values of the parameter, that is for $-c_1 < c < c_1$ where $c = \frac{2}{3}a\sqrt{\frac{a}{3b}}$ is the local minimum and $-c_1$ is the local maximum value of $g(c,0)$ for different values of the parameter c in order to show the bifurcation diagram of our CNN model. For $c = -c_1$ or $c = c_1$ the equation is at a bifurcation point. For the parameter values $c < -c_1$ and $c > c_1$ the equation again has stable orbit structure. The bifurcation diagram is given in Fig.1.
If we start the system with a very large negative value of c, after a long time the system will be very near the stable equilibrium state on the right leg of the cubic. Now, let us continuously increase the value of the parameter c. Since the system was near the stable state when we began to very c it will stay near this stable state for small variations in c. In fact, as we increase the parameter c the system will follow the stable equilibrium on the right until $c = c_1$. At this point the system will jump to a different equilibrium state on the left leg of the cube. As we continue to increase the parameter c, the system will follow the state equilibria on the left. Now, if we start decreasing the parameter c form a very large positive value, the system will follow the equilibria on the left leg of the cubic until $c = -c_1$, at which point it will jump to the right leg. The important observation about this experiment is that the system

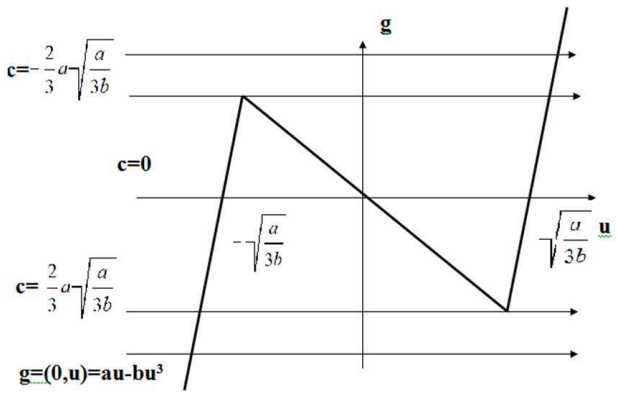

Figure 1: Bifurcation diagram for the function $g(c, u)$

experience a jump at two different values of the parameter.
There has been many studies on traveling wave solutions of spatially discrete or both spatially and time discrete systems. In our case we shall study the existence and structure of traveling wave solutions of autonomous Cellular Neural Networks. There are two possibilities of the structure of the traveling wave solutions- in one dimensional

$$x_i = \Phi(i - ct) \tag{13}$$

or two dimensional case respectively.

$$x_{ij}(t) = \Phi(i\cos\theta + j\sin\theta - ct) \tag{14}$$

where $\theta \in \Re$ is given, $\Phi : R_1 \to R_1$. is a continuous function and c is unknown real number. Denote $s = i\cos\theta + j\sin\theta - ct$ or $(s = i - ct)$. Then $\Phi(s)$ and c satisfy the equation of the form:

$$-c\Phi'(s) = G(\Phi(s + r_0), \Phi(s + r_1), ..., \Phi(s + r_n)) \tag{15}$$

here r_0, r_i are real numbers for $i = 1$ to N. If the above equation depends on the past and future, i.e. if

$$r_{min} \equiv min\{r_i\}_{i=0}^{N} < 0 < r_{max} \equiv max\{r_i\}_{i=0}^{N} \tag{16}$$

then it is called mixed type. If $r_{min} = 0$ or $r_{max} = 0$ then it is called advance or delay type respectively. The above equation is called bistable if it has spatially homogeneous solutions $\Phi(s) \equiv x^-, x^0$ and x^+ and satisfying $x^- < x^0 < x^+$. Suppose that the equation is bistable and that it has a unique monotone solution satisfying the boundary conditions:

$$\lim_{x\to-\infty} \phi(s) = x^- and \lim_{x\to\infty} \phi(s) = x^+$$

Our objective is to study the structure of traveling wave solutions of Newell- Whitehead CNN model. Let us consider our CNN equation (3). The traveling wave solutions will be presented in the following form:

$$u_j(t) = u(\eta), 1 \leq j \leq n \tag{17}$$

where $\eta = -jg, h > 0$ is a parameter. Note that η is the coordinate moving along the array with a velocity equal to $c = \frac{1}{h}$. Substituting (17) in (3) we obtain

$$\dot{u} = u(\eta - h) - 2u(\eta) + u(\eta + h) + N(u) \tag{18}$$

where the dot denote differentiation with respect to $\eta, N(u) = au(\eta) - bu^3(\eta)$. The two different terms $[u(\eta - h) - u(\eta)] - [u(\eta + h)]$ can be replaced approximately by the first derivatives $-\frac{\dot{u}}{h}$ and $\frac{\dot{u}}{h}$ respectively. Hence, we obtain:

$$\dot{u} = \frac{1}{1 + 2c} N(u) \tag{19}$$

Clearly $u = 0$ and $u \equiv \pm\sqrt{\frac{a}{b}}$ are solutions of the stationary problem. So there are three equilibria $E_0 = (0, 0)$ and $E_1 = (\sqrt{\frac{a}{b}}, 0), E_2 = (-\sqrt{\frac{a}{b}}, 0)$. The following theorem for the traveling waves of the Newell- Whitehead CNN model (3) hold:

Theorem 1. *For the Newell- Whitehead CNN model (3), there exist $c > 0$, such that there is a*

(i) heteroclinic orbit connecting the equilibria E_0 and E_1 the traveling wave $u(\eta)$ is strictly monotonically increasing;

(ii) heteroclinic orbit connecting the E_0 and E_2 the traveling wave $u(\eta)$ is strictly monotonically decreasing

There are exact solutions of the Newell- Whitehead equation (1) for $a > 0$ and $b > 0$

$$\omega(x,t) = \pm\sqrt{\frac{a}{b}} \frac{C_1 \exp(\frac{1}{2}\sqrt{2ax}) - C_2 \exp(-\frac{1}{2}\sqrt{2ax}))}{C_1 \exp(\frac{1}{2}\sqrt{2ax}) + C_2 \exp(-\frac{1}{2}\sqrt{2ax}) + C_3 \exp(-\frac{3}{2}at)}$$

$$\omega(x,t) = \pm\sqrt{\frac{a}{b}} [\frac{2C_1 \exp(\sqrt{2ax}) + C_2 exp(\frac{1}{2}\sqrt{2ax} - \frac{3}{2}at)}{C_1 \exp(\sqrt{2ax}) + C_2 \exp(\frac{1}{2}\sqrt{2ax} - \frac{3}{2}at) + C_3} - 1]$$

where C_1, C_2 and C_3 are arbitrary constants. The following simulations of our CNN model are made for different values of cell parameters.

References

[1] N.F.Britton, *Reaction-Diffusion Equations and Their Applications to Biology*, Acad. Press, New York, 1986.

[2] L.O.Chua, L.Yang, Cellular neural networks: Theory, IEEE Trans. Circuits Syst.,35:1257-1272,1988.

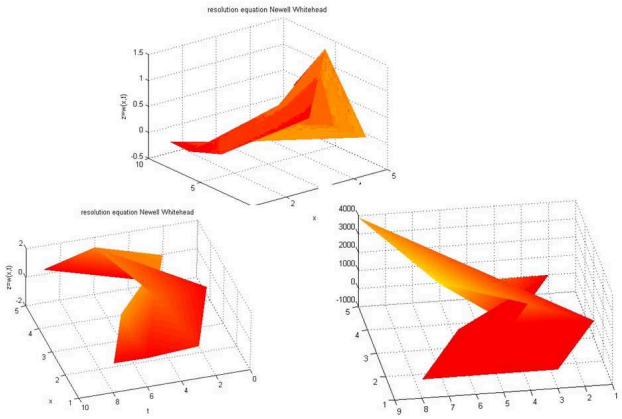

Figure 2:

[3] Chua L.O., Hasler M., Moschytz G.S., Neirynsk J., Autonomous cellular neural networks: a unified paradigm for pattern formation and active wave propagation, *IEEE Trans. CAS-I*, vol. 42, N 10, pp. 559-577, Oct. 1995.

[4] Genesio R., Tesi A., Villoresi F., A frequency approach for analyzing and controlling chaos in nonlinear circuits, *IEEE Trans. CAS-I*, vol. 40, N 11, pp. 819-827, Nov. 1993.

[5] J.Guckenheimer, Ph.Holmes, *Nonlinear Oscillations, Dynamical Systems, and Bifurcations of Vector Fields*, Springer, 1983.

[6] C.-H.Hsu, S.-S.Lin,W.Shen, Travelling waves in Cellular Neural Networks, Int.J.Bifurcation and Chaos, vol.9,N0.7, pp.1307-1319, 1999.

[7] A.I.Mees, *Dynamics of Feedback Systems*, Wiley, London, 1981.

[8] Polyanin A.D., Zaitsev V.F., Handbook of nonlinear partial differential equations, Chapman & Hall/CRC, Boca Raton, 2004.

[9] Roska T., Chua L.O., Wolf D., Kozek T., Tetzlaff R., Puffer F., Simulating nonlinear waves and partial differential equations via CNN- Part I: Basic techniques, *IEEE Trans. CAS-I*, vol. 42, N 10, pp. 807-815, Oct. 1995.

[10] A.Slavova, Applications of some mathematical methods in the analysis of celullar neural networks, J.Comp.Appl.Math. 114, pp. 387-404, 2000.

Applications of topological games in Optimization and Nonlinear Analysis

Julian P. Revalski

1 Introduction

It seems that the first infinite positional game with perfect information appeared in 1936 in the well-known Scottish Book [10] which was created by the mathematical group of the Lvov University (at that time in Poland). Among the names of this group were those of Banach, Mazur, Steinhaus, Ulam and others. The game was formulated by Mazur in one of the problems in the Scottish book and an (unpublished) answer of the question, related to the game and posed by Mazur, was given by Banach. This is why it has become later known under the name *Banach-Mazur game*. In the period after the Second World War different other type of such games appeared, mostly played in topological spaces, which were thoroughly studied from different points of view (see e.g. the survey [9]). For a long period this study was mostly self-oriented. Since the 70's and 80's the applications of topological games to other fields of mathematics have started to grow, such as functional analysis, geometry of Banach spaces, topology and nonlinear analysis. The aim of this presentation is to outline two such applications: the first one is related to the validity of variational principles in optimization and the second one to geometry of Banach spaces and the existence of solutions to certain differential equations.

2 Banach-Mazur type games and variational principles in Optimization

Let X be a completely regular topological space and $f : X \to \mathbb{R} \cup \{+\infty\}$ be an extended real-valued function which is lower semicontinuous, bounded from below and proper. The latter means that the function f has at least one finite value, i.e. the set $\mathrm{dom}(f) := \{x \in X : f(x) < +\infty\}$, which is the effective domain of f, is nonempty. Let further $(Y, \|\cdot\|)$ be a Banach space of bounded and continuous functions in X. If the set $E(f) := \{g \in Y : f + g$ attains its infimum in $X\}$ is dense in Y we say that we have *a variational principle for the function f with perturbations from Y*. The interest to have such a principle lies in the fact that, even if the function f does not attain its infimum in X, we can perturb it with, as small perturbation as we want, in such a way that the perturbed function attains its infimum in X. If the set $E(f)$ is residual in Y (that is, its complement in Y is of the first Baire category in Y) then we say that we have *generic variational principle for f with perturbations from Y*–in this latter case the set $E(f)$ is substantially bigger from topological point of view than of being merely dense in Y. Such (or similar) setting is the case in several

well-known variational principles such as those of Ekeland, Borwein-Preiss, Deville-Godefroy-Zizler, Stegall and others–see e.g. the monograph [3]. These principles have numerous applications in various branches of mathematics.

We will consider below the case when the space Y is the family of all bounded and continuous functions $C(X)$ in X equipped with its usual sup-norm. It turns out that in this case, the validity of generic variational principles as above is related to the Banach-Mazur game and its variants. Two players, named α and β, play a game in X, by choosing, at each step $n \geq 1$, alternatively nonempty open sets U_n for β (who starts the game) and V_n for α so that $U_{n+1} \subset V_n \subset U_n$ for every $n \geq 1$. The obtained sequence $\{U_n, V_n\}$ is called *a play*. The player α wins this play if $\cap_n U_n = \cap_n V_n$ is nonempty. Otherwise β wins the play. This is one of the most known variants of the Banach-Mazur game and is denoted by $BM(X)$. A *strategy* s for the player α is a rule which to any possible finite sequence of the type $(U_1, V_1, \ldots, U_n)$ which consists of possible moves of the players in the game, assigns a nonempty open set $V_n := s(U_1, V_1, \ldots, U_n)$. The play $\{U_n, V_n\}$ is called *an s-play* if any set V_n in this play is obtained according to s. The strategy s is called *winning* for α if she wins any s-play in the game $BM(X)$. One defines a (wining) strategy for the player β in an analogous way.

The following fact is the first one relating the validity of generic variational principles with the existence of winning strategies in this game.

Theorem 2.1. ([6]) *If $f : X \to \mathbb{R}$ is a continuous bounded function, then the set $E(f) = \{g \in C(X) : f + g$ attains its minimum in $X\}$ is residual in $C(X)$ if and only if the player α has a winning strategy in the Banach-Mazur game $BM(X)$.*

If we want to have a generic variational principle for a lower semicontinuous function f we have to involve a variant of the Banach-Mazur game: in this game, again two players which we will denote by Σ and Ω play a game in X by alternatively choosing nonempty sets A_n for Σ, who starts the game, and B_n for Ω in such way that$A_{n+1} \subset B_n \subset A_n$ for any $n \geq 1$ and, in addition, B_n must be relatively open in A_n for every $n \geq 1$. The player Ω wins the play $\{A_n, B_n\}$ if $\cap_n \overline{A}_n = \cap_n \overline{B}_n$ is nonempty (here $\overline{A}$ means the closure of a set A in X). Otherwise, Σ wins this play. This game, which is denoted by $G(X)$ was considered for the first time by Michael [8] for the study of completeness properties of metric spaces. One sees that in this variant the player Σ has much more freedom in her choices compared with the player β in the classical variant of the Banach-Mazur game. The player Ω however continues to be obliged to play relatively open sets in her opponent choices. The definitions of (winning) strategies for the players Σ and Ω in this game are similar to those in the Banach-Mazur game given above.

With the above notions in hand we have the following generic variational principle:

Theorem 2.2. ([2, 7]) *Let $f : X \to \mathbb{R} \cup \{+\infty\}$ be a proper lower semicontinuous function which is bounded from below in X. Let the player Ω has a winning strategy in the game $G(X)$. Then the set $\{g \in C(X) : f + g$ attains its infimum in $X\}$ is residual in $C(X)$.*

Two remarks are in order here: First, it should be mentioned that in the above case the existence of a winning strategy for the player Ω in the game $G(X)$ is only a sufficient condition for the validity of the generic variational principle. There are examples showing that this condition is not necessary (cf., [2]). Second, if one wants that the perturbations $f+g$, $g \in E(f)$, not only attain their infimum in X, but something stronger is true, such as, uniqueness of the minimum, or the so-called well-posedness of $f+g$, then special winning strategies have to exist in the above games–see e.g. [2, 6, 7].

3 Point-hyperplane game with applications to geometry of Banach spaces and Eikonal equations

The game that we will discuss in this section is related to the following classical property known as the Denjoy-Clarkson property: *if $u : \mathbb{R} \to \mathbb{R}$ is an everywhere differentiable function in $\mathbb{R}$ then, for any open set $U \subset \mathbb{R}$ the set $\{x : u'(x) \in U\}$ is either empty or of positive Lebesgue measure.* C.E. Weil [11] raised the question whether this property remains valid for the gradient of an everywhere differentiable function of several variables and this question is known as the Weil gradient problem. The question was answered in negative by Buczolich [1] who constructed an everywhere differentiable function $u : \mathbb{R}^2 \to \mathbb{R}$ such that $\nabla u(0) = 0$ but $\|\nabla u(x)\| \geq 1$ for almost all points $x \in \mathbb{R}^2$ (and thus, u fails to satisfy Denjoy-Clarkson property in the open unit ball of $\mathbb{R}^2$).

The construction of the function u is not easy and a significant simplification was proposed by Malý and Zelený [5] by use of the following infinite game in $\mathbb{R}^2$: two players, Player I and Player II, play a game in $\mathbb{R}^2$ as follows: Player I starts by choosing a point a_0 in the open unit ball of $\mathbb{R}^2$ and Player II answers by choosing a line L_0 passing through a_0; then Player I continues by choosing a point a_1 on L_0 which stays in the open unit ball of $\mathbb{R}^2$ and Player II answers by choosing a line L_1 that passes through a_1, and so on. The Player II wins if the sequence $(a_n)_n$ is convergent in $\mathbb{R}^2$, otherwise Player I wins. This game is called *point-line* game. The (winning) strategies for the players are defined similarly to the corresponding notions in the Banach-Mazur games.
Malý and Zelený proved [5] that the Player II has a winning strategy in the point-line game. And this is what one needs to simplify the Buczolich proof. It should be noted that the proof of the existence of a winning strategy is not evident.

This game has a natural generalization in more dimensions which was proposed and studied by Deville and Matheron in [4]: Let X be a (real) Banach space and B_X be its open unit ball. Players I and II play a game in X as follows: Player I chooses a point $a_0 \in B_X$ and Player II answers by a closed hyperplane H_0 so that $a_0 \in H_0$; then Player I continues by a point $a_1 \in H_0 \cap B_X$ and Player II answer is a closed hyperplane H_1 containing a_1; and so on. Player II wins if the sequences $(a_n)_n$ converges in X. Otherwise Player I wins. The game is called *point-hyperplane game*. If, in the above scheme, one replaces the closed hyperplanes H_n by closed (open) half-spaces F_n so

that each a_n lies on the boundary (or in the interior) of F_n, with the same winning conditions, the game is called *point-closed slice game* (resp. *point-open slice game*). The (winning) strategies in these games are defined in a similar as above way.

These generalizations are useful in the characterization of an important geometric propertiy, the Radon-Nikodym property (RNP). This property in a Banach space X is equivalent to the validity of Radon-Nikodym theorem about representations of absolutely continuous measures and can be given the following geometric form: *The Banach space X has RNP if for any $\varepsilon > 0$ there is an open half-space F so that the slice $F \cap B_X$ has norm-diameter less than ε.* The Radon-Nikodym property has turned out to be very useful in Banach space geometry (in operator theory, differentiability of convex functions, etc.).

The RNP can be characterized by the existence of winning strategies in the above games in the following way:

Theorem 3.1. (Deville-Matheron [4]) *Let X be a Banach space. The following conditions are equivalent:*

(a) *X has RNP;*

(b) *Player II has a winning strategy in the point-hyperplane game;*

(c) *Player II has a winnings strategy in the point-closed (open) slice game.*

Let us mention that in the above definitions of (winning) strategies for the players, at each step, the strategy depends on the whole history of the game before this step (i.e., depends on all choices of the players before the corresponding step). If there is a strategy that depends only on the previous move of the opponent player, such a strategy is called *tactic*. The following result shows a situation when we have the existence of a winning tactic for one of the players in the above games.

Theorem 3.2. (Deville-Matheron [4]) *If X is a superreflexive Banach space than Player II has a winning tactic in the point-closed slice game.*

Finally, Deville and Matheron used the existence of a winning strategy for the Player II in the above games in order to prove the following existence of solutions to an Eikonal equation in finite dimensions, which is also another counterexample for the Denjoy-Clarkson property in $\mathbb{R}^n$, $n \geq 2$. Namely, the following theorem holds:

Theorem 3.3. ("Exotic" solutions of Eikonal equations: Deville-Matheron [4]) *Let Ω be an open subset of $\mathbb{R}^n$, $n \geq 2$, $x_0 \in \Omega$ and $\|\cdot\|$ be any norm in $\mathbb{R}^n$. Then there exists a 1-Lipschitz function $u : \overline{\Omega} \to \mathbb{R}$ so that:*

(a) *u is bounded and everywhere differentiable on Ω;*

(b) *$\nabla u(x_0) = 0$;*

(c) *$\|\nabla u(x)\| = 1$ almost everywhere in $\mathbb{R}^n$;*

(d) *$u|_{\partial\Omega} \equiv 0$.*

References

[1] Z. Buczolich, Solution to the problem of C.E. Weil, *Revista Mat. Iberoamericana*, **21**(2005), 889–910.

[2] M.M. Čoban, P.S. Kenderov and J.P. Revalski, Variational principles and topological games, submitted for publication.

[3] R. Deville, G. Godefroy and V. Zizler, Smoothness and renormings in Banach spaces, Pitman monographs and Surveys in Pure and Appl. Math., Longman Scientific & Technical, 1993.

[4] R. Deville, E. Matheron, Infinite games, Banach space geometry, and Eikonal equations, *Proc. London Math. Soc.*, **95**(2007), 49–68.

[5] J. Malý and M. Zelený, A note on Buczolich solution of the Weil gradient problem, *Acta. Math. Hungarica*, **113**(2006), 145–158.

[6] P.S. Kenderov and J.P. Revalski, The Banach-Mazur game and generic existence of solutions to optimization problems, *Proc. Amer. Math. Soc.*, **118**(1993), 911–917.

[7] P.S. Kenderov and J.P. Revalski, Dense existence of solutions of perturbed optimization problems and topological games, *Compt. rend. Acad. bulg. Sci*, **63**, No.7(2010), 937–942.

[8] E. Michael, A note on completely metrizable spaces, *Proc. Amer. Math. Soc.*, **96**(1986), 513–522.

[9] R. Telgárski, Topological games: On the 50-th anniversary of the Banach-Mazur game, *Rocky Mount. J. Math.* **17**(1987), 227–276.

[10] S.M. Ulam, The Scottish Book, Los Alamos, CA, 1977.

[11] C.E. Weil, On properties of derivatrives, *Trans. Amer. Math. Soc.*, **114**(1965), 363–376.

Numerical Implementation of Fourier-transform Method for Generalized Wave Equations

M. D. Todorov, C. I. Christov

1 Problem Formulation

Consider the Boussinesq equation in two spatial dimensions (so called Boussinesq Paradigm Equation)

$$u_{tt} = \Delta(u - \alpha u^2 + \beta_1 u_{tt} - \beta_2 \Delta u) \tag{1}$$

where $u = u(x, y, t)$ is the surface elevation, t is the time, $\beta_1, \beta_2 > 0$ are two dispersion coefficients and α is an amplitude parameter. The initial conditions can be prepared by a single soliton (computed numerically and semi-analytically) or as a superposition of two solitons (see, for example [2], [1], [3] and [4]). The possible ways to solve numerically the above problem can be summarized in three groups: (*i*) by using a semi-implicit difference scheme; (*ii*) by using a fully implicit difference scheme; (*iii*) by using pseudospectral methods. In this paper we focus our attentions to the last ones.

2 Fourier Integral-Transform Method

Instead of using a multigrid solver (see, for example [5]) we can use a 2D Fourier transform. Applying it to the original equation (1) we get a second order Ordinary Differential Equation (ODE) with respect the time in the configurational space

$$[1 + 4\pi\beta_1(\xi^2 + \eta^2)]\hat{u}_{tt} = -4\pi^2(\xi^2 + \eta^2)\left[1 + 4\beta_2\pi^2(\xi^2 + \eta^2)\right]\hat{u} + 4\pi^2\alpha(\xi^2 + \eta^2)\hat{N} \tag{2}$$

where $\hat{u}(\xi, \eta, t) := \mathcal{F}[u]$ and $\hat{N}(\xi, \eta, t) := \mathcal{F}[u^2]$. Solving the last ODE is straightforward and requires very few operations per time step for given $\hat{N}$ but the lion's share of the computational resources are consumed by the computation of the contribution of the nonlinear term. An implicit scheme would require inverting the matrix that results from the discrete approximation of the convolution integral representing the Fourier transform of the nonlinear term u^2. The concept of the pseudospectral method is to use inverse Fourier transform to represent the sought function in the configurational space and to compute the square there, and then to "return" to the spectral space via the Fourier transform. The straightforward application of the pseudo-spectral method leads to an inherently explicit scheme, and in many case the latter us fully enough. Yet, for computations at very large times, one needs a fully conservative energy-conserving scheme. The latter is the object of the present note. We use the concept of "internal iterations" as introduced in [6].

3 Numerical Implementation of the Pseudo-spectral Method

We introduce a uniform grid (ξ_m, η_n) in the Fourier space and discretize the Fourier integral. Suppose that we know $\hat{u}^k$, $\hat{u}^{k-1}$,..., $\hat{u}^0$. Then the next $(n+1)$-st time stage is computed from the following three-stage difference scheme

$$[1+4\pi\beta_1(\xi_m^2+\eta_n^2)]\frac{\hat{u}_{mn}^{k,l+1}-2\hat{u}_{mn}^{k}+\hat{u}_{mn}^{k-1}}{\tau^2} = -2\pi^2(\xi_m^2+\eta_n^2)[1+4\beta_2\pi^2(\xi_m^2+\eta_n^2)](\hat{u}_{mn}^{k,l+1}+\hat{u}_{mn}^{k-1}) + \frac{4}{3}\pi^2\alpha(\xi_m^2+\eta_n^2)\mathcal{D}_F\left[(\mathcal{D}_F^{-1}[\hat{u}_{mn}^{k,l}])^2+\mathcal{D}_F^{-1}[\hat{u}_{mn}^{k,l}]\mathcal{D}_F^{-1}[\hat{u}_{mn}^{k-1}]+(\mathcal{D}_F^{-1}[\hat{u}_{mn}^{k-1}])^2\right], \quad (3)$$

where τ is the time step, and $\mathcal{D}_F[\cdot]$ denotes the discrete Fourier transform, and $\mathcal{D}_F^{-1}[\cdot]$ is the inverse, respectively. The concept of internal iterations requires that at each time stage the linear scheme Eq. (3) starts with $u_{mn}^{k,l}=u_{mn}^{k}$, $l=0$ and is repeated with increasing the number l until convergence is reached for some $l+1=L$. Then it is set up that $u_{mn}^{k+1}:=u_{mn}^{k,L}$. Then, following [6], we show that the scheme is fully nonlinear and fully implicit and conserves the energy within the tolerance level set for the convergence of the internal iterations (can be chosen close the the round-off error of the computer). Note that the inverse Fourier transform gives a discrete function $u_{ij}^k:=\mathcal{D}_F^{-1}[\hat{u}_{mn}^k]$, where i and j are the indices of a specific grid point in the configurational space.

4 Numerical Tests and Validations

We treat two 1D wave equations. In order to approximate the Fourier integrals we use specialized Filon's quadrature [8] on a uniform mesh

$$\int_{-x_\infty}^{x_\infty} u(x)\mathrm{e}^{\mathrm{i}\xi x}\mathrm{d}x \approx \left(\frac{1}{\mathrm{i}\xi}+\frac{1-\mathrm{e}^{-\mathrm{i}\xi h}}{\xi^2 h}\right)v_M-\left(\frac{1}{\mathrm{i}\xi}+\frac{\mathrm{e}^{-\mathrm{i}\xi h}-1}{\xi^2 h}\right)v_0 + \frac{4}{\xi^2 h}\sin^2\frac{\xi h}{2}\sum_{m=1}^{M-1}v_m,$$

with $v\equiv u(x)\mathrm{e}^{\mathrm{i}\xi x}$, spatial step h and "actual" infinities $[-x_\infty, x_\infty]$.
The advantage of above quadrature consists in both – for $\xi h\le 1$ it becomes a generalized trapezoidal formula with $O(h^2)$ error and when $\xi h>1$ the order of error is as $O(M\xi^{-3}u_{xx})$ [7], [9]. Having in mind the localized nature of the sought solutions it is obvious that $\lim_{x\to\pm\infty}u_{xx}=0$ and the decay of the quadrature error for $\xi\gg 1$ and given x_∞ in the problems in question is obeyed.

4.1 Cauchy problem for 1D string equation

Let us consider the well-known Cauchy problem

$$u_{tt} = c^2 u_{xx}, \qquad c = \text{const} > 0, \quad -\infty < x < \infty, \quad t > 0 \tag{4}$$

$$u(x,0) = f(x), \qquad u_t(x,0) = g(x) \tag{5}$$

with exact solution given by D'Alembert's formula

$$u(x,t) = \frac{1}{2}[f(x-ct) + f(x+ct)] + \frac{1}{2c}\int_{x-ct}^{x+ct} g d\theta.$$

The image of the problem (4)-(5) in the configurational space (again Cauchy problem with respect an ODE with algebraic right hand side) reads

$$\hat{u}_{tt} = -c^2\xi^2\hat{u}, \quad \hat{u}(\xi,0) = \hat{f}(\xi) \qquad \hat{u}_t(\xi,0) = \hat{g}(\xi) \tag{6}$$

and exact solution $\hat{u}(\xi,t) = \hat{f}(\xi)\cos c\xi t + \frac{\hat{g}(\xi)}{c\xi}\sin c\xi t$ where $\mathcal{F}^{-1}[\hat{u}] = u(x,t)$.
Following the idea in (3), we build a standard three-stage explicit difference scheme for (6)

$$\frac{\hat{u}_m^{k+1} - 2\hat{u}_m^k + \hat{u}_m^{k-1}}{\tau^2} = -\frac{c^2\xi^2}{2}(\hat{u}_m^{k+1} + \hat{u}_m^{k-1}) \tag{7}$$

setting the phase velocity $c = 1$, and (i) $f(x) = \mathrm{e}^{-(x-X)^2}$, $g(x) = 2(x-X)\mathrm{e}^{-(x-X)^2}$, X stands for the initial position of the center of the solitary wave; (ii) the functions $f(x)$ and $g(x)$ in the initial conditions are sech-like (see the next subsection). Let us note that the scheme is stable, when $ch/\tau \leq 1$.

4.2 Regularized Long Wave Equation

If $\beta_1 = 0$ the Boussinesq equation reduces to the so-called Regularized Long Wave Equation (RLWE)

$$u_{tt} = (u - \alpha u^2 + \beta u_{tt})_{xx} \tag{8}$$

and possesses the following exact solitary-wave solution (see [6]):

$$w = -\frac{3}{2}\frac{c^2-1}{\alpha}\mathrm{sech}^2\left(\frac{x-ct}{2c}\sqrt{\frac{c^2-1}{\beta}}\right). \tag{9}$$

Here c is the phase velocity, α is the parameter of the nonlinearity, and β is the dispersion parameter. For the mechanical meaning of Eq. (8) we refer the reader to [6]. To begin the time stepping, we set

$$u(x,0) = w(x,0) \quad \text{and} \quad u(x,\tau) = w_t(x,0)\tau + w(x,0) \tag{10}$$

and transform the latter to spectral space, thus providing the two initial conditions for the 1D version of the scheme (3).

5 Results and Conclusions

We show and discuss two groups of results concerning the 1D linear string equation and the 1D nonlinear RLWE. Figure 1 demonstrates the excellent comparison between the D'Alembert solution (dashed lines) and the numerical solution by the pseudospectral method (solid lines). Two running waves with Gaussian shape start from the coordinate origin $X = 0$ and go unchanged to the left and to the right with phase velocities $c_l = -c_r = 1$. The conclusion is that the linear wave equations can be

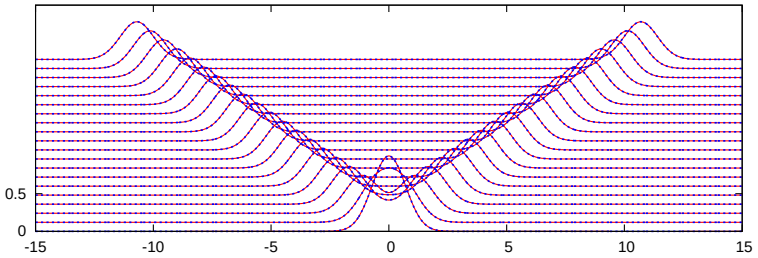

Figure 1: Comparison of the numerical solution with the D'Alembert formula.

discretized and solved numerically in the spectral space and only after the solution is obtained at each time stage, the inverse Fourier transformation can be used to restore the solution in the configuration space. As rule, the mapped differential equations are simpler compared to the original ones.
In Figure 2 the wave shapes are the same but the initial condition is a superposition of two running waves starting from different positions $-X_l = X_r = 3.5$ again with phase velocities $c_l = -c_r = 1$ which collide between them elastically.

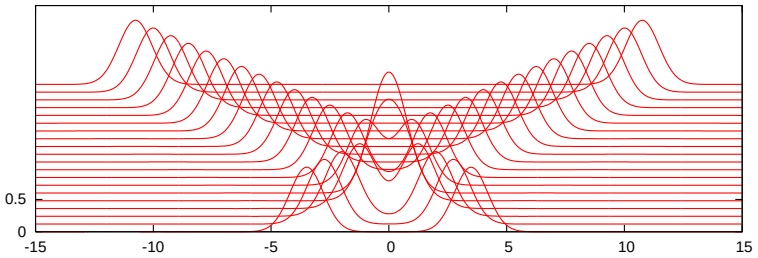

Figure 2: Superposition and elastic interaction of two Gaussian pulses.

The second part of investigation concerns 1D nonlinear dispersive generalized wave equations using RLWE as a featuring example. In the following figures the obtained numerical solutions with the described here algorithm are presented. To test the reliability of the method we compare the obtained results with these obtained by a finite difference method in [6].

In Figures 3 and 4 the head-on collisions for supercritical phase speeds that are still below the threshold of the blow-up are presented. The first figure presents a case where the nonlinearity is weaker, while in the second of these figures, the nonlinearity is considerable. In both cases, the solitons retain their individualities after the collision and no significant radiation is observed despite the fact that RLWE is not a fully integrable case. The only sign of inelasticity is the phase shift experienced by the colliding waves. For the sake of saving space it is not presented here.

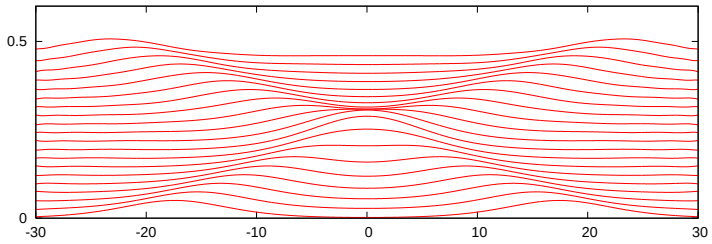

Figure 3: The inelastic interaction in RLWE for slightly supercritical phase velocities, $c_l = -c_r = 1.05$, $\alpha = -3$, $\beta = 1$.

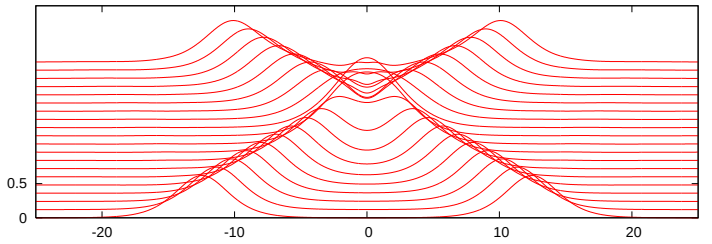

Figure 4: The interaction in RLWE near to the threshold of nonlinear blow-up, $c_l = -c_r = 1.5$, $\alpha = -3$, $\beta = 1$.

In the end, we present in Figure 5 a case known to lead to a blow-up of the solution.

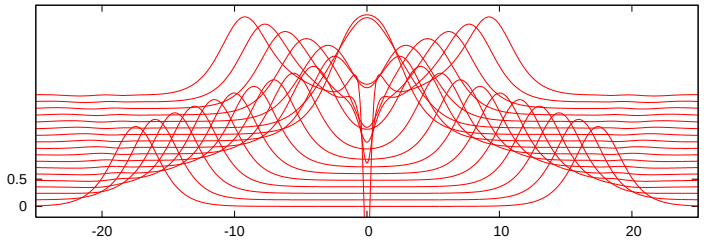

Figure 5: The blow-up in RLWE for large supercritical phase velocities, $c_l = -c_r = 2$, $\alpha = -3$, $\beta = 1$.

In all considered cases an excellent comparison with [6] is observed.

6 Conclusion

We have demonstrated that the pseudospectral methods and in particular Fourier transform can be efficient both for numerical treatment of linear and nonlinear wave equations. For the 2D and 3D equations one needs to apply 2D and 3D Fourier transforms and to follow the procedures described above.above.

Acknowledgement. This investigation is supported financially by the Science Foundation of Bulgarian Ministry of Education, Science, and Youth under grant DDVU02/71.

References

[1] A. Chertock, C. I. Christov, and A. Kurganov, "Central-Upwind Schemes for the Boussinesq Paradigm Equation," in *Computational Sci., & High performance Computing IV, NNFM*, edited by E. Krause *et al*, 2011, pp. 267-281.

[2] C. I. Christov and J. Choudhury, Perturbation Solution for the 2D Boussinesq Equation, *Mech. Res. Commun.*, (2011), galley proofs.

[3] C. I. Christov, N. Kolkovska, and D. Vasileva, "On the Numerical Simulation of Unsteady Solutions for the 2D Boussinesq Paradigm Equation," in *NMA 2010*, edited by I. Dimov, S. Dimova, and N. Kolkovska, 2011, *LNCS* **6046**, 386-394.

[4] C. I. Christov, M. D. Todorov, and M. A. Christou, Perturbation Solution for the 2D Shallow-Water Waves, in *Application of Mathematics in Technical and Natural Sciences*, AIP CP**1404**, pp. 53–60, 2011, doi: 10.1063/1.3659903.

[5] C. I. Christov and D. Vasileva, On the Numerical Investigation of Unsteady Solutions for the 2D Boussinesq Equation, accepted in this volume, 2012.

[6] C. I. Christov and M. G. Velarde, Inelastic Interaction of Boussinesq Solitons, *Int. J. Bifurc. and Chaos*, **4** (1994) 1095–1112.

[7] K. C. Chung, G.A. Evans, and J.R. Webster, A method to generate generalized quadrature rules for oscillatory integrals, *Applied Numer. Math.* **34** (2000), 85–93.

[8] L. N. G. Filon, On a quadrature formula for trigonometric integrals, *Proc. Roy. Soc., Edinb.* **49**, (1928-29), 38.

[9] N. N. Kalitkin, *Numerical Methods*, Nauka, Moscow, 1978, p.104. (in Russian)

On the Numerical Investigation of Unsteady Solutions for the 2D Boussinesq Paradigm Equation in a Moving Frame Coordinate System

Daniela Vasileva, Christo I. Christov

Introduction. One of the most important features of the generalized wave equations containing nonlinearity and dispersion, is that they possess solutions of type of permanent waves as shown in the original Boussinesq work [1]. In 1D, a plethora of deep mathematical results have been obtained for solitons, but it is of crucial importance to investigate also the 2D case, because of the different phenomenology and the practical importance. The accurate derivation of the Boussinesq system combined with an approximation, that reduces the full model to a single equation, leads to the Boussinesq Paradigm Equation (BPE) [2]:

$$u_{tt} = \Delta\left[u - F(u) + \beta_1 u_{tt} - \beta_2 \Delta u\right], \quad F(u) := \alpha u^2, \tag{1}$$

where u is the surface elevation of the wave, $\beta_1,\ \beta_2 > 0$ are two dispersion coefficients, and $\alpha > 0$ is an amplitude parameter. The main difference of (1) from the original Boussinesq Equation is the presence of a term proportional to $\beta_1 \neq 0$ called "rotational inertia".
It has been recently shown that the 2D BPE admits stationary translating localized solutions [3, 4, 5], which can be obtained approximately using finite differences, perturbation technique, or Galerkin spectral method. Results about their time behaviour and structural stability are presented in [6, 7, 8], and here we continue their investigation using a moving frame coordinate system. It allows us to keep the localized structure in the center of the coordinate system, reducing the effects of reflection from the boundary.

Numerical method for solving BPE. We introduce the following new dependent function

$$v(x, y, t) := u - \beta_1 \Delta u \tag{2a}$$

and substituting it in Eq. (1) we get the following equation for v

$$v_{tt} = \frac{\beta_2}{\beta_1}\Delta v + \frac{\beta_1 - \beta_2}{\beta_1^2}(u - v) - \Delta F(u).$$

We set $z := y - ct$, where c is the velocity of the stationary propagating soliton and obtain the following equation for $w(x, z, t) := v(x, z + ct, t)$

$$w_{tt} - 2c w_{tz} + c^2 w_{zz} = \frac{\beta_2}{\beta_1}\Delta w + \frac{\beta_1 - \beta_2}{\beta_1^2}(u - w) - \alpha \Delta F(u). \tag{2b}$$

Thus we obtain a system consisting of an equation for u, Eq. (2a), and an equation for w: Eq. (2b).
The following implicit time stepping can be designed for the system (2)

$$\begin{aligned}
&\frac{w_{ij}^{n+1} - 2w_{ij}^{n} + w_{ij}^{n-1}}{\tau^2} - c\frac{V^z[w_{ij}^{n+1} - w_{ij}^{n-1}]}{\tau} + \frac{c^2}{2}\Lambda^{zz}[w_{ij}^{n+1} + w_{ij}^{n-1}] \\
&= \frac{\beta_2}{2\beta_1}\Lambda\left[w_{ij}^{n+1} + w_{ij}^{n-1}\right] + \frac{\beta_1 - \beta_2}{2\beta_1^2}[u_{ij}^{n+1} - w_{ij}^{n+1} + u_{ij}^{n-1} - w_{ij}^{n-1}] \\
&\qquad - \Lambda G(u_{ij}^{n+1}, u_{ij}^{n-1}),
\end{aligned} \tag{3a}$$

$$u_{ij}^{n+1} - \beta_1 \Lambda u_{ij}^{n+1} = w_{ij}^{n+1}, \quad i = 0, \ldots, N_x + 1, \quad j = 0, \ldots, N_y + 1. \tag{3b}$$

Here τ is the time increment, $G(u_{ij}^{n+1}, u_{ij}^{n-1}) = \left[(u_{ij}^{n+1})^2 + u_{ij}^{n+1}u_{ij}^{n-1} + (u_{ij}^{n-1})^2\right]/3$, $\Lambda = \Lambda^{xx} + \Lambda^{zz}$ stands for the difference approximation of the Laplace operator Δ on a non-uniform grid, for example

$$\Lambda^{xx}\phi_{ij} = \frac{2\phi_{i-1j}}{h_{i-1}^x(h_i^x + h_{i-1}^x)} - \frac{2\phi_{ij}}{h_i^x h_{i-1}^x} + \frac{2\phi_{i+1j}}{h_i^x(h_i^x + h_{i-1}^x)} = \frac{\partial^2\phi}{\partial x^2}\Big|_{ij} + O(|h_i^x - h_{i-1}^x|),$$

and V^z is a central difference approximation of $\frac{\partial}{\partial z}$

$$V_z\phi_{ij} = \frac{h_{j-1}^z\phi_{ij+1}}{h_j^z(h_j^z + h_{j-1}^z)} - \frac{h_i^z\phi_{ij-1}}{h_{j-1}^z(h_j^z + h_{j-1}^z)} - \frac{(h_j^z - h_{j-1}^z)\phi_{ij}}{h_i^z h_{j-1}^z} = \frac{\partial\phi}{\partial z}\Big|_{ij} + O(|h_j^z - h_{j-1}^z|).$$

Another way to approximate w_{zt} for $c > 0$ is by the following "upwind" approximation

$$w_{zt} = \frac{w_{ij+1}^{n+1} - w_{ij}^{n+1} - w_{ij+1}^n + w_{ij}^n}{2\tau h_j^z} + \frac{w_{ij}^n - w_{ij-1}^n - w_{ij}^{n-1} + w_{ij-1}^{n-1}}{2\tau h_{j-1}^z} + O(|h_j^z - h_{j-1}^z| + \tau^2).$$

The values of the sought functions at the $(n-1)$-st and n-th time stages are considered as known when computing the $(n+1)$-st stage. The nonlinear term G is linearized using what we call internal iterations (translating the Picard's idea to the case of differential equations), i.e., we perform successive iterations for u and w on the $(n+1)$-st stage, starting with initial conditions from the already computed n-th stage.
The following non-uniform grid is used in the $x-$direction

$$x_i = \sinh[\hat{h}_x(i - n_x)],\ x_{N_x+1-i} = -x_i,\ i = n_x + 1, \ldots, N_x + 1,\ x_{n_x} = 0,$$

where N_x is an odd number, $n_x = (N_x + 1)/2$, $\hat{h}_x = D_x/N_x$, and D_x is selected in a manner to have large enough computational region. The grid in the $z-$direction is defined in the same way.
Because of the localization of the wave profile, the boundary conditions can be set equal to zero, when the size of the computational domain is large enough. The initial conditions are created using the best-fit approximation provided in [5]. The coupled system of equations (3) is solved by the Bi-Conjugate Gradient Stabilized Method with ILU preconditioner [9].

Numerical experiments. Denote by $u^s(x, y; c)$ the best-fit approximation of the stationary translating (with speed c) localized solutions, obtained in [5]

$$\begin{aligned} u^s(x, z; c) &= f(x, z) + c^2\left[(1 - \beta_1)g_a(x, z) + \beta_1 g_b(x, z)\right] \\ &+ c^2\left[(1 - \beta_1)h_1(x, z) + \beta_1 h_2(x, z)\right]\cos\left[2\arctan(z/x)\right], \end{aligned}$$

where the formulas for the functions $f,\ g_a,\ g_b$ may be found in [5]. For $t = 0$, the first initial condition is obvious: $u(x, z, 0) = u^s(x, z; c)$, and the second initial condition may be chosen as $u(x, z, -\tau) = u^s(x, z; c)$.
In the next examples solutions for $\beta_1 = 3,\ \beta_2 = 1,\ \alpha = 1$ are presented.

Example 1. The first example is for a phase speed $c = 0.27$. The basic grid has 161×161 points in the region $[-20, 20]^2$, $\tau = 0.1$. The results are for computations in fixed coordinates, for the moving frame coordinate system with upwind approximation of w_{tz}, for the moving frame coordinate system with central differences approximation of w_{tz}, for finer grid with 321×321 points and $\tau = 0.05$, and for a larger computational region with 641×641 points in $[-200, 200]^2$, $\tau = 0.1$. The behaviour of the solution is almost the same in all cases.

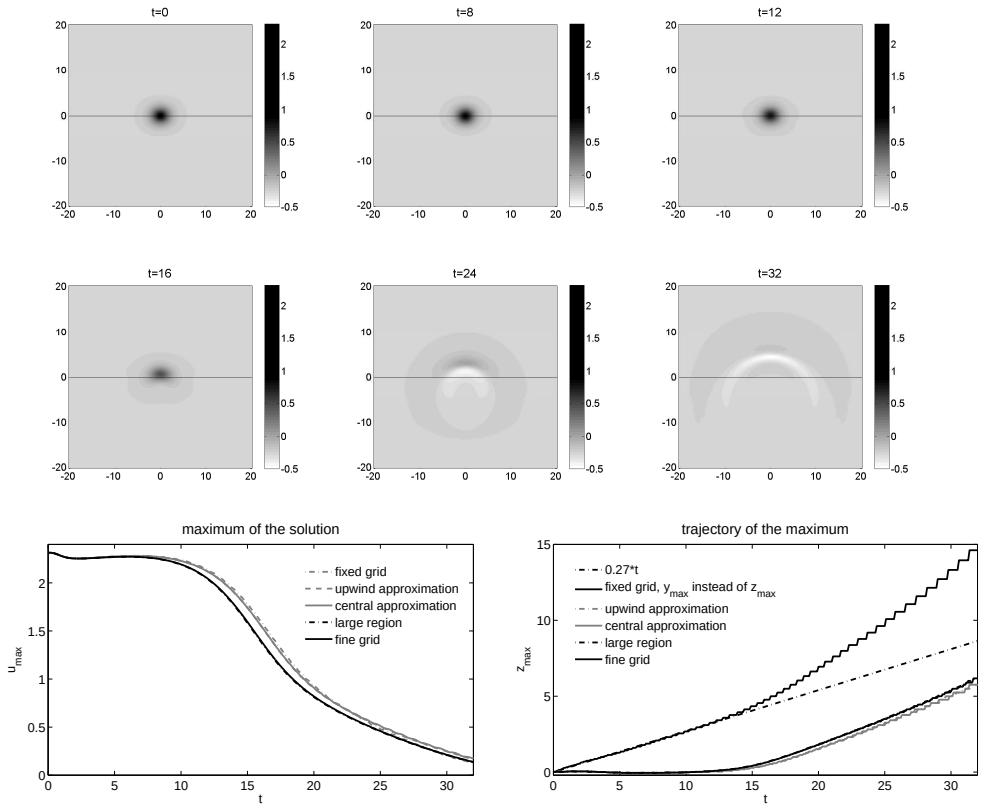

Figure 1: Evolution of the solution for $c = 0.27$, the maximum $u(0, z_{\max})$, and the trajectory of the maximum.

For $t < 10$ the solution stays near the center of the moving coordinate system and behaves like a soliton, i.e., preserves its shape, although its maximum slightly decreases. For larger times the solution transforms into a diverging propagating wave. As the structure is moving the weaves are not concentric – just like when we throw a stone in a pond at an angle. The evolution of the solution, as well as values of the maximum of the solution $u_{\max}$ and the trajectory of the maximum $z_{\max}$ ($y_{\max}$ for fixed coordinates) are shown in Fig.1.

Example 2. In Fig.2 results for $c = 0.28$ are presented. For $t < 10$ the solution stays near the center of the moving frame coordinate system and behaves like a soliton, i.e., preserves its shape, although its maximum slightly varies. For larger times the solution turns to grow and blows-up for $t \approx 20$. The results for the fixed and moving frame coordinate system are very similar.
The results from the Experiments 1 and 2 show that the mechanism for having a balance between the nonlinearity and dispersion is present, but the solution is not robust (even when it is stable as a time stepping process) and eventually takes the path to the attractor presented by the propagating wave.

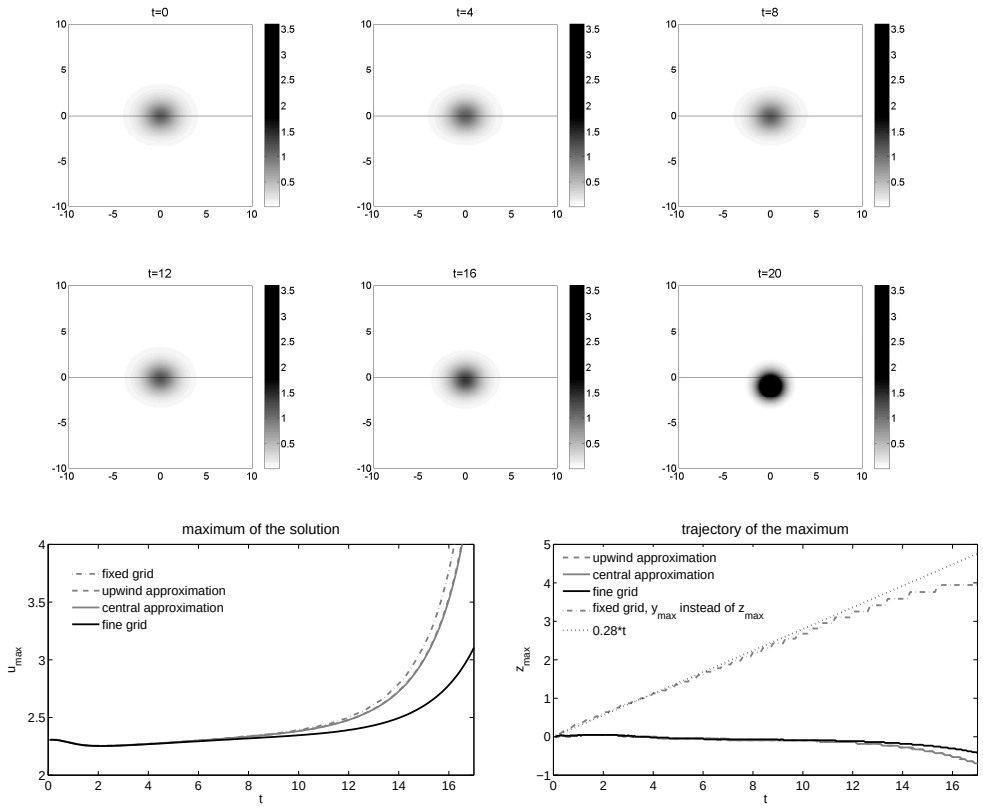

Figure 2: Evolution of the solution for $c = 0.28$, the maximum $u(0, z_{\max})$, and the trajectory of the maximum.

Example 3. In order to show that the lack of robustness is a intrinsically 2D effect rather than due to the imperfections of the scheme, we use the exact solution for the 1D case [2] as initial data:

$$u(x,z,0) := u^{\mathrm{sech}}(x) = (1-c^2)\frac{1.5}{\alpha}\mathrm{sech}^2\big(0.5x\sqrt{(1-c^2)/(\beta_2-\beta_1 c^2)}\big).$$

The boundary conditions on $z = -20$ and $z = 20$ are $u(x, \pm 20, t) := u^{\mathrm{sech}}(x)$. The maximum of the difference between the numerical and the exact solution $\Delta u := \max|u - u^{\mathrm{sech}}|$ and the order of convergence l are shown in Table 1. As it is seen, the results confirm both the solitonic behaviour of the 1D solution and the second order convergence of the difference scheme (3). The central difference and upwind approximations of u_{tz} lead to practically the same values in the numerical solution. The comparison between the moving frame and fixed grid computations shows that the latter produces larger errors on non-uniform grids, but smaller errors on uniform grids.

Conclusion. A difference scheme in a moving frame coordinate system is designed for the investigation of the time evolution of the localized solutions of the 2D Boussinesq

Table 1: Convergence in space and time for $c = 0.27$

		$t = 4$		$t = 8$		$t = 12$	
τ	N_x+1	Δu	l	Δu	l	Δu	l
moving frame, non-uniform grid							
0.1	160	1.36e-3		5.04e-3		1.70e-2	
0.05	320	3.56e-4	1.93	1.32e-3	1.93	4.44e-3	1.94
fixed grid							
0.1	160	1.81e-3		6.78e-3		2.42e-2	
0.05	320	4.69e-4	1.95	1.75e-3	1.95	6.21e-3	1.96
moving frame, uniform grid							
0.1	160	1.05e-2		3.36e-2		1.13e-1	
0.05	320	2.66e-3	1.98	8.41e-3	2.00	2.74e-2	2.04
fixed uniform grid							
0.1	160	1.00e-2		2.82e-2		8.61e-2	
0.05	320	2.56e-3	1.97	7.18e-3	1.97	2.15e-2	2.00

Paradigm Equation (BPE). The grid is non-uniform and the truncation error is second order in space and time. The results obtained for the time evolution of supposedly stationary propagating waves for different phase speeds are very similar to those in [7, 8] – for phase speeds $0 \neq c \leq 0.27$, the initially localized wave disperses in the form of ring-wave expanding to infinity. Respectively, for $c \geq 0.28$ the initial evolution resembles a stationary propagation, but after some period of time a blow-up of the solution takes place. The results are in good agreement with [6], where a similar ($c = 0.3$) threshold is established for the appearance of the blow-up.

The moving frame coordinate system helps us to keep the localized structure in the center of the coordinate system, where the grid is much finer. It also reduces the effects of the reflection from the boundaries, and thus allows us to use a smaller computational box.

Acknowledgment. This work has been partially supported by Grant DDVU02/71 from the National Science Fund by Ministry of Education, Youth, and Science of Republic of Bulgaria.

References

[1] Boussinesq, J.V.: Théorie des ondes et des remous qui se propagent le long d'un canal rectangulaire horizontal, en communiquant au liquide Journal de Mathématiques Pures et Appliquées **17** (1872) 55–108

[2] Christov, C.I.: An energy-consistent Galilean-invariant dispersive shallow-water model. *Wave Motion*, **34** (2001) 161–174

[3] Christou, M.A., Christov, C.I.: Fourier-Galerkin method for 2D solitons of Boussinesq equation. *Math. Comput. Simul.*, **74** (2007) 82–92

[4] Christov, C.I.: Numerical implementation of the asymptotic boundary conditions for steadily propagating 2D solitons of Boussinesq type equations, *Math. Comp. Simul.*, Appeared online August 10, 2010 `http://dx.doi.org/10.1016/j.matcom.2010.07.030`Doi:10.1016/j.matcom.2010.07.030

[5] Christov, C.I., Choudhury, J.: Perturbation solution for the 2D Boussinesq Equation. *Mech. Res. Commun.*, **38** (2010), 274–281

[6] Chertock, A., Christov, C.I., Kurganov, A.: Central-upwind schemes for the Boussinesq paradigm equation. *Proc. 4th Russian-German Advanced Research Workshop on Comp. Science and High Performance Computing*, *NNFM*, **113** (2011), 267–281

[7] Christov, C.I., Kolkovska, N., Vasileva, D.: On the Numerical Simulation of Unsteady Solutions for the 2D Boussinesq Paradigm Equation, *Lecture Notes Computer Science*, **6046** (2011) 386–394

[8] Christov, C.I., Kolkovska, N., Vasileva, D.: Numerical Investigation of Unsteady Solutions for the 2D Boussinesq Paradigm Equation, 5th Annual Meeting of the Bulgarian Section of SIAM, Sofia, Bulgaria, *BGSIAM'10 Proceedings*, 2011, 11-16

[9] van der Vorst, H.: Iterative Krylov methods for large linear systems. *Cambridge Monographs on Appl. and Comp. Math.*, **13** (2009)

Part B
List of participants

Ivanka Tr. Angelova
FNSE, University of Rousse
8 Studentska Str.
7017 Rousse, Bulgaria
iangelova@uni-ruse.bg

Roumen Anguelov
Department of Mathematics and
Applied Mathematics
University of Pretoria
Pretoria 0002, South Africa
roumen.anguelov@up.ac.za

Emanouil Atanassov
Institute of Information and
Communication Technologies
Bulgarian Academy of Sciences
Acad. G. Bontchev str., bl. 25A
1113 Sofia, Bulgaria
emanouil@parallel.bas.bg

Gergana Bencheva
Institute of Information and
Communication Technologies
Bulgarian Academy of Sciences
Acad. G. Bonchev Str., bl. 25A
1113 Sofia, Bulgaria
gery@parallel.bas.bg

V. Beschkov
Institute of Engineering Chemistry,
Bulgarian Academy of Sciences
1113 Sofia, Bulgaria

Petia Boyanova
Institute of Information and
Communication Technologies
Bulgarian Academy of Sciences
Acad. G. Bonchev Str., bl. 25A
1113 Sofia, Bulgaria
petia@parallel.bas.bg

Christo I. Christov
Dept. of Mathematics
University of Louisiana at Lafayette
P.O.Box 41010
Lafayette, LA, 70504-1010, USA
christov@louisiana.edu

Colin J. Cotter
Department of Aeronautics,
Imperial College London,
London SW7 2AZ, UK

Dimitar Dimitrov
Institute of Information and
Communication Technologies
Bulgarian Academy of Sciences
Acad. G. Bontchev str., bl. 25A
1113 Sofia, Bulgaria
d.slavov@bas.bg

Neli Dimitrova
Institute of Mathematics and Informatics
Bulgarian Academy of Sciences
Acad. G. Bontchev str., bl. 8
1113 Sofia, Bulgaria
nelid@iph.bio.bas.bg

Ivan Dimov
Department of Parallel Algorithms
Institute of Information and
Communication Technologies
Bulgarian Academy of Sciences
Acad. G. Bonchev Str., Bl. 25A
1113 Sofia, Bulgaria
ivdimov@bas.bg

Milena Dimova
Institute of Mathematics and Informatics
Bulgarian Academy of Sciences
Acad. G. Bontchev str., bl. 8
1113 Sofia, Bulgaria
mkoleva@math.bas.bg

Stefka Dimova
Faculty of Mathematics and Informatics
Sofia University
5, James Bourchier Blvd.
1164 Sofia, Bulgaria
dimova@fmi.uni-sofia.bg

Nina Dobrinkova
Institute of Information and
Communication Technologies
Bulgarian Academy of Sciences
Acad. G. Bontchev str., bl. 2
1113 Sofia, Bulgaria
nido@math.bas.bg

Mariya Durchova
Institute of Information and
Communication Technologies
Bulgarian Academy of Sciences
Acad. G. Bonchev Str., bl. 25A
1113 Sofia, Bulgaria
mabs@parallel.bas.bg

Stefka Fidanova
Institute of Information and
Communication Technologies
Bulgarian Academy of Sciences
Acad. G. Bonchev str., bl. 25A
1113 Sofia, Bulgaria
stefka@parallel.bas.bg

Ivan Georgiev
Institute of Mathematics and Informatics
Bulgarian Academy of Sciences
Acad. G. Bonchev str., bl. 8
1113 Sofia, Bulgaria
john@parallel.bas.bg

Krassimir Georgiev
Institute of Informatrion and
Communication Technologies
Bulgarian Academy of Science
Acad. G. Bontchev str., bl. 25A
1113 Sofia, Bulgaria
georgiev@parallel.bas.bg

Irina Georgieva
Institute of Mathematics and Informatics
Bulgarian Academy of Sciences
Acad. G. Bontchev str., bl. 8
1113 Sofia, Bulgaria
irina@math.bas.bg

Rayna Georgieva
Institute of Information and
Communication Technologies
Bulgarian Academy of Sciences
Acad. G. Bontchev str., bl. 25A
1113 Sofia, Bulgaria
rayna@parallel.bas.bg

Vladimir Gerdjikov
Institute for Nuclear Research and
Nuclear Energy
Bulgarian Academy of Sciences
72 Tsarigradsko chaussee
1784 Sofia, Bulgaria
gerjikov@inrne.bas.bg

J. V. Gonzalez
Department of Systems Biology and
Bioinformatics
University of Rostock
Germany

Todor Gurov
Institute of Information and
Communication Technologies
Bulgarian Academy of Sciences
Acad. G. Bontchev str., bl. 25A
1113 Sofia, Bulgaria
gurov@parallel.bas.bg

Clemens Hofreither
DK Computational Mathematics
Johannes Kepler University Linz
Altenberger Str. 69
4040 Linz, Austria
clemens.hofreither@dk-compmath.jku.at

Darryl D. Holm
Department of Mathematics
Imperial College London,
London SW7 2AZ, UK

Rossen Ivanov
School of Mathematical Sciences
Dublin Institute of Technology
Kevin Street, Dublin 8, Ireland
rivanov@dit.ie

Sofiya Ivanovska
Institute of Information and
Communication Technologies
Bulgarian Academy of Sciences
Acad. G. Bontchev str., bl. 25A
1113 Sofia, Bulgaria
sofia@parallel.bas.bg

Aneta Karaivanova
Institute of Information and
Communication Technologies
Bulgarian Academy of Sciences
Acad. G. Bontchev str., bl. 25A
1113 Sofia, Bulgaria
anet@parallel.bas.bg

Mikhail Kolev
University of Warmia and Mazury,
Słoneczna 54,
10-710 Olsztyn, Poland
mkkolev@yahoo.com

Miglena Koleva
FNSE, University of Rousse
8 Studentska Str.
7017 Rousse, Bulgaria
mkoleva@ru.acad.bg

Natalia Kolkovska
Institute of Mathematics and Informatics
Bulgarian Academy of Sciences
Acad. G. Bonchev str., bl. 8
1113 Sofia, Bulgaria
natali@math.bas.bg

Mikhail Krastanov
Institute of Mathematics and Informatics
Bulgarian Academy of Sciences
Acad. G. Bontchev str., bl. 8
1113 Sofia, Bulgaria
krast@bas.bg

Ivan Lirkov
Institute of Informatrion and
Communication Technologies
Bulgarian Academy of Sciences
Acad. G. Bontchev str., bl. 25A
1113 Sofia, Bulgaria
ivan@parallel.bas.bg

Maria Lymbery
Institute of Informatrion and
Communication Technologies
Bulgarian Academy of Sciences
Acad. G. Bontchev str., bl. 25A
1113 Sofia, Bulgaria
mariq@parallel.bas.bg

Svetozar Margenov
Institute of Informatrion and
Communication Technologies
Bulgarian Academy of Sciences
Acad. G. Bontchev str., bl. 25A
1113 Sofia, Bulgaria
margenov@parallel.bas.bg

Pencho Marinov
Institute of Information and
Communication Technologies
Bulgarian Academy of Sciences
Acad. G. Bonchev str., bl. 25A
1113 Sofia, Bulgaria
pencho@parallel.bas.bg

Valentin Marinov
Institute of Information and
Communication Technologies
Bulgarian Academy of Sciences
Acad. G. Bontchev str., bl. 2
1113 Sofia, Bulgaria
datatech@abv.bg

Svetoslav Markov
Institute of Mathematics and Informatics
Bulgarian Academy of Sciences
Acad. G. Bontchev str., bl. 8
1113 Sofia, Bulgaria
smarkov@bio.bas.bg

Maya Markova
Department of Informatics
University of Russe
Studentska Str. 8
7017 Russe, Bulgaria
maya.markova@gmail.com

M. Nenov
Institute of Mechanics,
Bulgarian Academy of Sciences
Acad. G. Bontchev St., bl. 4
1113 Sofia, Bulgaria

Geno Nikolov
Faculty of Mathematics and Informatics
Sofia University
5, James Bourchier Blvd.
1164 Sofia, Bulgaria
geno@fmi.uni-sofia.bg

S. Nikolov
Institute of Mechanics,
Bulgarian Academy of Sciences
Acad. G. Bontchev St., bl. 4
1113 Sofia, Bulgaria

Tsvetan Ostromski
Institute of Information and
Communication Technologies
Bulgarian Academy of Sciences
Acad. G. Bonchev str., bl.25A
1113 Sofia, Bulgaria
ceco@parallel.bas.bg

James R. Percival
Department of Earth Science and Engineering
Imperial College London,
London SW7 2AZ, UK

Petar Popivanov
Institute of Mathematics and Informatics
Bulgarian Academy of Sciences
Acad. G. Bontchev str., bl. 8
1113 Sofia, Bulgaria
popivano@math.bas.bg

Evgenija D. Popova
Institute of Mathematics and Informatics
Bulgarian Academy of Sciences
Acad. G. Bontchev str., bl. 8
1113 Sofia, Bulgaria
epopova@bio.bas.bg

Tsviatko Rangelov
Institute of Mathematics and Informatics
Bulgarian Academy of Sciences
Acad. G. Bontchev str., bl. 8
Sofia 1113, Bulgaria
rangelov@math.bas.bg

Victoria Rashkova
Department of Informatics
University of Russe
Studentska Str. 8
7017 Russe, Bulgaria
viktoriqi_78@abv.bg

Julian Revalski
Institute of Mathematics and Informatics
Bulgarian Academy of Sciences
Acad. G. Bontchev str., bl. 8
1113 Sofia, Bulgaria
revalski@math.bas.bg

Angela Slavova
Institute of Mathematics and Informatics
Bulgarian Academy of Sciences
Acad. G. Bontchev str., bl. 8
1113 Sofia, Bulgaria
slavova@math.bas.bg

M. D. Todorov
Technical University of Sofia
8 Kliment Ohridski Blvd.
1000 Sofia, Bulgaria
mtod@tu-sofia.bg

Daniela Vasileva
Institute of Mathematics and Informatics
Bulgarian Academy of Sciences
Acad. G. Bonchev str., bl. 8
1113 Sofia, Bulgaria
vasileva@math.bas.bg

Lubin Vulkov
FNSE, University of Rousse
8 Studentska Str.
7017 Rousse, Bulgaria
lvalkov@ru.acad.bg

Olaf Wolkenhauer
Department of Systems Biology and Bioinformatics
University of Rostock
Germany